2018

Ex-vivo modeling of misfolded protein neurotoxicity in brain slices: Implications for mechanistic and translational discovery in chronic neurodegenerative diseases

Naveen Kondru
Iowa State University

Ex-vivo modeling of misfolded protein neurotoxicity in brain slices: Implications for mechanistic and translational discovery in chronic neurodegenerative diseases

by

Naveen Kondru

A dissertation submitted to the graduate faculty

in partial fulfillment of the requirements for the degree of

DOCTOR OF PHILOSOPHY

Major: Biomedical Sciences

Program of Study Committee:
Anumantha G. Kanthasamy, Major Professor
Arthi Kanthasamy
Heather West Greenlee
Jodi Smith
Elizabeth Whitley

The student author, whose presentation of the scholarship herein was approved by the program of study committee, is solely responsible for the content of this dissertation. The Graduate College will ensure this dissertation is globally accessible and will not permit alterations after a degree is conferred.

Iowa State University
Ames, Iowa
2018

DEDICATION

This dissertation is dedicated to my parents, Subba Rao Kondru and Vijaya Lakshmi Kondru for their unconditional support and being my constant source of inspiration.

TABLE OF CONTENTS Page

ACKNOWLEDGMENTS

I am deeply indebted to my major professor and Ph.D. mentor, Dr. Anumantha Kanthasamy, who recognized my desire to become a researcher and helped to make my dream come true. I would also like to thank my committee members, Dr. Arthi Kanthsamy, Dr. Heather West Greenlee, Dr. Elizabeth Whitley, Dr. Jodi Smith and Dr. Vellareddy Anantaram for their support and serving on my doctoral research. I am deeply indebted to my wife, Dr. Sireesha Manne for becoming a dual career professional with me in the lab and encouraging my workaholic nature. I express my deep love to my son, Akyath Narayan Kondru (Akki), for inspiring me through his little achievements. I am indebted to Gary Zenitsky for proofreading my manuscripts prior and during publication process and making the jokes that I understand. I would like to thank all lab members and neighboring lab members that I worked with since August 2012.

I would also like to my teaching mentor, Dr. Walter Hsu for his support and recognize my teaching skills. I'd like to thank other teaching mentors who I served as a teaching assistant - Drs. Kenneth B. Platt, Karin VanMeter, Chis Minion, Paul Kapke, Kathleen Mullin, Vellareddy Anantharam, Arthi Kanthasamy, Richard Martin, Elizabeth Whitley, Jodi Smith, Carrie Berg, Keri Carstens, Johann Coetzee, Suzanne Millman, Michael Cho and William Robertson. Thanks to my teaching colleagues Diou, Emir, Hiruni and Ms. Linda Zeller and Amanda Brockman. Lastly but most importantly, I thank my parents, Subba Rao Kondru and Vijaya Lakshmi Kondru for supporting me and providing me with education. I would like to thank my sister, Sravanthi Bachana for her constant support and love.

ABSTRACT

Protein misfolding has a major implication in the development of neurodegenerative diseases like Alzheimer's, Parkinson's, Prions, Huntington's and dementia. Elucidation of misfolded protein neurotoxicity for such chronic diseases has been challenging to model in the lab. Using cell cultures, the biology of misfolded proteins can be studied in short term, but the biologically integrated models remain to be established for long-term modeling. Therefore, in chapter I, we established an organotypic brain slice culture model that maintains the 3-dimensional environment and functionally relevance for chronic studies. Further, we have experimentally demonstrated the applications such as viability assessment, response to toxicants, cytokine release, modeling traumatic brain injury, targeted gene delivery. In chapter II, we report a novel organotypic slice culture assay coupled with seeding assays such as real-time quaking-induced conversion (OSCAR) assay. We hypothesized that the brain slice cultures coupled with sensitive readouts would provide fast and efficient alternative to modeling prions *ex-vivo*. OSCAR model was characterized for seeding activity at various time points and the titers are quantified. OSCAR supports investigating the biological mechanisms of prions and supports screening of anti-prion therapeutics. chronic wasting disease (CWD) is a prion disease of cervids that has been rapidly expanding in several states in USA including Iowa and Canada. Therefore, in chapter III, I developed a CWD brain slice culture model to characterize the CWD prions. Using traditional prion detection and ultra-sensitive detection such as Real-Time Quaking-Induced Conversion (RT-QuIC) and Protein Misfolding Cyclic Amplification (PMCA), we characterize the seeding ability of CWD prions. Further, we demonstrate infectious ability of the CWD prions from slices to infect the mice. We also demonstrate

the diagnostic ability of this model to detect CWD prions from a biological sample. Environmental factors such as Manganese can induce neuroimmune transformations that possibly alter the course of neurodegenerative processes. Therefore, in chapter IV, we systemically characterized the transcriptome of microglia in response to the neurotoxicant Manganese, misfolded α-syn, and the influence of their interaction. Our findings provide novel insights into global transcriptome of microglia. α-syn predominately activated innate immune genes particularly, cytokine and chemokines, TNF, NF-kB, and TLR signaling. In contrast, Mn caused distinct changes to pathways related to cellular senescence, NOD-like receptor signaling, HIF-1 signaling, and pyrimidine metabolism. Mn and α-syn co-treatment caused major perturbations in Rho GTPase signaling and inflammasome activation. Co-treatment also caused profound changes in transcripts that triggered microglia to switch to their more cytotoxic, M1 phenotype. Collectively, we report the brain slice cultures to model the *in-vivo* like propagation of amyloids in environmentally linked neurodegenerative disorders. The reliability of this quantitative model for protein misfolding diseases could help us in understanding the mechanisms of diseases and to identify potential therapeutic targets. Additionally, we identified novel microglial genes and pathways that are perturbated in response to Mn and α-syn that allow us to discover therapeutic targets for treatment of synucleinopathies such as Parkinson's disease.

CHAPTER I: GENERAL INTRODUCTION

Thesis Layout and Organization

The alternative format was chosen for this dissertation and consists of manuscripts that have either been published or are in preparation for submission. There is a general introduction containing merged literature review and research, three research chapters in the format of their corresponding journals, and a general conclusions/future directions section. Each research chapter contains references in the format of the journal it was published, or it will be submitted to.

In chapter-I, we review the current state of organotypic slice cultures for modeling protein misfolding biology. We also develop this *ex-vivo* method of brain slice cultures from various brain regions and demonstrate this model as a faithful method to understand the disease process. Additionally, this model is also suitable to study the compounds of toxicological interest and environmental exposure such as Manganese, Lead, MPP+, 6-OHDA that are implicated in Parkinson's disease models.

Chapter-II is published in the journal *Scientific Reports.* In this manuscript, we report the integrated organotypic slice culture models coupled to RT-QuIC assay (OSCAR) to study the prion misfolding. The conclusion is that the OSCAR model can be a practical, sensitive, and fast approach to study slow progressive neurodegeneration in the lab setting. Another advantage of using this model is studying the misfolded proteins in the context of 3D environment and can support the studies in an intact *brain-like* environment for several weeks.

In Chapter-III, the robustness of OSCAR model allowed me to characterize another strain of misfolded prion, that causes chronic wasting disease (CWD) in Cervids and have a

public health concern. CWD is a devastating disease that been rapidly expanding to several states in the USA and have a zoonotic concern. This manuscript will be submitted to the journal *Scientific Reports.*

In chapter-IV, we provide a transcriptome analysis of misfolded α-Synuclein and Manganese (Mn) induced changes in the microglia. Using this study, we elucidate gene-environment interactions and to identify several important genes and signaling pathways. This manuscript will be submitted to journal *Glia.*

In chapter V, I summarize general conclusions and pointing some important directions that have potential to become translational targets.

This dissertation contains the experimental results obtained by the author during his Ph.D. study under the supervision of his major professor Dr. Anumantha G. Kanthasamy at Iowa State University, Department of Biomedical Sciences.

CHAPTER II: BRAIN SLICE CULTURES FOR EX-VIVO MODELING OF NEURODEGENERATIVE DISORDERS: CURRENT PROGRESS AND FUTURE PERSPECTIVES

A manuscript to be submitted to *Toxicological Sciences*

Naveen Kondru[1], Sireesha Manne[1], Adhithaya Charli[1], Gary Zenitsky[1], Carrie Berg[1], Huajun Jin, Vellareddy Anantharam[1], Arthi Kanthasamy[1], and Anumantha Kanthasamy[1*]

1. Department of Biomedical Sciences, College of Veterinary Medicine, Iowa State University, Ames, IA 50011, USA.

* Corresponding author: akanthas@iastate.edu

Abstract

Modeling of protein misfolding *ex-vivo* in neurodegenerative disorders is crucial for the advancement of biologically relevant modeling. Brain slices support salient features of amyloid pathology and faithfully recapitulate the 3D environment and cellular diversity. Protein misfolding and aggregation has been increasingly important as a pathological event in neurodegenerative diseases and cancer, but biological modeling of this phenomena remains to be a challenge. The common hallmark manifestation in the degenerative process is the formation of abnormal aggregates of the proteins. While cellular models served to understand some of the mechanisms, organotypic slice cultures prove to be a realistic model for the advancement as the biologically relevant models. Here, we discuss the evolution of brain slice cultures for broad applications in diseases such as Alzheimer's, Parkinson's, Huntington, ALS and Prion diseases. We also provide experimental evidence to demonstrate the suitability of brain slices for long-term biological modeling of neurodegeneration and environment

connected neurotoxic mechanism. Further, we demonstrate targeted genetic manipulation using viral vectors that can be explored for *ex-vivo* disease modeling or therapeutic development. Finally, we describe a novel TBI slice culture model using a multi-electrode array to assess electrophysiological activity. In summary, we review the current state of brain slices to model chronic neurodegeneration, demonstrate assessment of flow cytometry-based cell viability, multiplex cytokine detection and established a novel TBI model. (NIH ES 19276 and ES10586 and W. Eugene Linda Lloyd Endowed Chair)

Introduction

Many neurodegenerative diseases that have a protein component responsible for pathology are termed as proteinopathies. In prion diseases, misfolded proteins have conclusively been demonstrated as etiological agent although other protein misfolding diseases such as Alzheimer's, Parkinson's, Huntington, ALS are actively being investigated for prion-like propagation. A prion-like spreading of protein aggregates is emerging as a major pathophysiological mechanism in all these diseases but experimental modeling of these slow, progressive diseases remains to be addressed. Environmental neurotoxicant exposure has also been increasingly recognized as risk factors for these proteinopathies. Although the mechanisms underlying this process is poorly understood, prion theory argues that the self-templating mediated protein misfolding as a unifying denominator in this process. Several proteins are involved in this process that is specific for the disease. Therefore, these diseases are categorically referred to as Protein Misfolding Disorders (PMD). Organotypic brain slice cultures offer advantages over traditional cell culture methods as they resemble the intra-cerebral environment *ex-vivo*. The goal of the present study is to establish an organotypic brain slice culture model for the investigation of the protein-misfolding mechanisms underlying

environmentally linked proteinopathies. We have previously established organotypic slice cultures models for sensitive detection in prion disease. Misfolded prions from brain homogenates invade and amplify in the slice cultures over a relatively shorter time scale compared to animal models. It reduced animal suffering and may be a cost-effective approach to study the molecular aspects of these chronic diseases. The *ex-vivo* nature of these models allows easy experimental operation and downstream analysis such as immunohistochemistry, and biochemical analysis such as protein and RNA analysis. Several markers are characterized by quantitative assessment of the viability of slice cultures (Noraberg *et al.*, 1999). For example, propidium iodide (PI) uptake estimates cell death and can be imaged in a live slice and further be cultured. Similarly, Lactate dehydrogenase (LDH) efflux allows us to estimate the stress from the culture medium. Ordinary Nissl cell staining, Fluoro-Jade (FJ), and immunohistochemical staining can be used to assess the integrity of the neuronal cell death. Although several cell culture models were available to study the protein misfolding, most of these rely on either infecting with a brain homogenate or using protein expression constructs with a reporter tags. Cell cultures remain to be a popular method to study the disease process, but they suffer from some key limitations. These cells represent an isolated, monoclonal population or cells from a mixed origin with no crosstalk to other cell types. However, brain slices overcome few limitations such as preserving the have dynamic connections to other cell type and maintenance of the electrical activity that is typically present in physiological conditions. Organotypic brain slices allow easy experimental access and optimal viability over long periods (months). Experiments can be monitored in living slices (e.g., for imaging) during the entire culture period. Further, the slices can be fixed and cryosectioned for microscopic examination at the experimental endpoint. Different regions of the embryonic brain or spinal

tissue can be used in this protocol. Although brain slices are extracted from postnatal day 4 to 21 pups, blood vessels continue to develop. A transporter protein, GLUT-1 was reported to be expressed in blood vessels after 3 days in culture (Camenzind *et al.*, 2010). This suggests that endothelial transporters can be functionally maintained in slices that recapitulate blood-brain barrier. In this study, we review several applications of organotypic brain slice cultures and demonstrate some of their applications such as the effect of the environmental neurotoxicants like manganese and lead on protein aggregation. In summary, our results demonstrate the organotypic brain slice culture as a flexible model for studying the effects of environmental factors on protein misfolding in various proteinopathies of the central nervous system. The brain slice culture model will also greatly minimize the animal use for studying neurodegenerative diseases.

Evolution and diverse applications of organotypic brain slice cultures

The slice culture method was historically introduced by Hogue and colleagues using human fetal brain cells in 1947 (Hogue, 1947). However, not until several decades, the roller tube method came into existence and later the interface method of culture became popular. After this invention, the interface method became experimentally feasible in several labs and optimized for in culture settings in the early 90s. (see review by Stoppini and colleagues) (Stoppini *et al.*, 1991). This method of using interests have been applied for testing the long-term plasticity of neurons (Gähwiler *et al.*, 1997). Organotypic hippocampal slices from neonatal mice were prepared and maintained on a porous membrane that drives the nutrient-rich media through the capillary action from the membrane pores (Stoppini, et al., 1991). Due to this simplification step, this method of culturing the brain slices on a liquid-air interface became a standard method for slice culture maintenance. The membranes are typically loaded

with an insert that allows having an elevation to feed the culture medium from the basal chamber of the membrane insert. The slices can be typically cultured on a 30 mm diameter for a 6 well plate and with a porosity of 0.4 µM. When the membrane is hydrated, it is transparent allowing the bright field and fluorescence microscopy on a live culture. Slice cultures from postnatal P8–P10 brains were thought to be best for the brain slice cultures on membrane inserts. These slices were shown to have good survival for a prolonged time of several months (Marksteiner and Humpel, 2008). Organotypic slice cultures prepared from various brain regions such as mesencephalon, striatum, hippocampus, and cerebellum from embryonic (E21) to postnatal P7 rats were shown to have good viability when using roller tube technique (Ostergaard et al., 1990). Typically, the slices would be cultured for at least ten days to allow stabilization of intrinsic projections of the axons in developing slices. Further, this method minimizes the endogenous activation and release of signaling molecules such as calcium or glutamate, therefore, minimizing reactive astrogliosis. This stabilization period allows the slice culture to adhere to the membrane insert and making it flexible for downstream handling such as IHC. Slice cultures were prepared from the region encompassing both entorhinal and hippocampal regions to determine circuit development in culture. Using biocytin uptake labeling, the authors demonstrated the presence of live granule cells and axons of entorhinal neurons networking with mossy fibers in the 2-3 week old slice cultures that correspond to the development of the rat brain (Diekmann *et al.*, 1994). In addition to neurodegenerative diseases, slice cultures have also been used to model cancer. For instance, slice cultures from neonatal rats (p2) co-cultured with C6 glioma spheroids to demonstrate the cell migration, tumor cell invasion, that mimics the physiological system (Ohnishi *et al.*, 1998). Slices derived from mature mice have shown to have poor viability for chronic studies. Therefore, a different

study using antisense oligodeoxynucleotides (ASO) against Cx43 gap junctions reportedly enhance survival from trauma (Yoon *et al.*, 2010). This ASO treatment caused a transient decrease in expression levels of Cx43 gap junctions that lead to survival of neurons with normal morphology over a longer culture period. Adult hippocampal slices were maintained *ex-vivo* over 6 days using a medium that closely resembles cerebrospinal fluid (CSF) with supplements. The viability of slices was measured using population spike amplitude (PSA). Other studies have explored the microenvironment of the tumor using an organotypic slice co-culture assay for drug testing (Chadwick *et al.*, 2015; Ren *et al.*, 2015). Brain slices co-cultured with murine macrophage cell line (RAW 264.7) demonstrated soluble intermediates from HIV-1 Tat protein are responsible for neurotoxicity in the hippocampal slices (Brana *et al.*, 1999).

Organotypic slice culture models of Alzheimer's disease (AD)

Organotypic slice cultures prepared and maintained under low oxygen partial pressure were used to model amyloid-beta (1-40) toxicity. Melatonin, the pineal hormone was shown to have opposing effects on oxidative stress was observed using slice culture model of AD (Clapp-Lilly *et al.*, 2001). Low dose reduced the oxidative stress markers based on a reduction in the redox-active iron, heme-oxygenase-1 induction and 8-hydroxyguanosine. However, higher dose promoted opposite effects. Another study demonstrated neuroprotection by 17beta-estradiol in the slice cultures via glycogen synthase kinase-3 pathway (GSK-3) inhibition. Similarly, cultures prepared form 3xTg-AD mice were used to model Alzheimer's disease that recapitulates animal model (Croft *et al.*, 2017). Using slice cultures, a benzothiazole compound (BTA-EG4) that binds to amyloid, was shown to reduce tau phosphorylation via GSK-3 pathway. Similar to Prion infected slice cultures, Another study successfully showed *ex-vivo* replication of amyloid beta in the slices (reviewed in the section below). Using similar strategy

aggregation of synthetic Amyloid beta in a long-term hippocampal slice culture supplemented with homogenates in the culture media. Further, these amyloid aggregation was concurrent with microglial activation, neuronal and spine loss.

Organotypic slice culture models of Parkinson's disease (PD)

Development of dopaminergic neurons was studied using the slices prepared from ventral mesencephalon region of neonatal (P1) rats (Holmes *et al.*, 1995). The dopamine neurons, from immunoassay by tyrosine hydroxylase were radially grown towards striatal slices but not into cerebellar slices when co-cultured. This suggests the nigrostriatal pathway can be oriented in slice cultures by guidance and preservation of synaptic connections. Another co-culture system using a ventromedial portion of the mesencephalon and striatum was used to evaluate the 1-benzyl-1,2,3,4-tetrahydroisoquinoline, a PD toxin (Kotake *et al.*, 2003). Olfactory route hypothesis has been actively being investigated as an origin site for PD pathology. The rostral migratory stream (RMS) in rodents comprises of circuits with direct connectivity from subventricular zone (SVZ) neurons that reach the olfactory bulb (OB). Migration of neural stem cell precursors but not mesenchymal stem cells was observed when implanted in the slices. This was demonstrated using Bromodeoxyuridine (BrdU)-labelling and stem cell micrografts into the forebrain slices that help in preserving the rostral part of the lateral ventricle, the RMS, and the OB (Tanvig *et al.*, 2009). Therefore, the brain slice cultures facilitate neural precursors in a programmable manner. However, modeling stem cells in slice culture with pharmacological or genetic manipulation remains to be tested. Toxicological modeling of slice cultures is an active area under investigation. As we demonstrate in this manuscript, we modeled toxicity studies using the brain slice cultures. Rotenone, a neurotoxin is a potent complex I inhibitor of the electron transport chain and used to model dopaminergic

and cholinergic neuron toxicity in co-culture brain slices (Ullrich *et al.*, 2009). Rat midbrain slice cultures containing substantia nigra (SN) were also used to understand regional susceptibility catecholamine neurons suggesting the dorsal tier catecholamine neurons are more susceptible (Bywood *et al.*, 2000). Another study utilized th effect of mechanical transfection on the nigrostriatal neurons in the slice preparation (Daviaud *et al.*, 2014). Progressive loss of dopaminergic cell number created by the lesion was quantified using diffusion tensor magnetic resonance imaging suggesting the organotypic slices are a simple and rapid method to study dopaminergic neuronal degeneration. Hippocampal slices co-cultured with microglial cells (primary and n9) to study LPS induced inflammatory responses and role of histone deacetylases (Suuronen *et al.*, 2003). In another study, mesenchymal stem cell (MSC) were co-cultured with brain slices without direct contact. The MSCs purified using fluorescence-activated cell sorting from bulk bone-marrow-cell suspensions. This study demonstrated MSC cocultured brain slices have higher BDNF secretion, axonal regrowth and shown to support neuronal regeneration in a slice culture model of the mesocortical dopaminergic projection system (Sygnecka *et al.*, 2015).

Organotypic slice culture models of Prion disease

Prion diseases have prolonged incubation periods making the study of these diseases difficult in the lab and considered as biosafety level II or above. Although cells lines were developed to maintain infectivity, alternative models that reflect neuropathology remains to be addressed. Slice cultures from transgenic mouse were used to determine electrophysiological response in the presence or absence of prion protein. Slice cultures were prepared from 19- to 21-day-old mice and patch-clamp experiments on the Purkinje cells was performed. Whole-cell recordings suggested there is no difference in the resting membrane potential regardless of the genotype

of the animal (wild-type mice, tg35, tg20, and *Prnp-/-* genotypes tested). However, Ca^{2+} activated K^{+} currents are reduced in *Prnp-/-* mice are reduced due to an alteration of intracellular calcium homeostasis suggesting PrP plays role in depolarization (Herms *et al.*, 2001). Later, sagittal brain sections were prepared from the cerebellar region of 9-12-day old pups and with 350 µm thickness as an *ex-vivo* prion infective model (Falsig *et al.*, 2008a). The prions from infected brain homogenate (RML scrapie) was used to incubate the slices as free sections in the physiological buffer. The slices were washed twice and maintained as explants on the membrane inserts with culture media supplied. After several days in culture, the slices were collected, lysed and treated with proteinase K to digest cellular form of prion protein before immunoblotting (Falsig *et al.*, 2008b). The slices gained a proteinase K resistant bands that appeared on 21 days post culture and expression increased thereafter. Although the model is far superior to existing cell cultures, the proteinase K digestion and western blot requires a large amount of protein. Therefore, we developed a sensitive prion detection method using real-time quacking induced conversion (RT-QuIC) assay and termed as OSCAR (organotypic slice culture assay coupled to RT-QuIC) assay (Kondru *et al.*, 2017a). The advantage of OSCAR assay is that it is ultrasensitive and requires a very low amount of slice culture homogenate. Further, based on the traces, prion titers can be quantified. OSCAR also offers a cost-effective approach to rapidly test the compounds or inhibitors that uncouple prion replication and requires less number of animals. We are optimistic that OSCAR model is easy to setup and can help several research labs. Prion-infected slices have also been valuable to determine temporal alteration in the spine density of Purkinje neuronal cells (Campeau *et al.*, 2013). Further, this model has been used to explore other 22L prion strains and utilized immunohistochemistry for differential staining patterns (Wolf *et al.*, 2015).

Organotypic slice culture models of Huntington's disease and Amyotrophic Lateral Sclerosis diseases (HD & ALS)

HD and ALS are diseases with unique aggregation of either protein/RNA or both as manifested diagnostically by expansion repeats typically consisting of PolyQ domains. Organotypic striatal slice cultures from neonatal rats were used to model Huntington's disease (HD) (Ostergaard *et al.*, 1995). These striatal slices were also demonstrated for the presence of the spiny interneurons that are spared in HD and positive for neuropeptides – somatostatin, neuropeptide Y and NADPH-diaphorase. These slices were found to be positive for the projection neurons that are particularly vulnerable in HD. Analogous to the brain, the slice cultures have preserved connections such as the interneurons and projection neurons. In contrast, the enkephalin mRNA-containing neurons, which are *in-vivo* projection neurons, were significantly fewer in the cultures. The relative loss of projection neurons and preservation of interneurons in single slice cultures of striatal tissue apparently mimic some of the neurodegenerative changes of HD. The hippocampal slices prepared from the R6/2 mouse as a model for HD. Poly Q aggregates bind to Congo red and chrysamine G that delay neuropathology by inhibiting the aggregate formation. Organotypic spinal cord slice cultures were also used to study the misfolded superoxide dismutase (SOD1) in relation to conformation-dependent strain propagation in ALS models (Ayers *et al.*, 2016).

Traumatic Brain Injury (TBI)

Organotypic brain slices have been utilized to model and understand the traumatic brain injury (TBI). The major disadvantage of using these models are associated with difficulty in method setup for a controlled and reproducible damage. While brain slices provide a controllable environment for the accurate delivery, of the specific cellular trauma as a result of various

methods remains to be investigated. One study produced traumatic injury utilizing mechanical sheer created by rolling a steel cylinder on the slices. Next, a second injury was created in a small area of the slice. These two forces were created to imitate the head injury and hypoxic damage that results as a post-traumatic event such as hypoxia or swelling (Adamchik *et al.*, 2000). Similarly, using mechanical injury on rat brain slices, disruption of calcium homeostasis and associated apoptosis was demonstrated (Morrison *et al.*, 2000). Using deformable silicone membranes, a two-dimensional stretch of organotypic hippocampal slice cultures was used to create acute phases of TBI (Morrison *et al.*, 2006). We have taken a novel approach to study the TBI. In this manuscript, we demonstrated a novel *in-vivo* model of blast injury, followed by ex-vivo electrophysiological assessment using a multi-electrode array, as described in the results section.

Results

Progressive toxicant-induced cell death in organotypic slice cultures

Organotypic cerebellar slice cultures were prepared from 10-12-day old pups and cultured for 21 days post-infection (dpi) for the adaption in *ex-vivo.* These slices were exposed to 100 µm Manganese (Mn) for different time points. The slice cultures were measured for the viability using Propidium Iodide (PI) incorporation and Annexin V staining. PI stains the dead cells when the cell membrane is compromised. Mn increased the PI uptake in the slices in a time-dependent manner and the fluorescence intensity was quantified (Fig 1A). Although Mn treatment caused an increase in the fluorescence intensity as early at 24 and 48 hours post-treatment, it is not significantly different from controls. However, Chronic exposure of Mn to the slice cultures (5 and 7 days post-treatment) caused a significant increase in the PI update. Next, we evaluated the apoptotic population and cell viability based on Annexin V staining

(Fig 1B). The slices demonstrated to have remarkable viability with over 95% of the cells remain viable. Mn treatment for 24 and 48 hours post-treatment showed a slight decrease in the viability of the slices with a marginal increase in late apoptotic cells when compared to controls. The quantification of the cell populations in either early apoptosis or late apoptosis were shown in (Fig 1C) whereas the distribution of the cells in each quadrant as shown in (Fig 1D). The right quadrants contain the apoptotic cells while the bottom left quadrant consists of live cells. These results demonstrate using flow cytometry and imaging to accurately quantify the viability of the cells in the slice cultures.

Measuring cytokine response from the slice cultures

Slice cultures are exposed to toxicants (MPP^+, 6-OHDA, and Manganese) and the stress-induced cytokine release was measured using Luminex assay. We measured the following cytokines IFNγ, IL-1β, IL-2, IL-4, IL-5, IL-6, IL-10, IL-12 and TNFα (Fig 2 A-I). 6-OHDA and Mn have significantly increased the cytokine release from the slice cultures. Mn was able to elicit the significantly higher release of IL-6 and TNFα when exposed for the chronic duration (96 hr) when compared to a shorter time of 24 hrs. However, the other cytokines tend to be higher at 24-hour time points. However, the cytokine, IL-4 change is not statistically different between controls and treatments.

2. Ectopic gene delivery in organotypic brain slice cultures

Slice cultures have unique advantage of desired protein to be expressed for long term studies. We prepared from the brain slices from cerebellar region and mounted on the inserts for transduced with an adeno-associated virus (AAV). The AAV virus used had green fluorescent protein (GFP) reporter tag that will allow live imaging in real time. After the slices were

infected, the slices were maintained for several dpi for imaging at various time points. The expression of the GFP was live imaged at 7 dpi using a fluorescent microscope (Fig 3A-B). The slices demonstrate excellent transduction efficiency with a clear expression of GFP starting from 2 dpi while the intensity continued to increase up to 7 dpi and then peak fluorescence plateaued (data not shown). Further, the virus serotypes AAV 2 and AAV 5 demonstrated tropism for Purkinje cells. Next, we infected the slice cultures from different brain region to determine the transduction efficiency. The cortico-striatal slices were infected with AAV 5 and imaged at 7 dpi (Fig 3C-D) at a lower magnification (2x) was shown to visualize the entire right hemisphere. Similarly, the cerebellar slices, the cortico-striatal slice cultures are readily transduced with AAVs. A magnified image (20x) of the striatal region of the slice was shown (Fig 3E). Further, we tested whether lipophilic gene transfection agents lipofectamine2000 to express GFP containing plasmid (data not presented). Although there is a low population of cells that express GFP, this method is not as efficient as the viral transduction for gene delivery in slice cultures.

Immunohistochemistry in slice cultures to evaluate the morphology and neurodegeneration

Slices can be imaged either live using viable antibodies or can be fixed and stained as free-floating sections. Various markers for different cells types can be used as in traditional histochemistry. In Fig.4, we demonstrate the neurodegeneration as a result of toxicants Mn and Cu on the slice cultures. Cu caused loss of neurites and disruption in the tau protein levels that is crucial for the integrity of the microtubules. While Mn also caused loss of Tau protein, the effects are not as severe when compared to Cu. Confocal imaging demonstrates a severe loss

of dendrites as evident in Purkinje cell layer as sustained by calbindin antibody and the microtubule binding protein Tau is shown in red stain.

Micro-electrode array for electrical activity in the slice cultures -Modeling TBI

Multichannel Systems (Reutlingen, Germany) MEA2100 in vitro recording system with built-in amplifier, a stimulus generator, temperature control, and perforated 60-electrode arrays that allow slices to be continuously perfused top-to-bottom with oxygenated artificial cerebrospinal fluid buffer. In an ongoing study, we are exploring the neurophysiological consequences of mild traumatic brain injuries (mTBI) induced by compressed gas-driven, primary shock waves (Fig. 4). In this study, the recording from the hippocampal CA1 region (Fig 4A-C) and the medial prefrontal cortex (mPFC, Fig. 4D) is shown. The slices were prepared as 400-µm coronal brain slices harvested from wild-type C57BL mice sacrificed 30 days post-blast (n=10 animals/group). Using this system, we have been able to capture bilateral recordings for both brain regions from either side of each coronal slice's midline. We are examining both spontaneous spike rates and micro-stimulus-evoked spike activity. Although spike sorting and unit discrimination can be quantified similarly for any other model, our results suggest that the spontaneous spike activity may differ between TBI and sham-TBI mice.

Discussion

Organotypic brain slices derived from CNS tissue maintains homeostasis due to a network of glial and neuronal connections. Therefore, the CNS resident cells such as glia produce cytokines and other factors in response to an external stimulus or toxicant exposure. In addition to the connectivity, the slices are physiologically respond based on the electrical activity. The *ex-vivo* nature of these slices allows us to interrogate the experimental question at any point in

the culture period and help us easily integrate with other culture protocols. The components released from these slices can be harvested in real time from the spent culture media. Therefore, the organotypic slice culture model remains to be invaluable for studying the role of toxicants in biologically relevant and alternative models of toxicology. Slice cultures demonstrate Mn toxicity as early as 24 hours based on the viability and PI incorporation. However, there is a significant effect on viability only after long-term exposure (i.e.., 5 days). The serum from culture media could potentially attenuate the toxicant effects of low concentration of Manganese. However, prolonged Mn treatment caused a significant reduction of viability as evident by the increase in the PI uptake and Annexin V correlated with the toxicity. In addition to neurotoxicological studies, the slice cultures have a unique advantage to study genetic engineering for evaluating the role of a specific gene of interest. Previous studies used electroporation to express protein-coding DNA (plasmid) delivery in slices generated from embryonic pups at a specific area on the slice. The inconsistency in delivering the electric currents and targeting a broader area remains to be a concern using this method. Our method demonstrated using Adeno Associated Virus (AAV) for effective gene delivery. It overcomes the physical trauma to the slices as induced by electric current. Using AAV 2 and 5 serotypes, we demonstrated that these AAVs have preferential tropism for Purkinje neurons in cerebellum and neuronal population in cortico-striatal regions in the organotypic slice cultures. The intact slices attached to the membrane insert are processed without dislodging the slice off the membrane. This helps to preserve the structural integrity of the slices during experimental and post-fix processing and thus allow for *in-situ* imaging. For the electrophysiological studies, we used multielectrode array either from organotypic slices or acute slices after treating the mice. Using acute slices, multi-unit spontaneous firing rates of the thalamic reticular nucleus (TRN),

and evoked potentials were quantified. The evoked potentials are generated via micro stimulation through one or more electrodes underlying the adjacent internal capsule. The mice subjected to TBI showed a decrease in the spike firing rate in the medial prefrontal cortex. Taken together, we have reviewed the current state of the art applications of the slice cultures and established the organotypic *ex-vivo* slice culture model for studying neurotoxicology and disease modeling.

Methods:

Organotypic slice cultures: All the experiments involving animal protocols were approved by Iowa State University's Institutional Animal Care and Use Committee (IACUC). Organotypic slices were prepared as previously described from 9- to 12-day-old mouse pups (Kondru, et al., 2017a). After dissecting the brain, it was oriented in the sagittal or coronal plane in the Compresstome's specimen tube. 2% low-melting-point agarose was poured maintaining proper orientation and quickly solidified by chilling specimen tube. To maintain the brain slices, ice-cold Gey's balanced salt solution supplemented with the excitotoxic antagonist, kynurenic acid (GBSSK) was used. The brain slices were sectioned at 350-µm thick slices using medium settings. The slices were plated on Millicell inserts in a 6-well plate supplemented with slice culture media in a humidified atmosphere of 5% CO2 at 37 °C. Slices were cultured for 1 week before exogenous expression of genes. For transfection, lipofectamine 2000 was used. The 1 µg of plasmid was mixed with 10 µl of lipofectamine and total volume was made to 50 µl and used to transfect 5 cerebellar slices. For transduction, AAV virus expressing a GFP reporter was mixed with opti-MEM in equal volume and used to directly as a micro drop on the slice. After transduction, the slices were cultured for at least 3 days before imaging as evident for GFP expression that peaked after 7 days.

Multiplex Luminex immunoassays Cytokine release:

Cytokine release was measured using the Luminex immunoassay as described previously (Gordon *et al.*, 2011). A mixed panel of cytokines relevant for neuroinflammation as described previously were used and quantified with recombinant standards. Media from slice cultures were frozen until assayed for cytokines.

***Ex-vivo* MEA analyses of brain slices from mice:**

Mice were decapitated after being anesthetized with 4% isoflurane in 2 L/min O_2 for 90 sec. The extracted brain is sliced at 400 µm on a vibratome while immersed in ice-cold carbogenated sucrose cutting solution. Slices are stored in ice-cold carbogenated sucrose cutting solution until all slicing is completed. All slices were then incubated 30-min at 32°C in a holding tray of carbogenated normal artificial CSF (aCSF) recording solution before the holding tray is transferred to the bench at RT. We used a 60-channel perforated multi-electrode array (MCS model 60pMEA100/30iR-Ti-gr) with a 30-µm electrode diameter and an inter-electrode distance of 100-µm (10 x 6 electrode array is 0.93 x 0.53 mm). Preparation of the MEA recording session was done as described previously with modification (2014). The slices are set up on the stage of an inverted microscope (Nikon TE2000-U, Tokyo, Japan) equipped with a 4X objective to aid slice orientation and imaging of the MEA-slice preparation. Slice recordings will be made in carbogenated normal aCSF recording solution heated to 32°C and continuously exchanged at 2 mL/min, while the slice tissue itself will be perfused at 0.1 mL/min through the bottom of the array chamber. This slow vertical perfusion through the MEA increases adherence between the slice and electrodes and gets carbogenated aCSF to the

bottom of the slice at the neuronal-electrode interface. After at least 5 min, spontaneous action potential discharge activity was recorded for 2 min at a sampling rate of 25 kHz from which we will be able to determine the neuronal firing pattern or neuronal oscillation synchrony of the TRN. After recording spontaneous activity, we performed high-frequency stimulation (HFS: 120 Hz, 140 µA) and low-frequency stimulation (LFS: 1 Hz, 140 µA) to determine their effect on neuronal firing pattern or on neuronal oscillation synchrony (Anderson *et al.*, 2003; Fuentealba *et al.*, 2005). For stimulus-evoked activity, a 2-min baseline was recorded followed by a 2-min post-stimulus recording. Raw, unfiltered data streams were captured for data processing and multi-unit sorting and discrimination was conducted on bandpass-filtered data (300 Hz – 3 kHz).

References

1 Noraberg, J., Kristensen, B. W. & Zimmer, J. Markers for neuronal degeneration in organotypic slice cultures. *Brain Res Brain Res Protoc* **3**, 278-290 (1999).

2 Camenzind, R. S. *et al.* Preservation of transendothelial glucose transporter 1 and P-glycoprotein transporters in a cortical slice culture model of the blood-brain barrier. *Neuroscience* **170**, 361-371, doi:10.1016/j.neuroscience.2010.06.073 (2010).

3 Hogue, M. J. Human fetal brain cells in tissue cultures; their identification and motility. *The Journal of experimental zoology* **106**, 85-107 (1947).

4 Gähwiler, B. H., Capogna, M., Debanne, D., McKinney, R. A. & Thompson, S. M. Organotypic slice cultures: a technique has come of age. *Trends in Neurosciences* **20**, 471-477, doi:https://doi.org/10.1016/S0166-2236(97)01122-3 (1997).

5 Stoppini, L., Buchs, P. A. & Muller, D. A simple method for organotypic cultures of nervous tissue. *Journal of Neuroscience Methods* **37**, 173-182, doi:https://doi.org/10.1016/0165-0270(91)90128-M (1991).

6 Diekmann, S., Nitsch, R. & Ohm, T. G. The organotypic entorhinal-hippocampal complex slice culture of adolescent rats. A model to study transcellular changes in a circuit particularly vulnerable in neurodegenerative disorders. *J Neural Transm Suppl* **44**, 61-71 (1994).

7 Ohnishi, T., Matsumura, H., Izumoto, S., Hiraga, S. & Hayakawa, T. A novel model of glioma cell invasion using organotypic brain slice culture. *Cancer Res* **58**, 2935-2940 (1998).

8 Yoon, J. J., Nicholson, L. F., Feng, S. X., Vis, J. C. & Green, C. R. A novel method of organotypic brain slice culture using connexin-specific antisense oligodeoxynucleotides to improve neuronal survival. *Brain Res* **1353**, 194-203, doi:10.1016/j.brainres.2010.07.005 (2010).

9 Chadwick, E. J. *et al.* A Brain Tumor/Organotypic Slice Co-culture System for Studying Tumor Microenvironment and Targeted Drug Therapies. *J Vis Exp*, e53304, doi:10.3791/53304 (2015).

10 Ren, B. *et al.* Invasion and anti-invasion research of glioma cells in an improved model of organotypic brain slice culture. *Tumori* **101**, 390-397, doi:10.5301/tj.5000321 (2015).

11 Brana, C., Biggs, T. E., Mann, D. A. & Sundstrom, L. E. A macrophage hippocampal slice co-culture system: application to the study of HIV-induced brain damage. *J Neurosci Methods* **90**, 7-11 (1999).

12 Clapp-Lilly, K. L. *et al.* Melatonin acts as antioxidant and pro-oxidant in an organotypic slice culture model of Alzheimer's disease. *Neuroreport* **12**, 1277-1280 (2001).

13 Croft, C. L., Kurbatskaya, K., Hanger, D. P. & Noble, W. Inhibition of glycogen synthase kinase-3 by BTA-EG4 reduces tau abnormalities in an organotypic brain slice culture model of Alzheimer's disease. *Sci Rep* **7**, 7434, doi:10.1038/s41598-017-07906-1 (2017).

14 Holmes, C., Jones, S. A. & Greenfield, S. A. The influence of target and non-target brain regions on the development of mid-brain dopaminergic neurons in organotypic slice culture. *Brain Res Dev Brain Res* **88**, 212-219 (1995).

15 Kotake, Y., Ohta, S., Kanazawa, I. & Sakurai, M. Neurotoxicity of an endogenous brain amine, 1-benzyl-1,2,3,4-tetrahydroisoquinoline, in organotypic slice co-culture of mesencephalon and striatum. *Neuroscience* **117**, 63-70 (2003).

16 Tanvig, M. *et al.* A brain slice culture model for studies of endogenous and exogenous precursor cell migration in the rostral migratory stream. *Brain Res* **1295**, 1-12, doi:10.1016/j.brainres.2009.07.075 (2009).

17 Ullrich, C. & Humpel, C. Rotenone induces cell death of cholinergic neurons in an organotypic co-culture brain slice model. *Neurochem Res* **34**, 2147-2153, doi:10.1007/s11064-009-0014-9 (2009).

18 Bywood, P. T. & Johnson, S. M. Differential vulnerabilities of substantia nigra catecholamine neurons to excitatory amino acid-induced degeneration in rat midbrain slices. *Exp Neurol* **162**, 180-188, doi:10.1006/exnr.2000.7310 (2000).

19 Daviaud, N. *et al.* Modeling nigrostriatal degeneration in organotypic cultures, a new ex vivo model of Parkinson's disease. *Neuroscience* **256**, 10-22, doi:10.1016/j.neuroscience.2013.10.021 (2014).

20 Suuronen, T., Huuskonen, J., Pihlaja, R., Kyrylenko, S. & Salminen, A. Regulation of microglial inflammatory response by histone deacetylase inhibitors. *J Neurochem* **87**, 407-416 (2003).

21 Sygnecka, K. *et al.* Mesenchymal stem cells support neuronal fiber growth in an organotypic brain slice co-culture model. *Stem Cells Dev* **24**, 824-835, doi:10.1089/scd.2014.0262 (2015).

22 Herms, J. W., Tings, T., Dunker, S. & Kretzschmar, H. A. Prion protein affects Ca2+-activated K+ currents in cerebellar purkinje cells. *Neurobiol Dis* **8**, 324-330, doi:10.1006/nbdi.2000.0369 (2001).

23 Falsig, J. & Aguzzi, A. The prion organotypic slice culture assay--POSCA. *Nat Protoc* **3**, 555-562, doi:10.1038/nprot.2008.13 (2008).

24 Falsig, J. *et al.* A versatile prion replication assay in organotypic brain slices. *Nat Neurosci* **11**, 109-117, doi:10.1038/nn2028 (2008).

25 Kondru, N. *et al.* Integrated Organotypic Slice Cultures and RT-QuIC (OSCAR) Assay: Implications for Translational Discovery in Protein Misfolding Diseases. *Sci Rep* **7**, 43155, doi:10.1038/srep43155 (2017).

26 Campeau, J. L., Wu, G., Bell, J. R., Rasmussen, J. & Sim, V. L. Early increase and late decrease of purkinje cell dendritic spine density in prion-infected organotypic mouse cerebellar cultures. *PLoS One* **8**, e81776, doi:10.1371/journal.pone.0081776 (2013).

27 Wolf, H. *et al.* Deposition pattern and subcellular distribution of disease-associated prion protein in cerebellar organotypic slice cultures infected with scrapie. *Front Neurosci* **9**, 410, doi:10.3389/fnins.2015.00410 (2015).

28 Ostergaard, K., Finsen, B. & Zimmer, J. Organotypic slice cultures of the rat striatum: an immunocytochemical, histochemical and in situ hybridization study of somatostatin, neuropeptide Y, nicotinamide adenine dinucleotide phosphate-diaphorase, and enkephalin. *Exp Brain Res* **103**, 70-84 (1995).

29 Ayers, J. I. *et al.* Distinct conformers of transmissible misfolded SOD1 distinguish human SOD1-FALS from other forms of familial and sporadic ALS. *Acta Neuropathol* **132**, 827-840, doi:10.1007/s00401-016-1623-4 (2016).

30 Adamchik, Y., Frantseva, M. V., Weisspapir, M., Carlen, P. L. & Perez Velazquez, J. L. Methods to induce primary and secondary traumatic damage in organotypic hippocampal slice cultures. *Brain Res Brain Res Protoc* **5**, 153-158 (2000).

31 Morrison, B., 3rd, Eberwine, J. H., Meaney, D. F. & McIntosh, T. K. Traumatic injury induces differential expression of cell death genes in organotypic brain slice cultures determined by complementary DNA array hybridization. *Neuroscience* **96**, 131-139 (2000).

32 Morrison, B., 3rd, Cater, H. L., Benham, C. D. & Sundstrom, L. E. An in vitro model of traumatic brain injury utilising two-dimensional stretch of organotypic hippocampal slice cultures. *J Neurosci Methods* **150**, 192-201, doi:10.1016/j.jneumeth.2005.06.014 (2006).

33 Gordon, R. *et al.* A simple magnetic separation method for high-yield isolation of pure primary microglia. *J Neurosci Methods* **194**, 287-296, doi:10.1016/j.jneumeth.2010.11.001 (2011).

34 Dossi, E., Blauwblomme, T., Nabbout, R., Huberfeld, G. & Rouach, N. Multi-electrode Array Recordings of Human Epileptic Postoperative Cortical Tissue. *J Vis Exp*, e51870, doi:doi:10.3791/51870 (2014).

35 Fuentealba, P., Timofeev, I., Bazhenov, M., Sejnowski, T. J. & Steriade, M. Membrane Bistability in Thalamic Reticular Neurons During Spindle Oscillations. *Journal of neurophysiology* **93**, 294-304, doi:10.1152/jn.00552.2004 (2005).

36 Anderson, M. E., Postupna, N. & Ruffo, M. Effects of High-Frequency Stimulation in the Internal Globus Pallidus on the Activity of Thalamic Neurons in the Awake Monkey. *Journal of neurophysiology* **89**, 1150-1160, doi:10.1152/jn.00475.2002 (2003).

Fig 1

1a

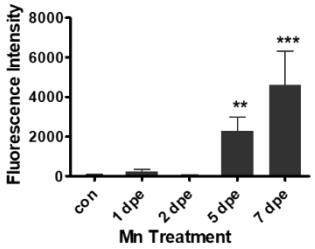

1b

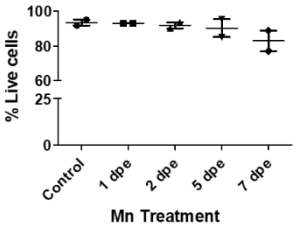

1c

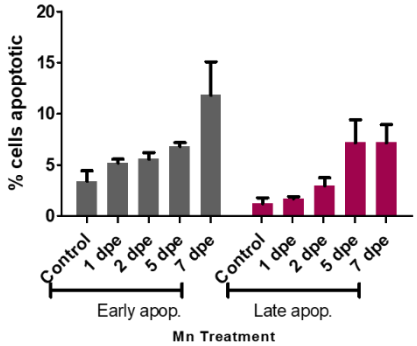

1d

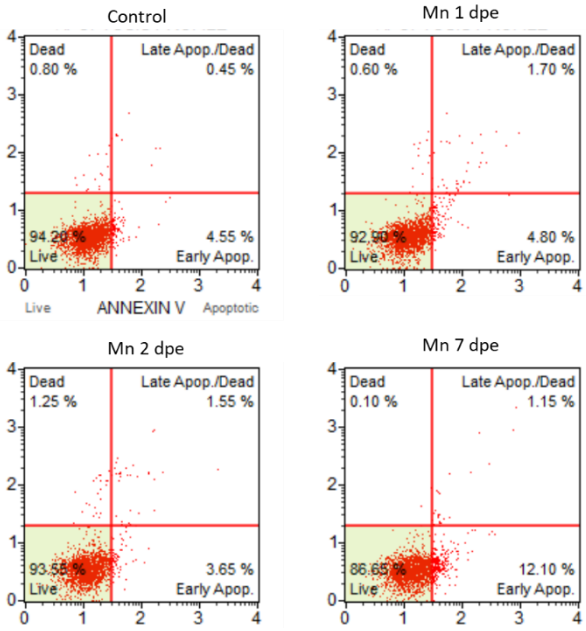

Figure 1: Characterization of organotypic slice cultures for the viability

(A) Characterization of toxicant-induced cell death in slice cultures. Dose-response relationship between increasing exposure time to Manganese (Mn) and cellular propidium iodide (PI) uptake, measured for the cerebellar slice cultures. There significant increase in PI uptake is noticed after 5 and 7 days post exposure (dpe) (B) Quantification of % live cells as evident by AnnexinV staining and flowcytometry of slice cultures after exposure. Viability drops down at 5 dpe and continues to decrease upon 7 dpe. (C) Data are shown as means ± SEM, as compared with control cerebellar slices ($n = 3$). and $*p < 0.05$ using one-way ANOVA with Bonferroni posttest. (D) Flowcytometric representation of Annexin V staining demonstrating the percentage of cells at the various stage of Apoptosis (early or late stage) and viability.

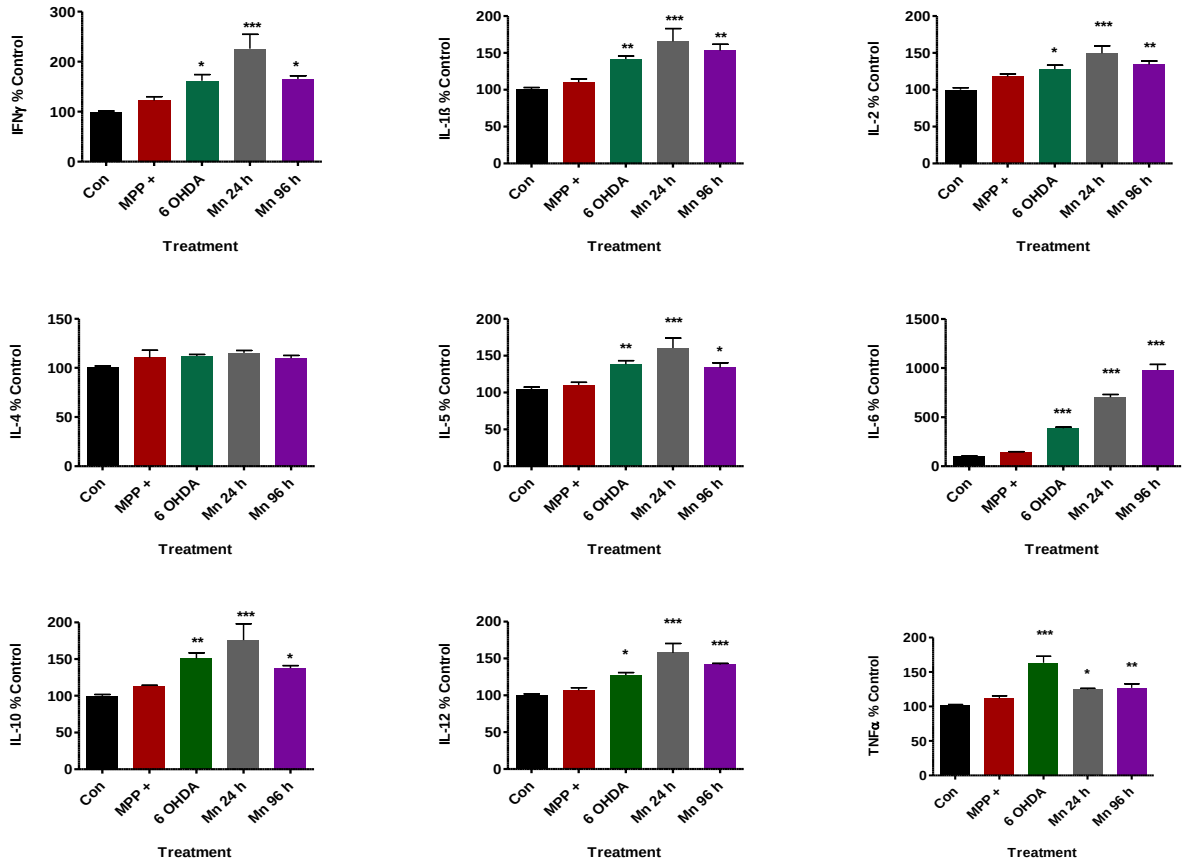

Figure 2: Secretion of cytokines in response neurotoxicants, MPP+, 6 OHDA, Mn (both short-term and long-term exposure):

Cytokines production in the organotypic slice cultures were quantified from spent culture media using Multiplex bead-based Luminex assay system. A panel of known proinflammatory cytokines was used. A significant increase in the pro-inflammatory cytokines was observed in Mn and 6-OHDA treatments (IFNγ, IL-1β, IL-2, IL-5, IL-10, IL-12) and A dose-dependent increase of TNFα and IL-6 was observed. Data represented as the group mean ± SEM (n = 3–4 per group). Asterisks (***p<0.001, **p<0.01 and *p<0.05) indicate significant differences between neurotoxicant treated groups vs control slices.

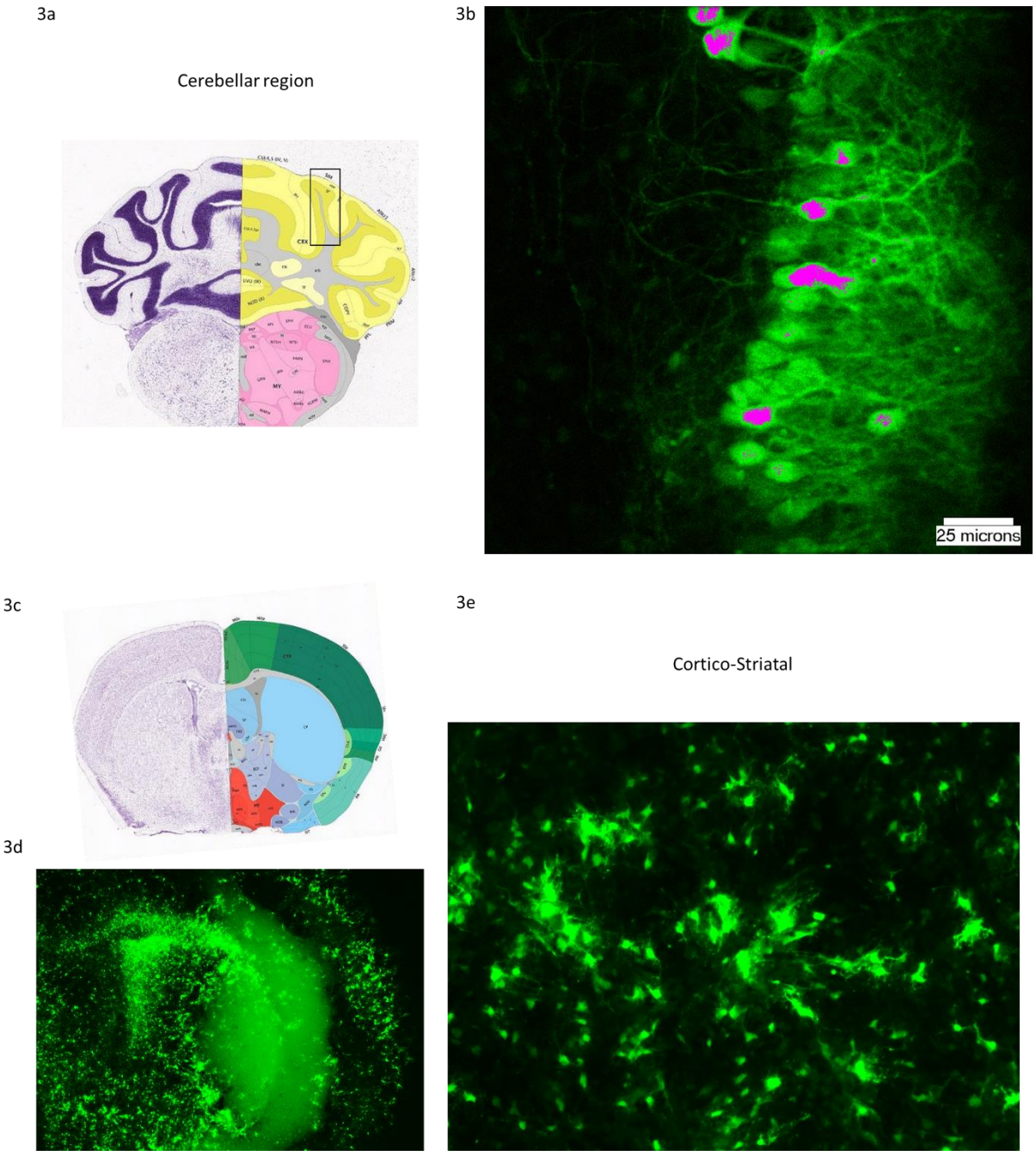

Figure 3: AAV virus-mediated transduction for targeted gene delivery

(A) Cerebellar slices- a schematic showing cerebellar folia with granular layer and Purkinje border highlighted in the rectangular box. (Source; mouse brain atlas). AAV virus with a GFP reporter was diluted in opti-MEM and Slices were transduced by placing a microdrop (2uL/

cerebellar slice and 4 ul for corticostriatal slices on the dorsal surface of the slice. The liquid spreads across the surface owing to surface tension. The media was replaced with fresh culture media and slices were incubated for 5-7 days for live imaging. (B) Bright GFP expression in a Purkinje layer with a dense network of dendrites is shown. Scale bar 25µ. (C) Cortico-striatal slices used to transduce with GFP-AAV - schematic showing a slice with cortical and striatal region distinction cultured similarly as described for a cerebellar slice. The highlighted portion (right half) was imaged. (D) The low magnification demonstrates efficient transduction in cortico-striatal slice cultures as evident by the GFP expression (green) is observed throughout the slice culture. (E) A higher magnification (20x) image was shown to specify neuronal structures in the striatal region that are efficiently transduced.

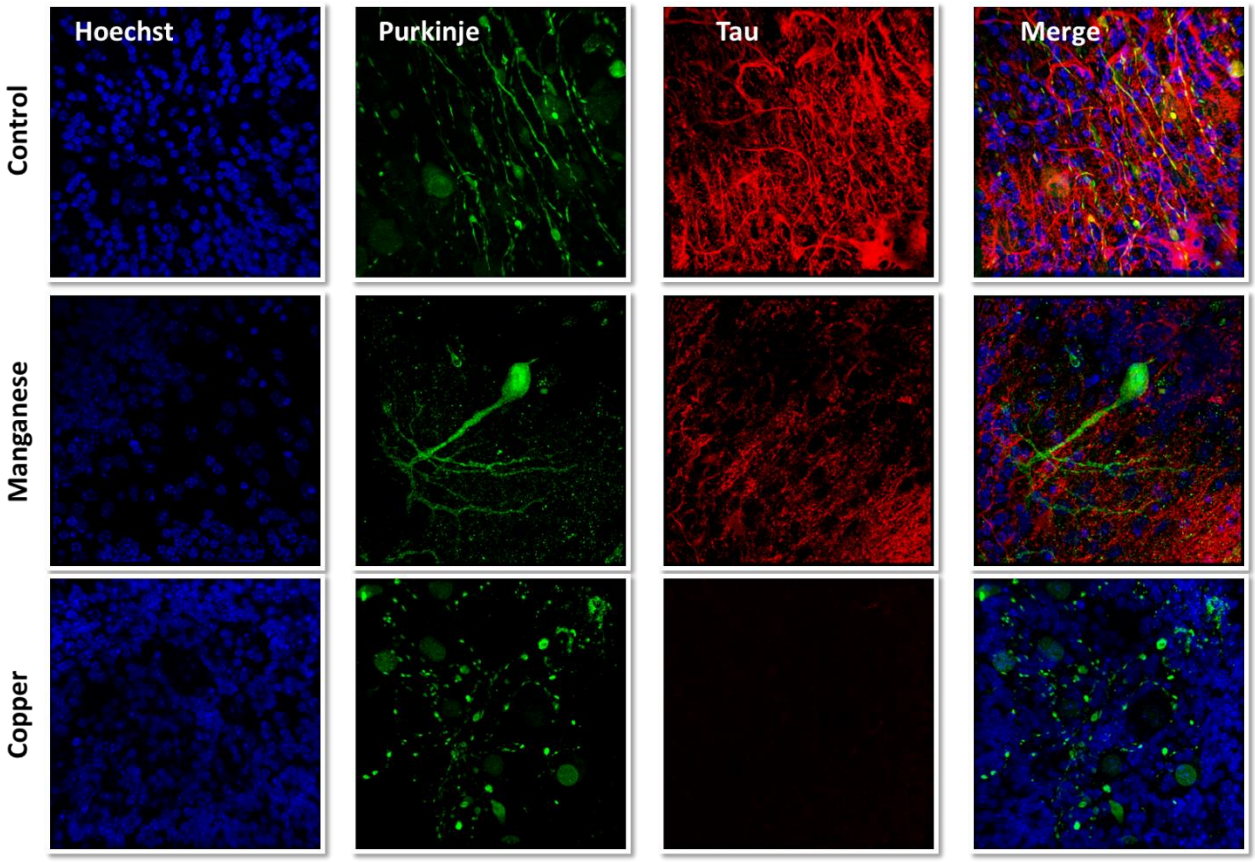

Figure 4: Immunohistochemistry of organotypic slice cultures

Slices were exposed to neurotoxicants, Manganese (Mn) 100 uM and Copper (Cu) 1uM for 24 hours, fixed and immunostaining and confocal imaging was performed. Slices were stained with Hoechst for nuclear staining, Calbindin for Purkinje neurites and Tau protein to stain for microtubule integrity. As evident by Red stain, partial loss of Tau protein was noticed in slices treated with Mn and profound loss of Tau immunoreactivity was evident with Cu treatment. Cu also caused major loss of dendrites as seen in the green channel.

Fig 5

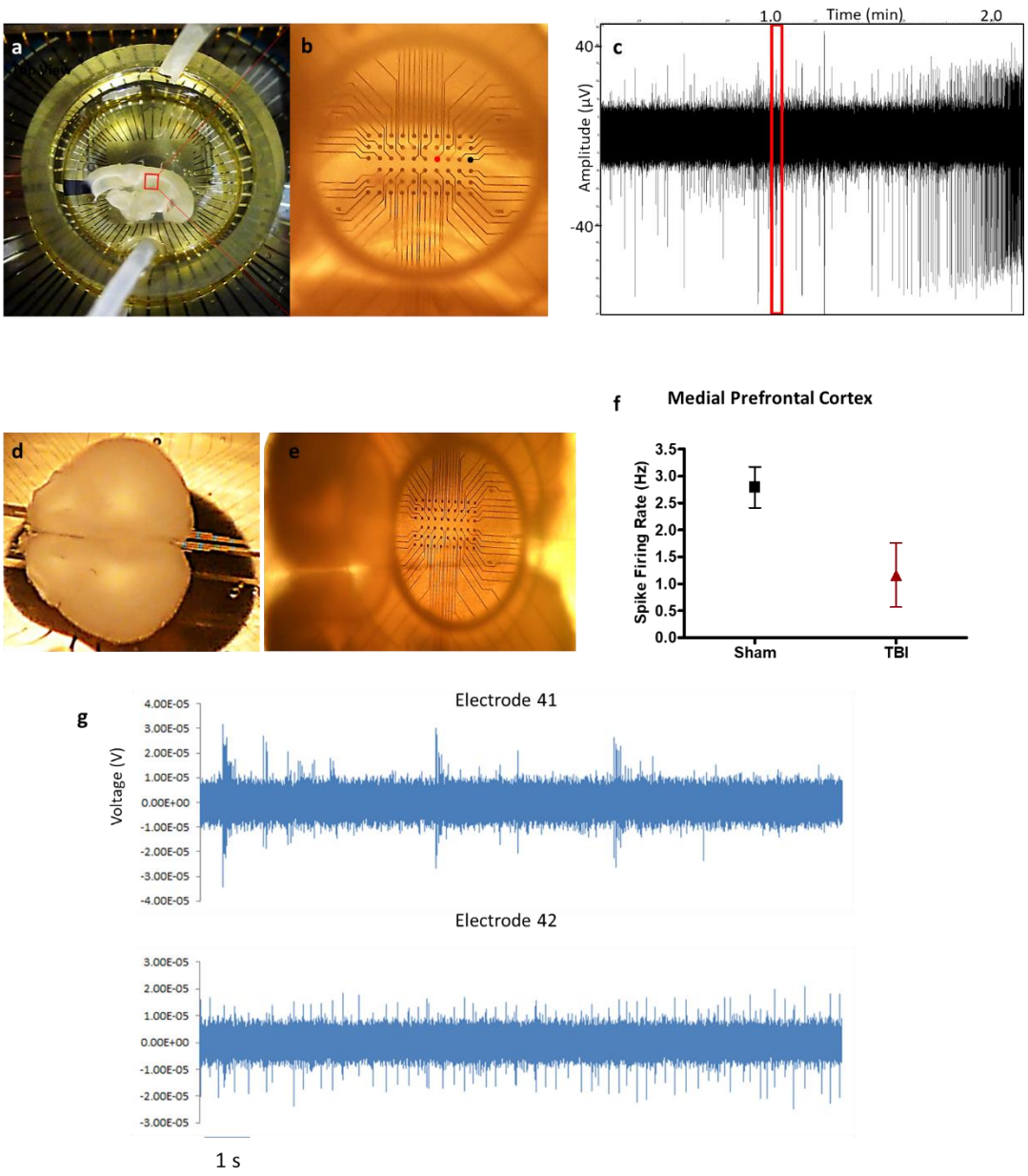

Figure 5: Extracellular recording of the mouse brain slices

(A) Using a micro-electrode array of 60 (10 x 6), 30-µm electrodes spaced 100 µm apart. Slice was positioned over electrodes to record from CA1 region. High-frequency stimulation (C, red rectangle) was delivered through one electrode (B, black dot) in the proximity of Schaffer collaterals after recording a 1-min baseline, which triggered a wave of activity across CA1 as

exemplified by one representative unit (B, red dot). The same MEA was also used to compare the spontaneous spike rate of the medial prefrontal cortex (D-E) in mice whose right side of the head was facing compressed gas blast-induced shock wave. (F) Spike firing rate was quantified and plotted to compare Sham and TBI. The spike firing rate was lower in the animals exposed to blat when compared to controls. (G) Spontaneous activity patterns in organotypic slice cultures. Cerebellar slices were cultured for 21 days on a membrane insert and transferred to a multi-electrode chamber, to observe the spontaneous firing activity from the slice. Firing patterns from two electrodes (#41 and 42) were presented for comparison.

CHAPTER III: INTEGRATED ORGANOTYPIC SLICE CULTURES AND RT-QUIC (OSCAR) ASSAY: IMPLICATIONS FOR TRANSLATIONAL DISCOVERY IN PROTEIN MISFOLDING DISEASES

Naveen Kondru[1], Sireesha Manne[1], Justin Greenlee[2], Heather WestGreenlee[1], Vellareddy Anantharam[1], Patrick Halbur[3], Arthi Kanthasamy[1], Anumantha Kanthasamy[1*]

1. Department of Biomedical Sciences, College of Veterinary Medicine, Iowa State University, Ames, IA 50011, USA.
2. Virus and Prion Research Unit, National Animal Disease Center, Agricultural Research Service, United States Department of Agriculture, Ames, Ia, USA.
3. Veterinary Diagnostic and Production Animal Medicine, College of Veterinary Medicine, Iowa State University, Ames, IA.

* Corresponding author: akanthas@iastate.edu

Abstract

Protein misfolding is a key pathological event in neurodegenerative diseases like prion diseases, synucleinopathies, and tauopathies that are collectively termed protein misfolding disorders. Prions are a prototypic model to study protein aggregation biology and therapeutic development. Attempts to develop anti-prion therapeutics have been impeded by the lack of screening models that faithfully replicate prion diseases and the lack of rapid, sensitive biological screening systems. Therefore, a sensitive model encompassing prion replication and neurotoxicity would be indispensable to the pursuit of intervention strategies. We present an ultra-sensitive screening system coupled to an *ex vivo* prion organotypic slice culture model to rapidly advance rationale-based high-throughput therapeutic strategies. This hybrid

Organotypic **S**lice **C**ulture **A**ssay coupled with **R**T-QuIC (OSCAR) permits sensitive, specific and quantitative detection of prions from an infectious slice culture model in a reduced time scale. We demonstrate that the anti-prion activity of test compounds can be readily resolved based on the power and kinetics of seeding activity in the OSCAR screening platform and that the prions generated in slice cultures are biologically active. Collectively, our results imply that OSCAR is a robust model of prion diseases that offers a promising platform for understanding prion proteinopathies and advancing anti-prion therapeutics.

Introduction

Prion diseases, or transmissible spongiform encephalopathies (TSEs), are chronic, lethal neurodegenerative disorders affecting both humans and animals, and a cure for these devastating brain diseases has yet to be identified. The common prion diseases of animals include bovine spongiform encephalopathy (BSE) in cattle, scrapie in sheep and goats, and chronic wasting disease (CWD) in cervids. Major human prion diseases are Creutzfeldt-Jakob disease (CJD), Gerstmann–Sträussler–Scheinker syndrome (GSS) and fatal familial insomnia (FFI)(Prusiner, 1998). Prion diseases are often hard to detect due to their long incubation periods as well as clinical presentations that overlap with other neurological disorders. In addition to classical prion diseases, emerging evidence suggests that other protein misfolding disorders (PMDs) like Parkinson's disease (PD) and multiple systems atrophy (MSA) have misfolded α-synuclein proteins that are experimentally transmissible(Bernis *et al.*, 2015; Prusiner *et al.*, 2015) and other PMDs like Alzheimer's, FTDs, Huntington's *etc.*, also have unique amyloids capable of prion-like aggregation and experimental propagation(Jaunmuktane *et al.*, 2015)·(Brundin *et al.*, 2010). The normal cellular form of prion protein (PrP^C) is richly distributed throughout the nervous system and lymphoid tissues. PrP^C is known to play a role

in oxidative stress, apoptotic signaling, and other biological functions including interactions with metals(Anantharam *et al.*, 2008; Choi *et al.*, 2010; Harischandra *et al.*, 2014). Although the mechanisms underlying the templated conversion of PrP^{C} into its misfolded isomer, PrP^{Sc} (*Sc* denotes scrapie; also referred to as PrP^{res} for protease-resistance), remains poorly understood, PrP^{Sc} associated with TSEs are oligomers, fibrils or aggregates that contribute to neuropathological processes(Solomon *et al.*, 2010).

Detection of misfolded prion in a high-throughput format is necessary for rational therapeutic designs(Karapetyan *et al.*, 2013; Mallucci *et al.*, 2005). Currently, mouse bioassays serve as a predominant method of assessment for prion infectivity. However, these models present several obstacles to developing high-throughput assays. For instance, incubation times can extend to excessively long durations and clinical signs are typically not manifested until the terminal stages of infection(Harischandra, et al., 2014). Furthermore, working with infected animals raises concerns about occupational safety and the increasing costs associated with care and management of laboratory animals(Falsig, et al., 2008b; Martin *et al.*, 2011). Efforts to establish *in vitro* models of prion diseases met with limited success due to the inability of cells to maintain persistent infectivity over time. Results generated from one or two cell models has not readily translated to other preclinical and clinical models of different prion strains of animals and human prions(Giles *et al.*, 2016; Giles *et al.*, 2015). Notably, *in vitro* cell models fail to recapitulate the neuropathological features of prion disease. Thus, a suitable alternative to chronically infected animal models could help advance prion research via rapid validation of therapeutic options.

The recently developed real-time quaking-induced conversion (RT-QuIC) assay for prions is gaining wide acceptance for its ultra-sensitive detection of prions from a variety of

samples and has the potential to become a rapid and sensitive prion detection assay. This robust and reproducible, high-throughput prion detection assay can be adapted for both animal and human prion diseases, and it is compatible with a wide range of prion strains, allowing strain discrimination(Cramm *et al.*, 2015a; Cramm *et al.*, 2015b; Henderson *et al.*, 2013; McGuire *et al.*, 2012; Orru *et al.*, 2014). Notably, RT-QuIC was shown to detect prions with a million-fold greater sensitivity than had been achieved via the immunoblot detection of scrapie prions(Shi *et al.*, 2013) and also with superior specificity, stability, and reproducibility(Cramm, et al., 2015a) for diagnostic screening. This assay also was adopted for quantitative and qualitative estimation of prion titers in samples using endpoint titration of prions defined by seeding activity(Henderson *et al.*, 2015; Wilham *et al.*, 2010). Thus, we postulated that integrating the **O**rganotypic **S**lice **C**ulture **A**ssay with **R**T-QuIC (OSCAR) would prove to be the ideal platform for fulfilling a long-standing gap in the translational arena of prion diseases. Herein, we show that OSCAR is a rapid, specific and quantitative method that can be readily adopted for translational research and for understanding the molecular mechanisms underlying protein misfolding disease processes.

Results

***Ex vivo* cerebellar slice cultures exhibit hallmarks of prion infection and neurodegeneration.**

To test whether organotypic slices accumulate PK-resistant prions, the molecular hallmark of prion infection in culture, we prepared organotypic cerebellar slices from 9- to 12-day-old WT pups and maintained them as *ex vivo* slice cultures after infecting them with RML scrapie. After five weeks in culture, slices were harvested, and lysates were digested with Proteinase-K for the electrophoresis profile. The slices infected with RML scrapie show an obvious pattern

of di-, mono-, and non-glycosylated PK-resistant bands (PrP^{Sc}) on immunoblots with bands shifted lower than those from uninfected slices (Fig. 1A). This illustrates that the resulting PK-resistant fragments have lower molecular weight when compared to the undigested protein. This banding profile is consistent with the terminally sick brain homogenates of mice (Fig. 1B), indicating the amplification of prions in culture. Next, we evaluated slice viability using propidium iodide (PI) staining. The slice cultures showed significantly less PI-positive staining during the culture periods (<5%) tested up to 9 weeks when compared to a positive control (Sup Fig. 1). However, after 42 days in culture, slices infected and cultured with RML scrapie showed a significant increase in PI-positive cells, concentrated in the granular cell layer when compared to slices treated with NBH (Fig. 1C-D). Next, we examined the neuronal density of $NeuN^+$ cells in the slices. RML scrapie-infected slices displayed a significant neuronal loss in the granular layer of the cerebellum when compared to non-infectious brain homogenate (NBH)-treated slices after 42 dpi (Fig. 1E and 1F). Furthermore, we characterized pro-apoptotic markers in RML-infected cerebellar slice cultures. A pro-apoptotic signaling cascade in RML scrapie-infected slices was evidenced by caspase-3 activation and a significant increase in the novel protein kinase C isoform δ (PKCδ) and its cleaved fragment (Fig. 1G, full blots in Sup Fig. 5). Taken together, these results suggest that slices cultures serve as a representative model for prion replication and neurotoxicity in a culture environment while preserving the complex connections.

RT-QuIC assay provides a versatile platform for sensitive detection of prions in *ex vivo* slice cultures.

Following the establishment of mouse organotypic cerebellar slices cultured *ex vivo,* we evaluated the RT-QuIC assay for testing nanogram to femtogram quantities of misfolded

prions in slice cultures. Only the scrapie-infected slices and terminally sick mouse brain homogenates (positive control) were amplified consistently across multiple experiments (n>20), whereas NBH-treated slices or healthy mouse brain homogenates did not show seeded amplification over the course of 72 h of reaction (Fig. 2A). To confirm that this amplification occurred due to specific amplification of prions in slice cultures, we used transgenic prion mouse models to probe for prion seeding activity. We prepared slices from *Tga*20 pups that overexpress prion protein ~10 fold and/or $PrP^{-/-}$ pups with no PrP expression, infected them with either RML scrapie or mock normal brain homogenates and cultured them for 28 days before subjecting their samples to RT-QuIC assay. Only slices from *Tga*20 mice showed seeding activity (Fig. 2B), whereas NBH-treated slices or $PrP^{-/-}$ slices infected with RML scrapie did not show any seeding activity at any of the dilutions tested (Fig. 2C). The amplification kinetics from *Tga*20 slices were seed dose-dependent as demonstrated by the time required to reach threshold and maximum average fluorescence readings (Fig. 2 D-E). Collectively, these findings suggest that true prion replication in organotypic slice cultures and the seeding activity is governed by the expression of cellular prion protein.

Kinetics of prion augmentation in slice cultures.

We systematically characterized the seeding activity of misfolded prion following various dose and incubation times. The seeding activity in RT-QuIC assays of samples from organotypic slice cultures became progressively stronger as culture duration increased. Cultured slices infected with NBH or RML scrapie were harvested at multiple time points ranging from 1 to 42 dpi for RT-QuIC assay. Seeding activity was detected as early as 7 dpi (Fig. 3A). However, seeding activity increased substantially in RT-QuIC assays only after 14 dpi when PrP^{Sc} started to buildup. This is comparable with previous reports demonstrating PK-resistant material

deposition only after two weeks in RML scrapie-infected slices(Aguzzi *et al.*, 2012; Campeau, et al., 2013; Falsig, et al., 2008b). Nonetheless, slices harvested at 21 dpi showed even stronger seeding activity, and the seeding activity in RT-QuIC assays did not peak until around 42 dpi (Fig. 3A). The slices harvested immediately after starting the culture (1 dpi) did not show discernible seeding activity, suggesting that the seeding activity did not begin from the inoculum used to infect slices. This time-dependent intensification of seeding activity in RT-QuIC assays (Fig. 3A) clearly suggests the amplification of prions in the e*x vivo* cultured slices. To further determine the seeding efficiency of prions replicated in slice cultures at various time points after infection and culture (7, 14, 21, 35 and 42 dpi), we tested serial 10-fold dilutions of slice culture homogenates (5 ng - 50 fg) (Fig. 3B-F). Slices cultured for 42 and 35 dpi (Fig. 3B and 3C respectively) showed greater seeding activity and had both shorter lag phases and stronger relative fluorescence (RFU) values compared to 21 dpi (Fig. 3D). The seeding activity of prion-infected slice cultures at 14 dpi and 7 dpi was not as robust as at 21 dpi (Fig. 3E-F). Additionally, the slices harvested after 7 and 14 dpi took longer to reach thresholds and the average RFU was reduced 2- to 3-fold with respect to 35-dpi cultures. Furthermore, the ThT fluorescence intensity generated from the RT-QuIC seeds was correlated (r=0.855) with time spent in culture (Sup Fig. 2). These results clearly demonstrate that RT-QuIC captures both amount and rate of prion infection in the *ex vivo* brain culture model.

Quantitative estimation of infectious titers from prion-infected slice cultures based on seeding activity in RT-QuIC assay.

Quantifying the seeding activity of slice cultures would help us to understand the kinetics and dynamics of prion aggregation, which would further aid in developing disease-modifying therapies or improving existing compounds. To quantify prion seeding activity, we tested

endpoint seeding dilutions of slice cultures as described in previous reports using the Spearman-Kärber approach for calculating the 50% infective dose (ID_{50}) in virus titration experiments(Wilham, et al., 2010). We performed RT-QuIC assays on log dilutions (10 fold) of slice homogenates (as shown in figures 3B-F) to determine the seeding activity of different dilutions at each endpoint. The Spearman-Kärber method relies on the number of wells turning positive at each dilution point to determine arbitrary SD_{50} (seeding activity, 50%) values, representing the dilutions of slice homogenate at which 50% of the wells became positive in RT-QuIC reactions. Over a wide range of time points, SD_{50s} showed a clear pattern of increasing values with increasing culture durations for homogenates from both WT and *Tga*20 organotypic brain slices (Fig. 4A). In addition, the seeding activity for *Tga*20 slice cultures was always higher at all time points tested possibly due to a higher quantity of seeding prions. The average values (SD_{50}/g) obtained by this method peaked at 35 dpi for both WT slices (6.32×10^9) and for *Tga*20 slice cultures (3.64×10^{10}). Serial dilutions of RML scrapie brain homogenates that were used to calculate SD_{50} achieved a similar seeding activity per gram(Wilham, et al., 2010), suggesting that the prion titers accumulated in cultured slices were comparable to *in vivo* conditions (Sup Fig. 3). Next, we explored the threshold-crossing time (Tt), which is the time taken for the fluorescence intensity to cross the threshold, as a measure of seeding power of sample tested, as described in previously published reports, to indirectly calculate the amyloid formation rate (AFR), which is the inverse of Tt (in hours). To gain a comprehensive understanding of prion replication, we used this model to study the kinetics of amyloid formation based on Tt derived from different seeding dilutions (50 fg- 5 ng) of slice culture homogenates at 7-42 dpi (Fig. 4B). Not only was AFR correlated with the dpi of cultured slices, but also higher seed concentrations were directly proportional to AFR. The

lower dilutions that never turned positive in an RT-QuIC assay were predictably considered to have zero AFR. In addition to this, PrP immunoreactivity was examined semi-quantitatively using dot blot assay (as described in methods). Homogenates prepared from slices cultured 1-42 dpi (0.5 µg and 5 µg) were transferred to nitrocellulose membrane and treated with the prion antibody POM1 to visualize PrP immunoreactivity. The signal intensity of PrP, normalized to the loading control β-actin, increased in a time-dependent fashion (Fig. 4C-D). These results demonstrate that the OSCAR platform enables us to quantify the progressive increase in amyloid formation rate and determine the prion titers from cultured slices. This is advantageous when determining the effect of pharmacological modulators on amyloid formation as an indirect marker of disease progression under *in vivo* conditions.

Effect of anti-prion compounds on seeding activity in RT-QuIC assay of prion-infected slice cultures.

To extend the applicability of our OSCAR model, we applied some already known anti-prion compounds (astemizole, Congo red and quinacrine) to slice cultures to test their ability to influence the seeding activity of prions from RML scrapie-infected slice cultures. First, we measured the seeding ability of slice cultures tested in two independent experiments with high reproducibility (Sup Fig. 4). Next, we compared the seeding ability of the slice cultures treated with compounds at various dilutions (Fig. 5A-C). Both Congo red and quinacrine, but not astemizole, showed reduced seeding activity at 5 ng (Fig. 5A) and 0.5 ng (Fig. 5B) seed concentrations. Similarly, when a dilution of 50 pg was used as seed, both Congo red and quinacrine, but not astemizole, completely inhibited seeding activity (Fig. 5C). Quantification of percent positive wells tested for each treatment shows a clear pattern of seeding activity for the compounds (Fig. 5D). Anti-prion activity was clearly manifested by a reduction in AFR

(Fig. 5E) for two of the compounds. Together, these results suggest a true reduction in seeding activity upon addition of the anti-prion compounds Congo red and quinacrine. Furthermore, these results highlight the utility of the OSCAR model for determining the preclinical efficacy of compounds that are effective against prion seeding activity.

Serial propagation of prions and utility of non-cerebellar brain slice cultures to confirm prion infectivity.

To assess the infectivity of the prions generated in slice cultures, we tested the ability of homogenates prepared from RML scrapie-infected brain slice cultures (P1) to infect cerebellar slices (P2) that had been cultured uninfected in parallel with the infected batch. Slices were cultured for 30 days with log dilutions ranging from (0.5 ng – 50 fg) before testing via RT-QuIC assay. Both P1 and P2 slice cultures demonstrated comparable seeding activity at the dilutions shown (Fig. 6A). The use of cerebellar regions alone required a large number of pups for the study. Thus, to expand the number of slice cultures prepared from a given number of pups, we next tested whether other brain regions can be adopted for an organotypic culture model of prion infection. We infected and cultured non-cerebellar brain sections (corticostriatal slices) for 42 days before testing for seeding activity. To our surprise, these slices demonstrated excellent seeding congruent with the seeding activity obtained from cerebellar slice cultures (Fig. 6B), with seeded amplification occurring in a concentration-dependent manner across a high dynamic range (50 ng to 50 fg) of seed concentrations. Together, these results show the versatility and utility of OSCAR as a rapid bioassay for prion diseases.

Discussion

We developed a versatile system for quantifying prion seeding activity known as OSCAR that uses the RT-QuIC assay to detect prions in organotypic slice cultures. It is imperative to develop such integrated models for drug development against chronic neurodegenerative conditions like prions and related protein misfolding diseases that can remain asymptomatic for several years. The OSCAR model could advance the utility of the prion organotypic slice culture assay (POSCA) for this infectious disease (Falsig, et al., 2008a) However, the caveat for both approaches is that they require adequate technical expertise to prepare and long-term maintenance of the cultures. Nevertheless, we demonstrate the efficacy of prion-infected .organotypic slice cultures coupled with seeding assays like RT-QuIC to quantify seeding prions generated in the cultures in a more cost-effective way. Among various *in vitro* culture models, the major advantage of organotypic slice culture is that it preserves morphologic architecture and physiologic interconnectivity between various cell types like neurons and neuroglia. In addition, chronic animal distress associated with *in vivo* prion infection would be circumvented while permitting continuous access to brain tissue for experimental procedures throughout the course of infection. The slices were maintained in culture for several weeks with good viability. Slices infected with scrapie accumulated PK-resistant prions in culture while demonstrating neurotoxicity (Fig. 1A-G) consistent with previous reports(Aguzzi, et al., 2012; Campeau, et al., 2013; Falsig, et al., 2008b; Harischandra, et al., 2014). We found the RT-QuIC assay amplifies prions from minute quantities of protein extracted from slice cultures in both a seed concentration- and culture time-dependent manner (Fig. 3A-E) and can be quantified based on seeding characteristics (Fig. 4A-B). Importantly, prion knockout slices infected with RML scrapie did not show any seeding activity across a wide range of seed

dilutions (Fig. 2C). The level of seeding activity sustained in our WT slice cultures increased with the duration of the culture period and is comparable to published values(Falsig, et al., 2008b). Indeed, the seeding activity that we detected as early as 7 dpi was unexpected, suggesting that the OSCAR model is more sensitive than the prevailing methods of detecting infectivity such as Western blots. This rapid amplification is relevant to recent discoveries that the replication of PrP^{Sc} was observed in vasculature very early after microinjecting prions into mouse brains(Chesebro *et al.*, 2015). Furthermore, the inoculum used was not detectable in 1-dpi slices possibly due to 1) the washing steps involved in culturing the slices and 2) the homogenized slices were further diluted before testing.

We demonstrated the sensitivity of detecting prions with our OSCAR model of *ex vivo* prion infection and characterized the kinetics of prion amplification at various time points in culture (Fig. 3). The time course of prion amplification in slice cultures is analogous to the kinetic pattern of *in vivo* bioassays as PK-resistant prions rapidly reach maximum titer towards the terminal stage of infection, which becomes accelerated in the *ex vivo* preparation. Based on multiple endpoint titrations for RML scrapie prions in slice culture, seeding activity shows a progressive and time-dependent amplification. The SD_{50} values derived from the Spearman-Kärber method serve as reliable estimates of prion titers from infected slice cultures, indicating that after 35 dpi prion titers are comparable to terminally infected brains(Wilham, et al., 2010). Detection of prions by traditional methods depends on various factors such as PK concentration, incubation time, and choice of antibody that could create discrepancies in the results obtained between samples. Since RT-QuIC seeding activity is not solely based on protease resistance(Vascellari *et al.*, 2012), the OSCAR model could likely be adapted to other seeding prion species. However, it remains to be tested whether this model can be used

successfully for other strains and species. As the detection strategies continue to improve for a broad range of prions and strains(Orru *et al.*, 2015a; Orru *et al.*, 2015b; Orrú *et al.*, 2015; Vascellari, et al., 2012), we believe that our OSCAR model could be useful in developing procedures that disrupt prion propagation. Distinct kinetic traces from an OSCAR assay could help us to understand more characteristics of prion strains. Finally, using recombinant bank vole (*Myodes glareolus*) PrP as a substrate, a variety of prion strains could be rapidly amplified in an RT-QuIC assay to better understand mechanisms and alternative therapeutic approaches(Orrú, et al., 2015).

This OSCAR model offers a high-throughput platform for extending the utility of integrated prion models to support rapid drug discovery efforts and antemortem diagnostics. As proof-of-principle, we used the OSCAR system to test a small panel of anti-prion compounds that were characterized in animal models of prion diseases(Caughey *et al.*, 1994; Demaimay *et al.*, 2000; Karapetyan, et al., 2013). First, we used the OSCAR model to test Congo red for its potent curing effects in prion-infected cells(Caughey, et al., 1994). The mechanism of action of this polyanion is its high-binding affinity to amyloids that hyperstabilizes the aggregates,(Caspi *et al.*, 1998) thus interfering with the formation of toxic oligomers. Although Congo red is neuroprotective in prion-infected cerebellar slices(Falsig *et al.*, 2012), a paradoxical increase in PK-resistant prions as shown with stronger immunoblotted band intensity, has also been reported(Aguzzi, et al., 2012). Interestingly, using the OSCAR model, we found it reduced the seeding activity in RML scrapie-infected slice cultures (Fig. 5A-E), thereby supporting a neuroprotective role. Next, we evaluated the small molecule quinacrine. Previous reports suggest treatment with quinacrine results in a strong anti-prion effect in cell culture and it is routinely used in screening libraries(Doh-Ura *et al.*, 2000; Nguyen *et al.*, 2011).

However, efforts to translate this compound in human trials failed(Geschwind *et al.*, 2013). As further studies determined that quinacrine exhibits poor CNS bioavailability, attempts were made to increase its bioavailability using mice deficient in the P-glycoprotein multi-drug resistance (MDR) transporter. However, this study showed only a transient reduction in both PrP^{Sc} and its conformational stability while encouraging drug resistance(Ghaemmaghami *et al.*, 2009). In slice cultures, chronic treatment with quinacrine showed an intermediate decrease in seeding activity when compared to control slices infected with RML scrapie (Fig. 5A-E). This anti-prion effect in cultured slices could be attributed to direct interaction of the drug with the brain slices and early initiation of the treatment regimen. Lastly, we tested astemizole, as it was reported to show anti-prion activity in cell culture models and to marginally extend the survival of prion-infected mice (~4%) despite having no effect on reducing PrP^{C} levels or PrP mRNA levels in PK1 cells(Karapetyan, et al., 2013). Astemizole crosses the blood-brain barrier and reduced the PK-resistant PrP in the persistently infected cell culture model. Although its exact anti-prion mechanism of action is not known, it has been shown to stimulate autophagy. Conversely, in our study, astemizole did not show any reduction in seeding activity and the seeding kinetics remained similar to that of cerebellar slice cultures infected with RML scrapie (Fig. 5A-E). This difference may be attributed to a highly sensitive readout using RT-QuIC assay to detect seeding prions. These initial studies demonstrate the translational potential for the OSCAR model to further test novel compounds and may have utility in future treatment paradigms involving a wide range of prion strains.

Emerging evidence suggests that protein misfolding plays a key role in major neurodegenerative disorders that have prion-like templated conversion of proteins, including Parkinson's, Alzheimer's, frontotemporal dementias, multiple sclerosis, multiple system

atrophy and Huntington's diseases. No drugs are available for halting or reversing prion diseases or any other prion-like neurodegenerative disorders(Berry *et al.*, 2013). Additionally, drugs demonstrating excellent effects in cell culture and *in vivo* models of scrapie paradoxically fails to show any effect on CJD prions(Giles, et al., 2015) or in clinical trials(Geschwind, et al., 2013). Also, mouse cell lines persistently infected with prions were developed to establish *in vitro* models of scrapie(Butler *et al.*, 1988; Caughey *et al.*, 1989) for drug testing but compounds identified through a high-throughput drug screening(Klohn *et al.*, 2003) had little or no effect against CJD prions. Furthermore, no cell culture model can propagate the CJD prions in culture. We speculate that the OSCAR model could be extended to CJD human prions, thereby filling a critical void because currently available models are medically intractable against CJD prions.

In summary, we have established a highly sensitive integrated technique for the efficient detection of seeding prions (Fig. 7). Our OSCAR model using an organotypic slice culture assay coupled to the RT-QuIC assay may be able to accelerate translational research by testing a large number of anti-prion compounds, including small molecules, against prion infection. Furthermore, the OSCAR model could act as a prototype for other protein misfolding disorders (PMDs)that obey principles of aggregation and propagation. In addition, using OSCAR with transgenic mouse models and genetic manipulation may provide mechanistic insights into the cell-to-cell transmission of prion-like aggregates and the progression of neurodegenerative diseases.

Materials and Methods

Reagents: Dithiothreitol (DTT), ethylenediaminetetraacetic acid (EDTA), 45% glucose, kynurenic acid, proteinase K (PK), sodium chloride (NaCl), Tris-HCl and Triton X-100 were

purchased from Sigma (St. Louis, MO). Millicell 6-well plate inserts (Biopore filter CM, PTFE inserts 30-mm diameter and 0.4-um pore size, Cat No. PICM03050), E. *coli* Rosetta DE3 competent cells, Overnight Express™ Autoinduction System 1 (Cat. no. 71300-3) and BugBuster® Master Mix (Cat No. 71456-4) were purchased from Millipore (Billerica, MA). Bradford protein assay kit was purchased from Bio-Rad Laboratories (Hercules, CA). Horse serum, penicillin, streptomycin, and low-melting agarose (Cat No. 15517-022) were purchased from Invitrogen (Carlsbad, CA). Anti-PrP mouse monoclonal antibodies POM1 and 6D11 were purchased from Prionatis AG (Schlieren, Switzerland) and Covance, respectively. Anti-β-actin antibody was purchased from Sigma-Aldrich. Alexa Fluor 680 conjugated goat anti-mouse IgG was purchased from Invitrogen. Goat anti-rabbit IR800 conjugated IgG was purchased from Rockland Immunochemicals (Gilbertsville, PA), propidium iodide (PI) from Molecular Probes (Cat No. P3566), and Halt™ Protease and Phosphatase Inhibitor Cocktail (Cat No. 78440) from Life Technologies. All other reagents were obtained from Thermo Fisher Scientific (Waltham, MA) unless otherwise mentioned.

Slice cultures and infections: All the experiments involving animals followed protocols approved by Iowa State University's Institutional Animal Care and Use Committee (IACUC) and by the IACUC at the National Animal Disease Center (protocol number: 3985). Organotypic cerebellar slices for prion assay were prepared as previously described(Falsig, et al., 2008a; Harischandra, et al., 2014). In brief, brain slices were prepared from 9- to 12-day-old mouse pups from either wild-type (WT, C57BL/6) or transgenic prion-overexpressing or knockout mice (*Tga*20 or prnp $^{-/-}$, respectively) using a microtome (Compresstome™ VF-300, Precisionary Instruments). After dissecting the cerebellum from the whole brain, the cerebellum was oriented in the sagittal plane in the Compresstome's specimen tube, which had

been prefilled with 2% low-melting-point agarose. The agar was quickly solidified by clasping the specimen tube with a chilling block, and then the specimen tube was inserted into the slicing reservoir filled with freshly prepared, ice-cold Gey's balanced salt solution supplemented with the excitotoxic antagonist, kynurenic acid (GBSSK). To prepare GBSS, we added the following in solution in the following order from 10x stocks to obtain the final concentrations per liter 8 g NaCl, 0.37 g KCl, 0.12 g Na_2HPO_4, 0.22 g $CaCl_2 \cdot 2H_2O$, 0.09 g KH_2PO_4, 0.07 g $MgSO_4 \cdot 7H_2O$, 0.210 g $MgCl_2 \cdot 6H_2O$, 0.227 g $NaHCO_3$. The compression lip located in the cutting chamber helps stabilize the brain specimen while obtaining 350-µm thick slices with the blade set at a medium vibration speed. Slices were collected at the specimen tube's outlet and transferred to another plate with fresh prefilled GBSSK. Slices were exposed on ice for 1 h to either normal brain homogenate (NBH) or Rocky Mountain Labs scrapie brain homogenate (RML scrapie) with 100 µg/ml of brain homogenate total mass diluted in 1 mL GBSSK. Later, the slices were washed twice in 6 ml ice-cold GBSSK, transferred to Millicell 6-well plate inserts (7-9 slices per insert) and were incubated in a humidified atmosphere of 5% CO_2 at 37^{o}C. Culture media was exchanged every other day with fresh media until the infected slices reached their pre-determined endpoints. For scaling up the experiments, we cultured a pool of ~50 slices per 6-well plate, all from a single litter with the same genotype, and exposed to either NBH or RML scrapie brain homogenates. These slices were triple-washed in ice-cold GBSSK before plating and maintained as described above. Slice cultures were harvested at various endpoints by washing twice in 2 ml of ice-cold PBS. Lysates were prepared in 1X PBS by three freeze-thaw cycles and subjected to five 30-sec sonication pulses each in a cup sonicator. When testing anti-prion compounds, the compounds were added from stock solutions (1000X) to slices at 15 days post-inoculation (dpi), and then fresh media with

compounds were exchanged every other day and harvested at 31 dpi as described above.

Viability assays: Viability assays in organotypic cerebellar slices were performed as previously described with modifications(Herrmann *et al.*, 2015a). Dead cells were selectively stained by incubating the slices in culture media with 5 µg/ml of PI, which is a nontoxic dye that selectively binds to nuclei of dead cells and can be used to image live slice cultures. After 30 min, the PI media was replaced with fresh culture media before imaging at 2X and 10X magnification through a Nikon TE2000-U microscope (Tokyo, Japan) coupled to a SPOT digital camera (Diagnostic Instruments, Sterling Heights, MI). All the images were processed using ImageJ with constant threshold settings.

Immunoblotting: Western blot analyses and limited proteolysis were performed as described previously(Aguzzi, et al., 2012; Anantharam *et al.*, 2004; Choi, et al., 2010; Harischandra, et al., 2014) with minor modifications. Briefly, slices were washed twice in ice-cold PBS and harvested with PBS, unless otherwise specified. After protein assay, equal homogenates were separated on 15% SDS-PAGE gels. After electrophoresis, proteins were transferred to a nitrocellulose membrane. The membranes were blocked using LI-COR blocking buffer (LBB) for 1 h and probed overnight with the primary antibody followed by secondary antibody treatments using Alexa Fluor-conjugated anti-mouse or anti-rabbit antibodies. An Odyssey IR Imaging (LI-COR) system was used to capture and analyze images using Odyssey 2.0 software, and densitometry was done using ImageJ. For Limited proteolysis, we used partial Proteinase-K digestion methods as previously described with a few modifications(Falsig, et al., 2008b; Harischandra, et al., 2014; Martin, et al., 2011). At 35 dpi, RML scrapie- and NBH-inoculated slice cultures were homogenized in lysis buffer (1% Triton-X in PBS). After determining the protein concentration by Bradford assay, 200 µg of protein was digested with

25 µg/ml of Proteinase-K and incubated for 30 min at 37°C. When brain homogenates were used, 100 µg of protein was digested with 25 µg/ml of Proteinase-K for 45 min at 37°C. The digestion reactions were stopped by boiling the samples for 10 min. Samples were stored at -80°C until Western blots analyses were performed as described above. Membranes were incubated with the POM1 PrP antibody (1:5000, Prionatis AG) overnight at 4°C and then triple-washed with 0.1% Tween in 1X PBS. Secondary antibody incubations and washings were done as described above and fluorescence was captured using the Odyssey IR Imaging system.

Dot Blot: Immunoreactivity of PrP from the prion-infected slice cultures was determined by dot-blot using Bio-Dot® Microfiltration System using manufacturer's protocol as described previously(Sun *et al.*, 2005). In brief, the slice cultures were harvested at pre-determined endpoints, and homogenates were prepared and protein concentrations were determined as described above. Next, 0.5 µg and 5 µg of homogenates were mixed with 200 µl of tris-buffered saline (1X TBS) with 0.1% Tween-20 and allowed to adsorb onto a nitrocellulose membrane for 1 h. The membrane was washed twice with 200 µl of 1X TBS using a gentle vacuum, blocked with 1X LBB for 30 min, incubated with mouse monoclonal POM1 anti-PrP antibody (dilution 1:5000) for 1 h at RT, and triple-washed with 1X TBS. Membranes were then incubated with Alexa Fluor 680-conjugated anti-mouse secondary antibody in LBB (1: 10,000) for 30 min followed by 3 washes in 1X TBS. As the loading control, membranes were probed with β-actin. Antibody-bound proteins were detected with the Odyssey IR Imaging system and densitometry was performed with ImageJ.

Immunohistochemistry: After fixing the slices, antibody treatments were performed as described previously(Aguzzi, et al., 2012; Harischandra, et al., 2014; Sonati *et al.*, 2013) with minor changes. Slices were rinsed twice with 1 ml of 1X PBS and fixed in 4%

paraformaldehyde (PFA) overnight at 4ºC. Before antibody treatments, slices were washed twice with PBS for 15 min each at RT to remove residual PFA and incubated with blocking buffer (0.05% TritonX-100 and 3% goat serum in 1X PBS) for 1 h at RT. Primary antibodies were diluted (1:1000 unless otherwise stated) in blocking buffer and incubated for 2-3 days at 4ºC. The following antibodies were used: anti-NeuN (clone A60, Alexa Fluor®488 conjugated (Millipore, Cat No. MAB377X) and anti-PKCδ (Santa Cruz). After incubation with primary antibody, membranes were washed 4 times with PBS for 15 min each and incubated 1 h in the dark with the following secondary antibodies diluted 1:1500 in blocking buffer: Alexa Fluor 555-conjugated anti-mouse secondary antibody or Alexa Fluor 488-conjugated anti-rabbit secondary antibody. The cell-permeable dye Hoechst 44432 (1:5000 for 3 min in PBS) was used to stain all nuclei. The culture membranes were removed from the inserts and mounted directly on microscope slides, with membranes facing the slide, using Fluoromount mounting medium (Sigma) and imaged with a SPOT color digital camera attached to a Nikon TE2000-U microscope.

Recombinant prion protein expression and purification: Recombinant prion protein (rPrP) was expressed and purified using previously reported protocols(Atarashi *et al.*, 2008; Orru *et al.*, 2011; Vascellari, et al., 2012; West Greenlee *et al.*; Wilham, et al., 2010). Briefly, N-histidine-tagged prion protein-encoding plasmids of Syrian golden hamster residues for full length (23-231) or truncated (90-231) in pET vector (EMD biosciences) were transformed into *E. coli* Rosetta^{TM}2 (DE3) cells and grown under kanamycin and chloramphenicol as selection media. Protein expression was induced using Overnight Express™ Autoinduction System 1 (EMD Millipore Cat No. 71300) with log phase mini-cultures as a starter culture. The bacteria were pelleted and lysed with BugBuster® Master Mix to isolate inclusion bodies. Inclusion

bodies were dissolved in 8 M of the denaturing agent guanidine hydrochloride (GuHCl) for 1 h and mixed to pre-equilibrated nickel-nitrilotriacetic acid (Ni-NTA Superflow) resin (Qiagen Cat No. 30430) for 50 min on a rotating mixer. The beads were packed in an Akta #XK26 column and purified using Ni-NTA-immobilized metal affinity chromatography (IMAC) on a Bio-Rad DuoFlow system operating at 4^{o}C. On-column refolding was performed using gradient reduction of GuHCl. Pure rPrP was eluted from the IMAC using competitive imidazole binding with a linear gradient. Chilled dialysis buffer was added to the peak eluted fractions, filtered and dialyzed against three changes of chilled dialysis buffer (10 mM $NaPO_4$, pH 5.8). Following dialysis, the rPrP was filtered, aliquoted and stored at -80^{o}C. Protein concentration was determined by absorbance at 280 nm over the extinction coefficient before freezing as well as after thawing and filtering through 100-kD cutoff filters. Protein concentration was typically in the range of 0.5-0.7 mg/ml after dialysis. Each batch was routinely tested for quality and activity using Western blot and RT-QuIC assay respectively before using on test samples.

RT-QuIC assay: RT-QuIC assay was performed using standard protocols from published reports(Haley *et al.*, 2015; Orru, et al., 2015b; Wilham, et al., 2010) with slight modifications. Unless otherwise specified, the reaction mixtures consisted of final concentrations of 350 mM NaCl, 0.1 mM EDTA, 10 μM ThT, 0.1 mg/ml rPrP and 0.0025% SDS in 1X PBS. First, 5 μL samples from either brain homogenates or slice culture homogenates were diluted in a total reaction mixture of 100 μL. Plates subjected to RT-QuIC assay were sealed with Nalgene Nunc plate sealer. Plates were incubated at 42^{o}C in either a CLARIOstar (BMG) or Cytation3 (BioTek) plate reader with alternating 1-min shake (double orbital) and rest cycles. All samples were run at least in triplicates, and samples were judged to be positive as reported previously

when samples were run in quadruplicates(Orru, et al., 2015b; West Greenlee, et al.). Whenever triplicates were run, we averaged their fluorescence readings, and additionally we selected 10xSD (standard deviation of negative controls) as the criteria for determining the threshold. Bottom plate recordings of ThT fluorescence (450±15 nm excitation and 480±10 nm emission) were taken every 30 min and data analysis was performed as reported previously(Orru, et al., 2014) using MARS version 5.2.R8 or Gen 5 version 2.07.17 software when CLARIOstar (BMG) or Cytation3 (BioTek) were used, respectively, and the data were exported to Microsoft Excel for graphing.

Acknowledgements

This work was supported by NIH grant ES19267 and ES026892, ISU Presidential Wildlife initiative, and the Iowa State University Veterinary Diagnostic Laboratory. The W. Eugene and Linda Lloyd Endowed Chair for AGK is also acknowledged. We thank Dr. Byron Caughey for providing constructs; Drs. Brian Lee, Andrew Hughson, Bradley Groveman, Lynne Raymond and Eric Minikel for technical assistance with rPrP purification. We also thank Gary Zenitsky for assistance in preparing this manuscript and Sarah Mientka for assistance with figures. We thank Kevin Hassall, Stevan Wilson and LAR staff for animal husbandry.

Author Contributions

NK and AGK conceived idea and designed the experiments. NK and SM performed the experiments. JG and HG contributed prnp-/- and *Tga*20 mice and provided helpful recommendations. NK, SM, AK, and AGK performed data analysis and wrote the manuscript. PH and VA assisted in data interpretation and the manuscript preparation. AGK supervised and coordinated the entire study.

Conflicts of interest

A.G.K. and V.A. are shareholders of PK Biosciences Corporation (Ames, IA), which is interested in developing therapeutic strategies for protein misfolding diseases including prion disease. Other authors declare no potential conflicts of interest.

References

1 Prusiner, S. B. Prions. *Proceedings of the National Academy of Sciences of the United States of America* **95**, 13363-13383 (1998).

2 Prusiner, S. B. *et al.* Evidence for α-synuclein prions causing multiple system atrophy in humans with parkinsonism. *Proceedings of the National Academy of Sciences* **112**, E5308-E5317, doi:10.1073/pnas.1514475112 (2015).

3 Bernis, M. E. *et al.* Prion-like propagation of human brain-derived alpha-synuclein in transgenic mice expressing human wild-type alpha-synuclein. *Acta Neuropathol Commun* **3**, 75, doi:10.1186/s40478-015-0254-7 (2015).

4 Jaunmuktane, Z. *et al.* Evidence for human transmission of amyloid-beta pathology and cerebral amyloid angiopathy. *Nature* **525**, 247-250, doi:10.1038/nature15369 (2015).

5 Brundin, P., Melki, R. & Kopito, R. Prion-like transmission of protein aggregates in neurodegenerative diseases. *Nat Rev Mol Cell Biol* **11**, 301-307, doi:10.1038/nrm2873 (2010).

6 Harischandra, D. S. *et al.* Role of proteolytic activation of protein kinase Cdelta in the pathogenesis of prion disease. *Prion* **8**, 143-153 (2014).

7 Choi, C. J. *et al.* Manganese upregulates cellular prion protein and contributes to altered stabilization and proteolysis: relevance to role of metals in pathogenesis of prion disease. *Toxicol Sci* **115**, 535-546, doi:10.1093/toxsci/kfq049 (2010).

8 Anantharam, V. *et al.* Opposing roles of prion protein in oxidative stress- and ER stress-induced apoptotic signaling. *Free Radic Biol Med* **45**, 1530-1541, doi:10.1016/j.freeradbiomed.2008.08.028 (2008).

9 Solomon, I. H., Schepker, J. A. & Harris, D. A. Prion neurotoxicity: insights from prion protein mutants. *Current issues in molecular biology* **12**, 51-61 (2010).

10 Mallucci, G. & Collinge, J. Rational targeting for prion therapeutics. *Nat Rev Neurosci* **6**, 23-34 (2005).

11 Karapetyan, Y. E. *et al.* Unique drug screening approach for prion diseases identifies tacrolimus and astemizole as antiprion agents. *Proc Natl Acad Sci U S A* **110**, 7044-7049, doi:10.1073/pnas.1303510110 (2013).

12 Falsig, J. *et al.* A versatile prion replication assay in organotypic brain slices. *Nat Neurosci* **11**, 109-117, doi:10.1038/nn2028 (2008).

13 Martin, D. P. *et al.* Infectious prion protein alters manganese transport and neurotoxicity in a cell culture model of prion disease. *Neurotoxicology* **32**, 554-562, doi:10.1016/j.neuro.2011.07.008 (2011).

14 Giles, K. *et al.* Optimization of aryl amides that extend survival in prion-infected mice. *J Pharmacol Exp Ther*, doi:10.1124/jpet.116.235556 (2016).

15 Giles, K. *et al.* Different 2-Aminothiazole Therapeutics Produce Distinct Patterns of Scrapie Prion Neuropathology in Mouse Brains. *J Pharmacol Exp Ther* **355**, 2-12, doi:10.1124/jpet.115.224659 (2015).

16 Orru, C. D. *et al.* A test for Creutzfeldt-Jakob disease using nasal brushings. *The New England journal of medicine* **371**, 519-529, doi:10.1056/NEJMoa1315200 (2014).

17 Cramm, M. *et al.* Stability and Reproducibility Underscore Utility of RT-QuIC for Diagnosis of Creutzfeldt-Jakob Disease. *Mol Neurobiol*, 1-9, doi:10.1007/s12035-015-9133-2 (2015).

18 Henderson, D. M. *et al.* Rapid antemortem detection of CWD prions in deer saliva. *PloS one* **8**, e74377, doi:10.1371/journal.pone.0074377 (2013).

19 McGuire, L. I. *et al.* Real time quaking-induced conversion analysis of cerebrospinal fluid in sporadic Creutzfeldt-Jakob disease. *Annals of neurology* **72**, 278-285, doi:10.1002/ana.23589 (2012).

20 Cramm, M. *et al.* Stability and Reproducibility Underscore Utility of RT-QuIC for Diagnosis of Creutzfeldt-Jakob Disease. *Mol Neurobiol*, doi:10.1007/s12035-015-9133-2 (2015).

21 Shi, S., Mitteregger-Kretzschmar, G., Giese, A. & Kretzschmar, H. A. Establishing quantitative real-time quaking-induced conversion (qRT-QuIC) for highly sensitive detection and quantification of PrPSc in prion-infected tissues. *Acta Neuropathol Commun* **1**, 44, doi:10.1186/2051-5960-1-44 (2013).

22 Henderson, D. M. *et al.* Quantitative assessment of prion infectivity in tissues and body fluids by real-time quaking-induced conversion. *The Journal of general virology* **96**, 210-219, doi:10.1099/vir.0.069906-0 (2015).

23 Wilham, J. M. *et al.* Rapid end-point quantitation of prion seeding activity with sensitivity comparable to bioassays. *PLoS Pathog* **6**, e1001217, doi:10.1371/journal.ppat.1001217 (2010).

24 Campeau, J. L., Wu, G., Bell, J. R., Rasmussen, J. & Sim, V. L. Early Increase and Late Decrease of Purkinje Cell Dendritic Spine Density in Prion-Infected Organotypic Mouse Cerebellar Cultures. *PloS one* **8**, e81776, doi:10.1371/journal.pone.0081776 (2013).

25 Aguzzi, A. & Falsig, J. Prion propagation, toxicity and degradation. *Nat Neurosci* **15**, 936-939, doi:10.1038/nn.3120 (2012).

26 Falsig, J. & Aguzzi, A. The prion organotypic slice culture assay--POSCA. *Nat Protoc* **3**, 555-562, doi:10.1038/nprot.2008.13 (2008).

27 Chesebro, B. *et al.* Early Generation of New PrPSc on Blood Vessels after Brain Microinjection of Scrapie in Mice. *mBio* **6**, doi:10.1128/mBio.01419-15 (2015).

28 Vascellari, S. *et al.* Prion seeding activities of mouse scrapie strains with divergent PrPSc protease sensitivities and amyloid plaque content using RT-QuIC and eQuIC. *PloS one* **7**, e48969, doi:10.1371/journal.pone.0048969 (2012).

29 Orrú, C. D. *et al.* Bank Vole Prion Protein As an Apparently Universal Substrate for RT-QuIC-Based Detection and Discrimination of Prion Strains. *PLoS Pathog* **11**, e1004983, doi:10.1371/journal.ppat.1004983 (2015).

30 Orru, C. D. *et al.* Rapid and sensitive RT-QuIC detection of human Creutzfeldt-Jakob disease using cerebrospinal fluid. *mBio* **6**, doi:10.1128/mBio.02451-14 (2015).

31 Orru, C. D. *et al.* Detection and discrimination of classical and atypical L-type bovine spongiform encephalopathy by real-time quaking-induced conversion. *Journal of clinical microbiology* **53**, 1115-1120, doi:10.1128/JCM.02906-14 (2015).

32 Caughey, B., Brown, K., Raymond, G. J., Katzenstein, G. E. & Thresher, W. Binding of the protease-sensitive form of PrP (prion protein) to sulfated glycosaminoglycan and congo red [corrected]. *J Virol* **68**, 2135-2141 (1994).

33 Demaimay, R., Chesebro, B. & Caughey, B. Inhibition of formation of protease-resistant prion protein by Trypan Blue, Sirius Red and other Congo Red analogs. *Arch Virol Suppl*, 277-283 (2000).

34 Caspi, S. *et al.* The anti-prion activity of Congo red. Putative mechanism. *J Biol Chem* **273**, 3484-3489 (1998).

35 Falsig, J. *et al.* Prion pathogenesis is faithfully reproduced in cerebellar organotypic slice cultures. *PLoS Pathog* **8**, e1002985, doi:10.1371/journal.ppat.1002985 (2012).

36 Doh-Ura, K., Iwaki, T. & Caughey, B. Lysosomotropic agents and cysteine protease inhibitors inhibit scrapie-associated prion protein accumulation. *J Virol* **74**, 4894-4897 (2000).

37 Nguyen, T., Sakasegawa, Y., Doh-Ura, K. & Go, M. L. Anti-prion activities and drug-like potential of functionalized quinacrine analogs with basic phenyl residues at the 9-amino position. *Eur J Med Chem* **46**, 2917-2929, doi:10.1016/j.ejmech.2011.04.016 (2011).

38 Geschwind, M. D. *et al.* Quinacrine treatment trial for sporadic Creutzfeldt-Jakob disease. *Neurology* **81**, 2015-2023, doi:10.1212/WNL.0b013e3182a9f3b4 (2013).

39 Ghaemmaghami, S. *et al.* Continuous Quinacrine Treatment Results in the Formation of Drug-Resistant Prions. *PLoS Pathogens* **5**, e1000673, doi:10.1371/journal.ppat.1000673 (2009).

40 Berry, D. B. *et al.* Drug resistance confounding prion therapeutics. *Proc Natl Acad Sci U S A* **110**, E4160-4169, doi:10.1073/pnas.1317164110 (2013).

41 Butler, D. A. *et al.* Scrapie-infected murine neuroblastoma cells produce protease-resistant prion proteins. *J Virol* **62**, 1558-1564 (1988).

42 Caughey, B., Race, R. E., Ernst, D., Buchmeier, M. J. & Chesebro, B. Prion protein biosynthesis in scrapie-infected and uninfected neuroblastoma cells. *J Virol* **63**, 175-181 (1989).

43 Klohn, P. C., Stoltze, L., Flechsig, E., Enari, M. & Weissmann, C. A quantitative, highly sensitive cell-based infectivity assay for mouse scrapie prions. *Proc Natl Acad Sci U S A* **100**, 11666-11671, doi:10.1073/pnas.1834432100 (2003).

44 Herrmann, U. S. *et al.* Prion infections and anti-PrP antibodies trigger converging neurotoxic pathways. *PLoS Pathog* **11**, e1004662, doi:10.1371/journal.ppat.1004662 (2015).

45 Anantharam, V., Kitazawa, M., Latchoumycandane, C., Kanthasamy, A. & Kanthasamy, A. G. Blockade of PKCdelta proteolytic activation by loss of function mutants rescues mesencephalic dopaminergic neurons from methylcyclopentadienyl manganese tricarbonyl (MMT)-induced apoptotic cell death. *Annals of the New York Academy of Sciences* **1035**, 271-289, doi:10.1196/annals.1332.017 (2004).

46 Sun, F., Anantharam, V., Latchoumycandane, C., Kanthasamy, A. & Kanthasamy, A. G. Dieldrin induces ubiquitin-proteasome dysfunction in alpha-synuclein

overexpressing dopaminergic neuronal cells and enhances susceptibility to apoptotic cell death. *The Journal of pharmacology and experimental therapeutics* **315**, 69-79, doi:10.1124/jpet.105.084632 (2005).

47 Sonati, T. *et al.* The toxicity of antiprion antibodies is mediated by the flexible tail of the prion protein. *Nature* **501**, 102-106, doi:10.1038/nature12402 (2013).

48 Orru, C. D. *et al.* Prion disease blood test using immunoprecipitation and improved quaking-induced conversion. *mBio* **2**, e00078-00011, doi:10.1128/mBio.00078-11 (2011).

49 Atarashi, R. *et al.* Simplified ultrasensitive prion detection by recombinant PrP conversion with shaking. *Nature methods* **5**, 211-212, doi:10.1038/nmeth0308-211 (2008).

50 West Greenlee, M. H. *et al.* Temporal Resolution of Misfolded Prion Protein Transport, Accumulation, Glial Activation, and Neuronal Death in the Retinas of Mice Inoculated with Scrapie. *The American Journal of Pathology*, doi:10.1016/j.ajpath.2016.05.018.

51 Haley, N. J. & Hoover, E. A. Chronic wasting disease of cervids: current knowledge and future perspectives. *Annual review of animal biosciences* **3**, 305-325, doi:10.1146/annurev-animal-022114-111001 (2015).

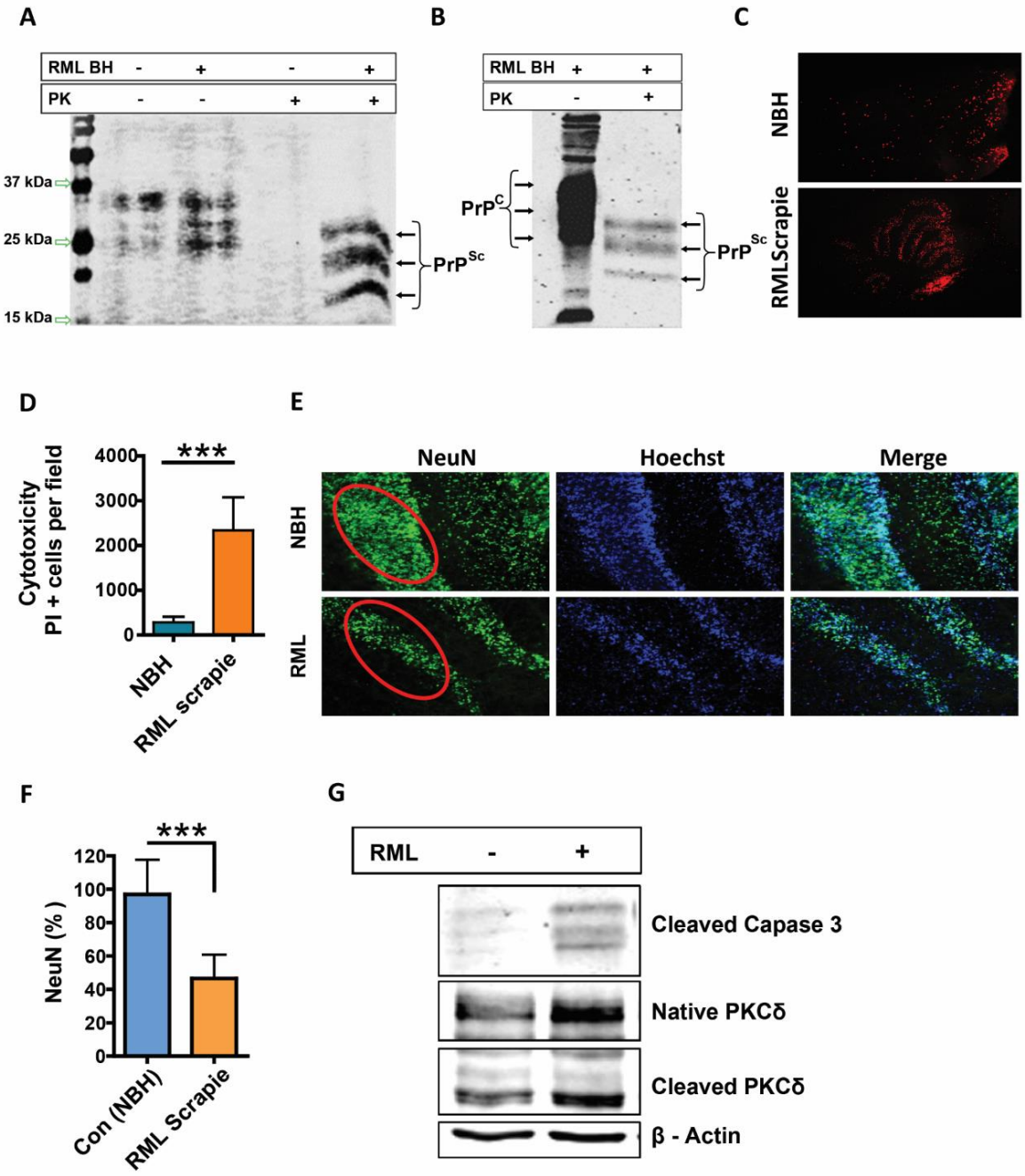

Figure 1. Prion infected organotypic slice cultures exhibit distinct biochemical and neurodegenerative changes. (A) Lysates from organotypic cerebellar slices exposed to NBH or RML scrapie and cultured for 35 days were subjected to PK treatment and then Western

blotted (undigested samples were loaded after diluting 10 fold to prevent over-exposure on blots). RML-treated slices accumulate the PK-resistant PrP signal, but NBH-treated slices did not. (B) An equal amount of brain homogenates from WT mice was infected with RML scrapie either undigested or digested with proteinase K (PK) to detect PK resistance (designated as PrP^{Sc}) on immunoblot. Membranes were probed with anti-PrP (α-helix 1) mouse monoclonal antibody, POM1. The banding profile showed differential migration with banding profiles consistent with PrP^{C} for undigested and PrP^{Sc} for digested samples. (C-D) Propidium Iodide (PI) incorporation to visualize dead cells in 49-dpi slice cultures. Quantification of PI+ cells from NBH or RML scrapie-infected slices using ImageJ. RML scrapie-infected cerebellar slices showed significantly higher cell death when compared to NBH-treated brain slice cultures. Data were analyzed using a two-tailed t-test; n = 6 biological replicates. Data are mean ± SEM (*$p<0.05$, **$p<0.01$, ***$P<0.001$). (E-F) Slices were stained with NeuN to determine any neuronal loss at 42 dpi. RML scrapie-infected slice cultures suffered significant neuronal loss as evidenced by $NeuN^{+}$ area of percent NBH-treated slices. (G) RML scrapie-infected slice cultures show pro-apoptotic signaling as evidenced by both upregulation and proteolytic activation of PKCδ and augmented cleaved caspase 3 when compared to controls. All the samples were normalized to the loading control β-actin.

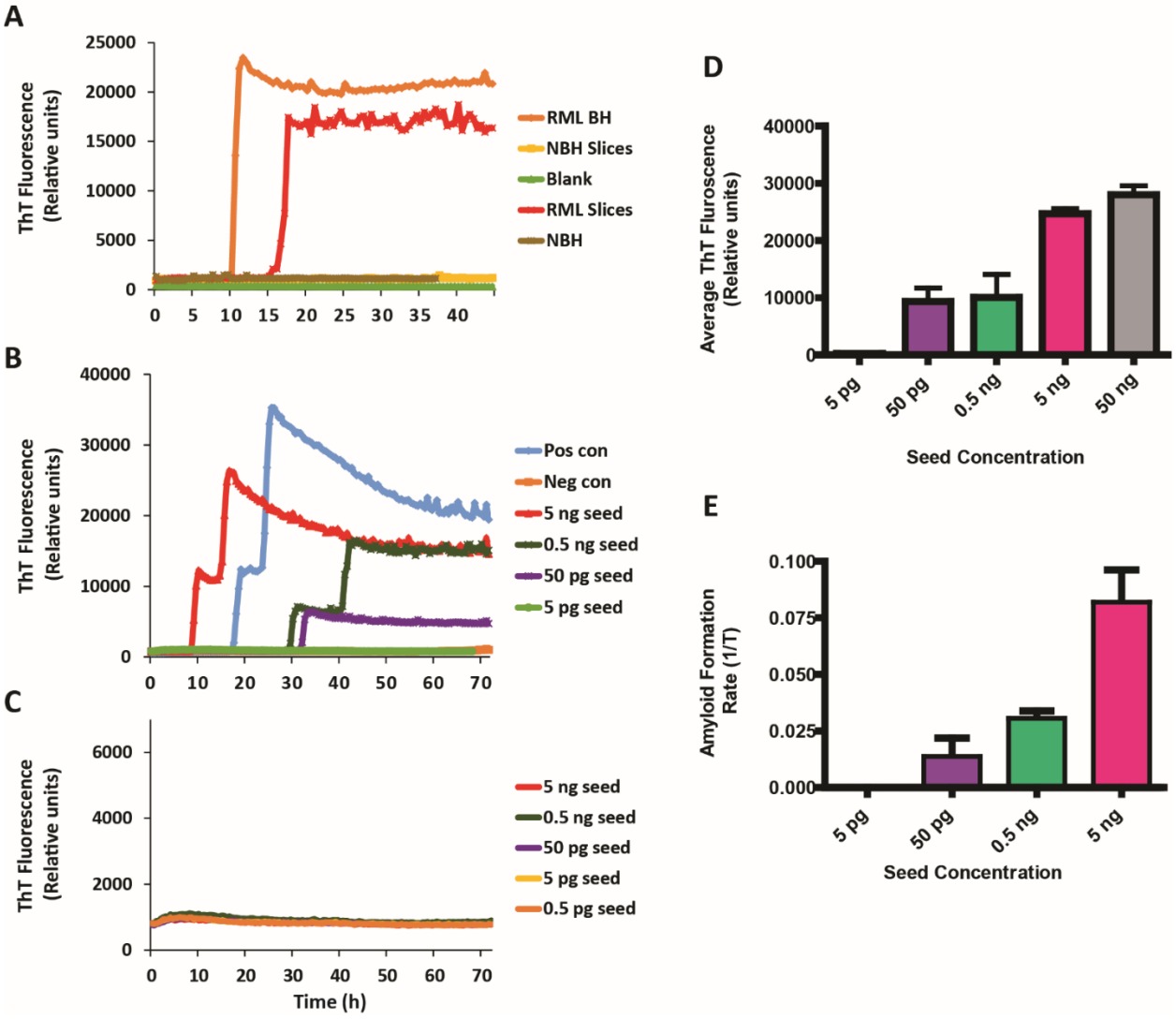

Figure 2. Sensitive and specific prion seeding activity from organotypic slice cultures on RT-QuIC assay. (A) Slice cultures from WT mice (*C57BL/6* background) efficiently seed the RT-QuIC assay. Representative RT-QuIC responses shown for the reactions seeded with 5 ng of WT homogenates from either NBH or RML scrapie-infected slice cultures (21 dpi) or brain homogenates from mock or terminally-infected scrapie mice. Uninfected samples did not show seeding activity and stayed at the baseline throughout the reaction. (B) RT-QuIC traces for a log dilution series from *Tga*20 slice cultures (21 dpi) showing clear concentration-dependent

seeding activity. (Positive control = mock or clinical scrapie mice. Neg Con = mock / normal brain homogenate-infected samples). (C) Cultured slices from *PrP*$^{-/-}$ did not show seeding activity (both NBH and RML scrapie groups) at any seed concentration. Data from the traces shown are average of three replicates for each dilution. (D) Quantification of average ThT fluorescence values obtained over 60-hour period for each seed concentration tested from *Tga*20 slice cultures (21 dpi) shows a seed concentration-dependent increase. (E) Quantification of average amyloid formation rate (AFR) for each seed concentration tested from *Tga*20 slice cultures (21 DPI) showed a seed concentration-dependent increase in AFR.

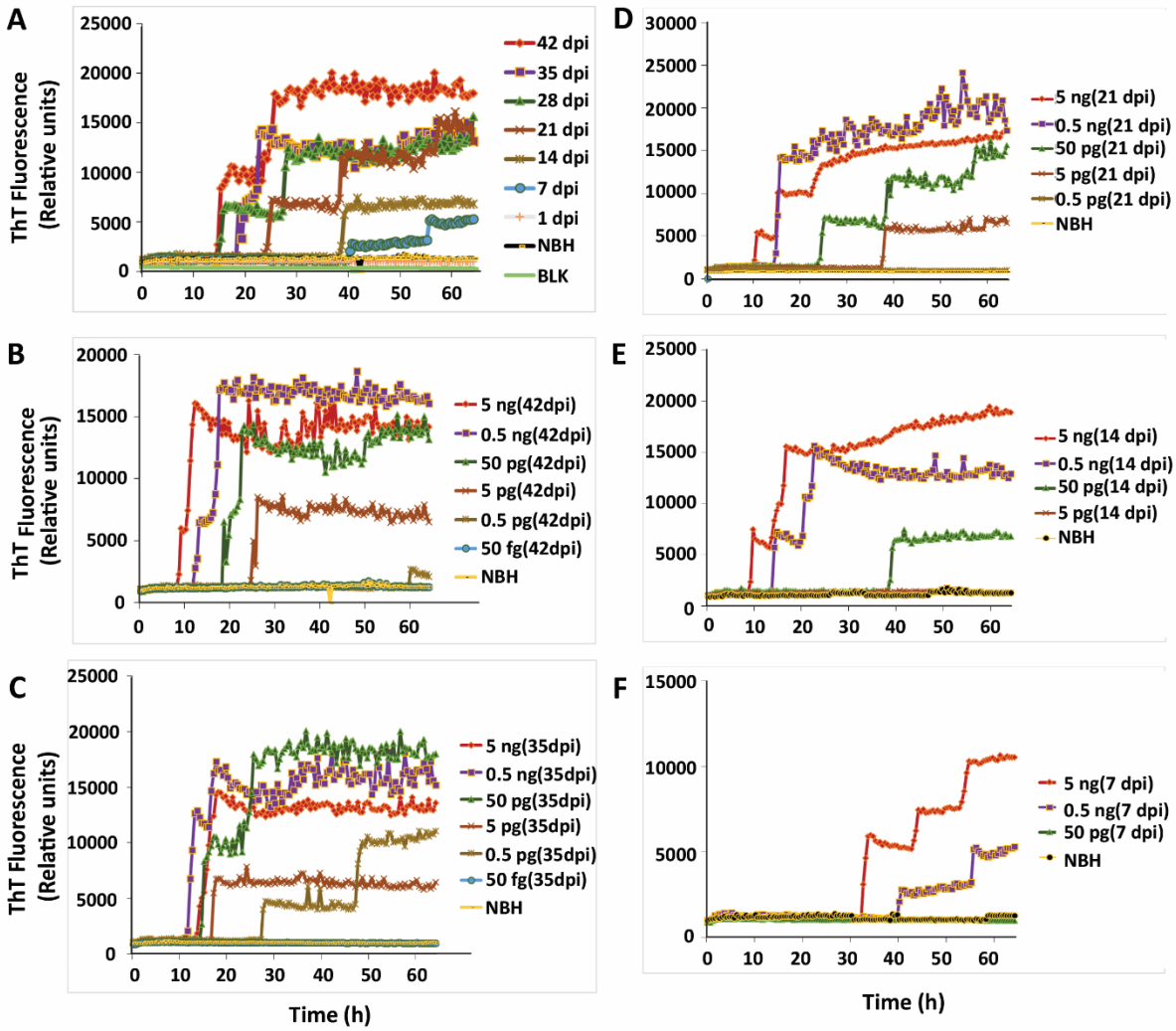

Figure 3. Temporal seeding activity from prion-infected organotypic slice cultures: RT-QuIC end-point dilution analysis in slice cultures from wild-type mice. (A) Organotypic cerebellar slices from WT mice infected with scrapie show time-dependent seeding activity. After RT-QuIC reactions were seeded with 5 ng of homogenate, seeding activity occurred only in RML scrapie-infected slice cultures, not in NBH-exposed slice cultures. NBH-treated slices and RML scrapie-infected slices at 1 dpi did not show seeding activity. The earliest detection of seeding activity was observed at 7 dpi with longer lag phases. Seeding strength showed a clear time-dependent increase as judged by time to reach threshold. Seeding activity was also

noted at 14 dpi, but the traces became stronger from slices at 21 dpi and continued to increase for later time points (28, 35 and 42 dpi). Data from each trace shown are the average ThT fluorescence of three replicate wells. (B-F) Seeded amplification of prions at log dilutions tested from cultured slices. Traces shown are average of 3 replicates from 42 dpi (B), 35 dpi (C), 21 dpi (D), 14 dpi (E) and 7 dpi (F).

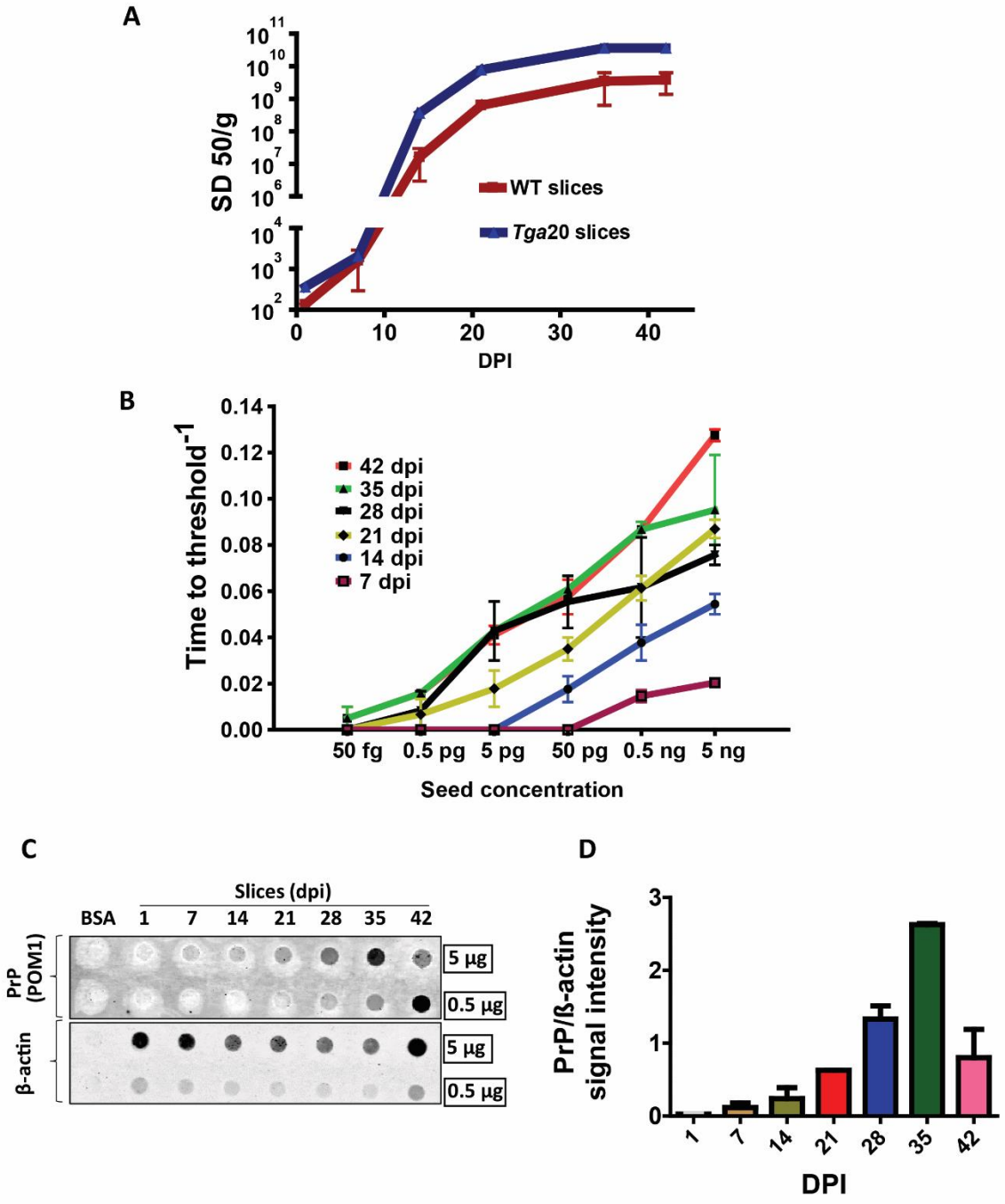

Figure 4. Rapid kinetics and quantitative assessment of prions from slice cultures using RT-QuIC assay. (A) The average SD_{50}/g of protein (Spearman-Kärber estimates) of slice cultures was calculated based on endpoint dilutions from (n=6 technical replicates) and plotted at time points (1, 7, 14, 21, 35 and 42 DPI) for both WT (n=3 biological replicates) and *Tga*20

(n=1 biological replicate) slice cultures. (B) The amyloid formation rate (AFR) was estimated by using the inverse of time in hours at which a trace crosses threshold fluorescence. The linear response AFR for cultured slices was both time- and seed concentration-dependent. (C) Dot-blot showing immunoreactivity against POM1 antibody. Progressive increase in immunoreactivity for PrP with respect to time spent in culture, starting at 14 dpi. Immunoreactivity against β-actin was used as a loading control for normalization. (D) Quantitative estimation of PrP immunoblot signal intensity.

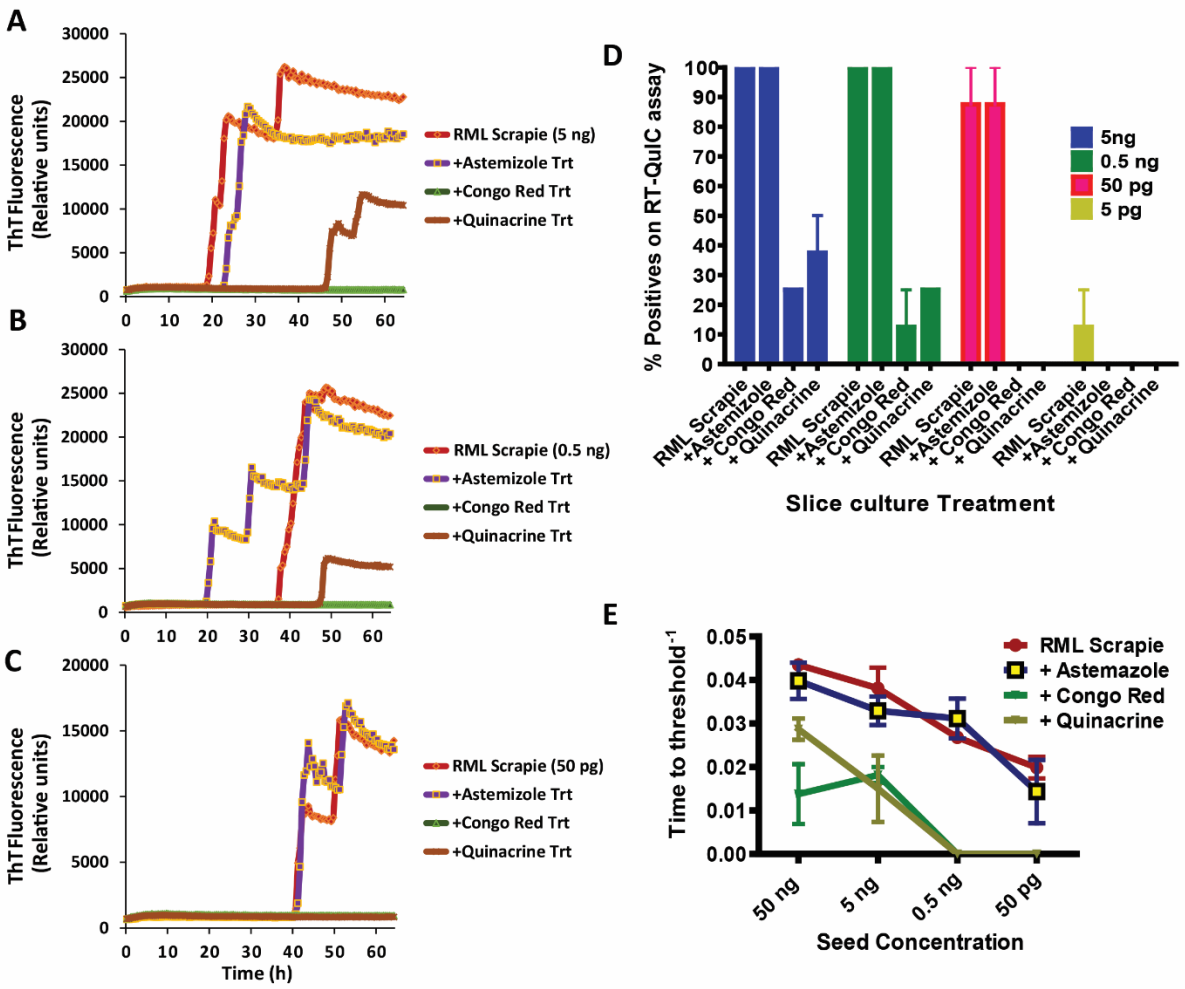

Figure 5. OSCAR model to determine the anti-prion activity of compounds. (A-C) Compounds known to have anti-prion activity against RML scrapie prions were tested. RT-QuIC responses shown for 3 different seed concentrations (5 ng, 0.5 ng, and 50 pg) with or without compounds. Each trace shown is an average of 4 replicates (n=2 biological replicates). (D-E) Quantification of anti-prion activity of compounds with respect to percent ThT-positive wells at different seed dilutions. Amyloid formation rate (AFR) represents the anti-prion activity of compounds tested.

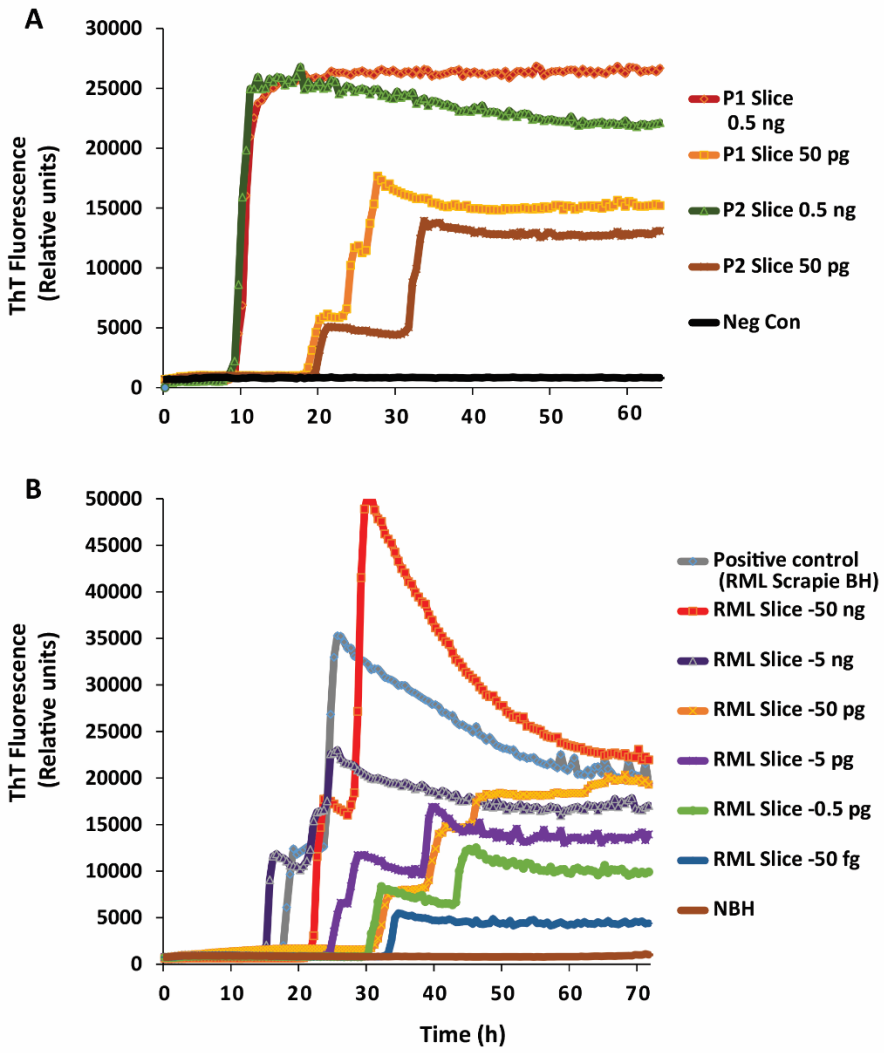

Figure 6. Prions generated in slice cultures are biologically active and OSCAR model can be adapted to whole brain slice cultures. (A) Efficient transmission of prions in slice cultures from serial passages shows comparable seeding activity between P1 and P2 slices. Traces are average of 3 technical replicates for each dilution. Additional dilutions were tested but only two seed concentrations (0.5 ng and 50 pg) shown here for brevity. Cerebellar slice cultures were prepared from *Tga*20 mice. Abbreviations: p1 = passage 1, WT slices treated with brain homogenate; p2 = passage 2, infected slice cultures harvested at 35 dpi, homogenized and used to treat fresh WT slice cultures) (B) corticostriatal slice cultures were prepared from 11-day-

old *Tga*20 pups in similar fashion as cerebellar slice cultures and maintained for 42 dpi before testing on RT-QuIC assay. The seeding activity from RT-QuIC traces demonstrates the competence of seeding activity is highly dynamic and similar to seeds obtained from organotypic cerebellar slices.

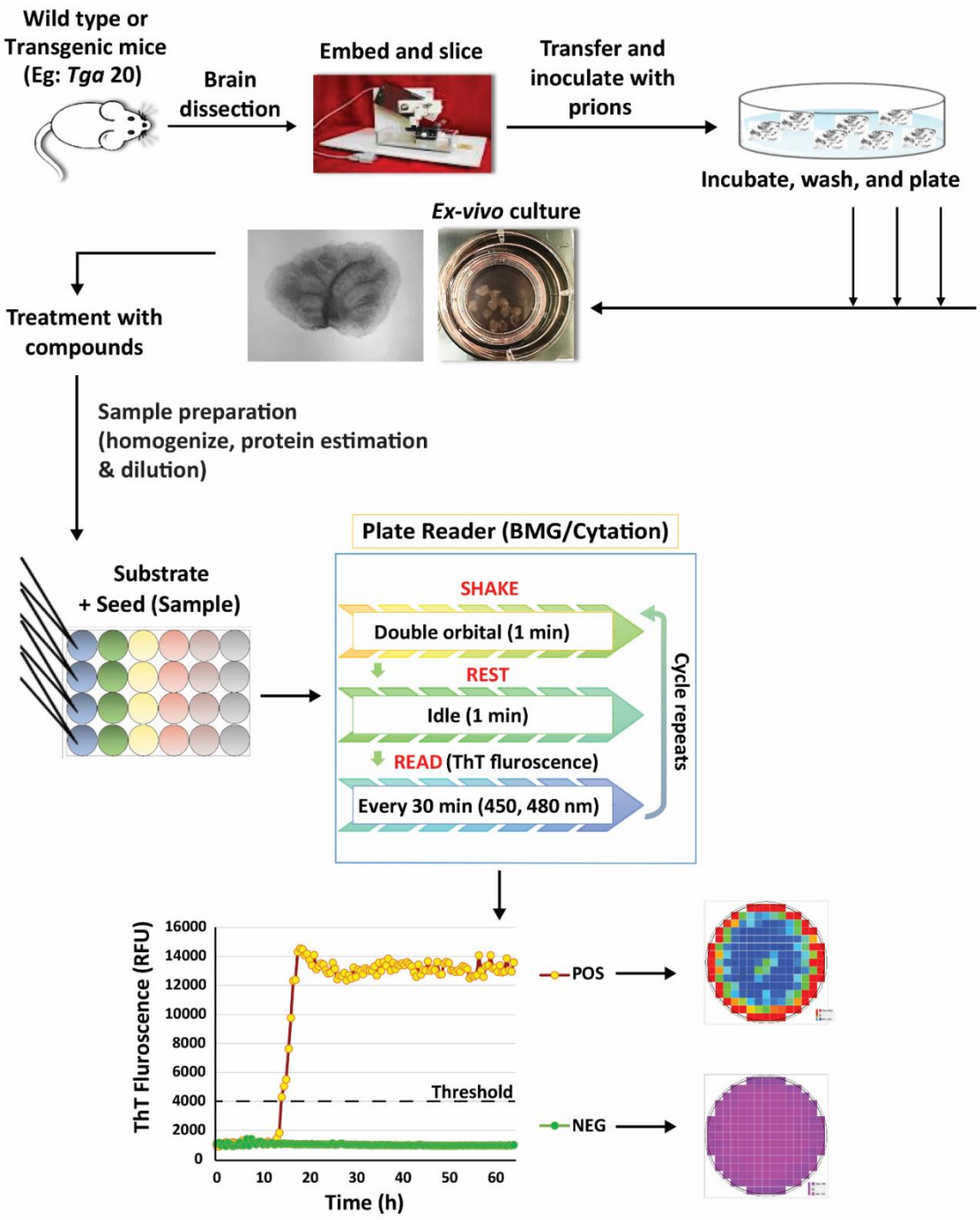

Figure 7. Schematic illustration of OSCAR workflow.

The brain slice cultures were prepared in organotypic fashion obtained from neonatal mice and embedded in compressing lip and sliced. The slices were incubated with either normal or prion-infected brain homogenates for 1 h, then washed and cultured with liquid air interphase on

membrane inserts. Treatments with compounds of interest began at 14 dpi in this study and slices were harvested at 31 dpi. Slices were homogenized and dilutions were used to seed RT-QuIC reactions. RT-QuIC assay was performed in 96-well plate using recombinant prion protein as a substrate with continuous shake/rest cycles. The seeding activity was monitored in real time based on seeding using a thioflavin T (ThT) fluorescence readout and quantified. Positive wells can be clearly visualized based on the traces that cross the threshold fluorescence and by the rapid increase in intensity. The well-area scan image shows the intense amyloid deposits in the well.

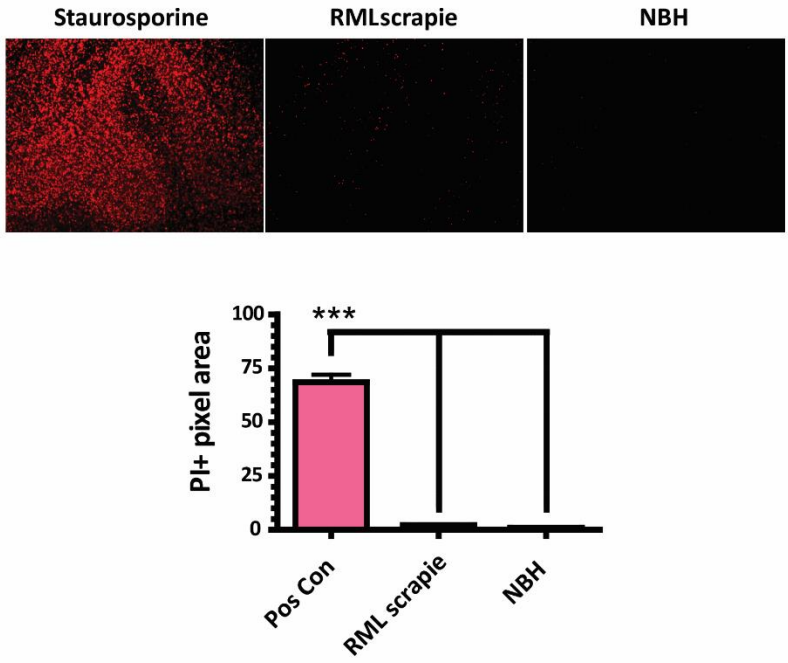

Supplementary Fig 1. Organotypic slices are viable for a long period of time in culture. Slices cultured for 63 days were assessed for viability using Propidium iodide (PI) fluorescence. Percentage of relative PI uptake intensity was used to compare cell death. Staurosporine evokes significantly stronger cell death as compared with the slices cultured post infection with either NBH or RML scrapie.

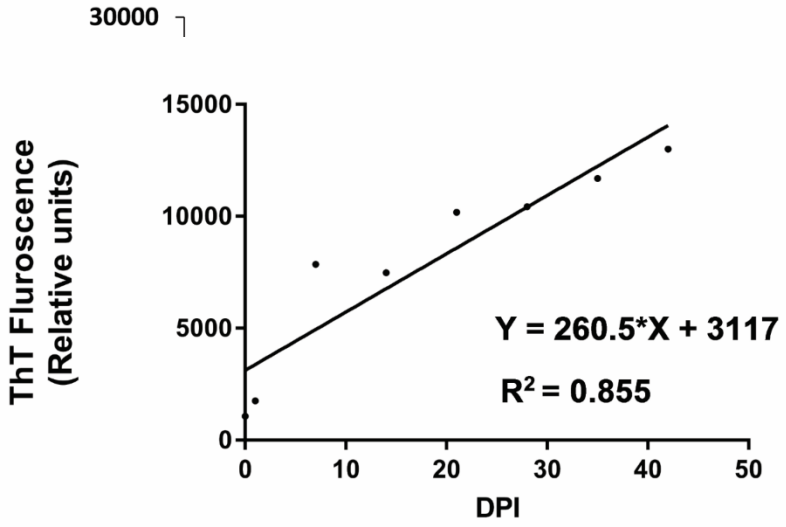

Supplementary Fig 2. Slice cultures illustrate the time-dependent increase in average fluorescence readings. Correlation between days post infection (DPI) versus an increase in the average fluorescence readings from the seeded reactions.

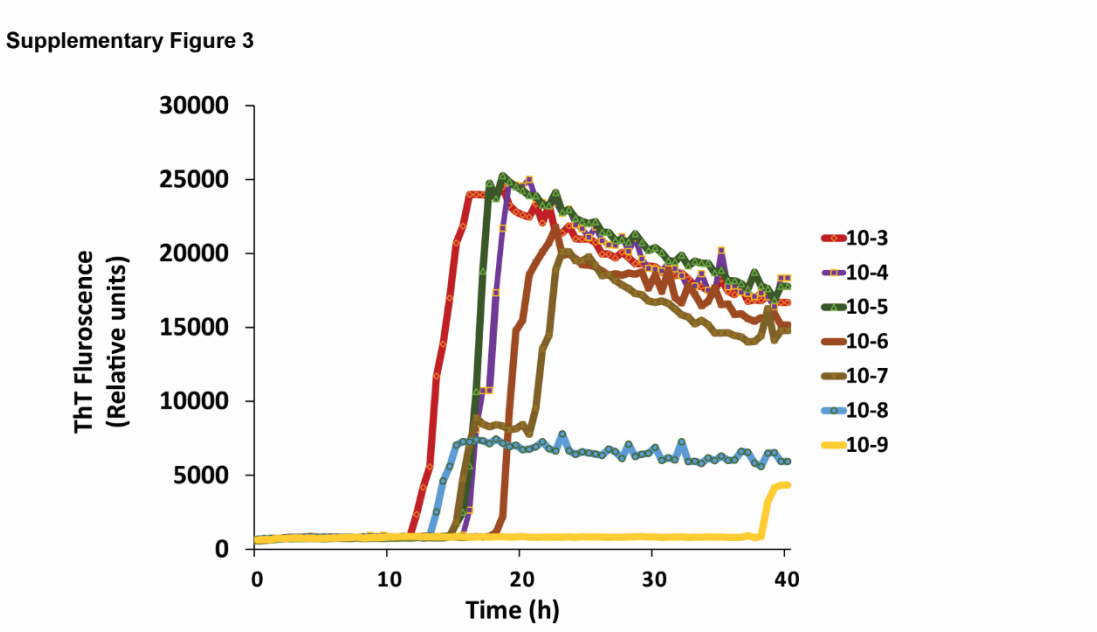

Supplementary Fig 3. Determining prion seeding activity from end point dilutions of infected scrapie brain homogenates. Serial dilutions of RML scrapie brain homogenates were used to seed RT-QuIC reactions; average of triplicate traces are shown. The 50% seeding dose (SD_{50}) was calculated based on the number of wells turned positive for each dilution, while the SD_{50} was calculated as described in methods. In this case, approximate SD_{50} for the RML scrapie brain homogenate was achieved with 5 ul seed from a 10^{-8} dilution.

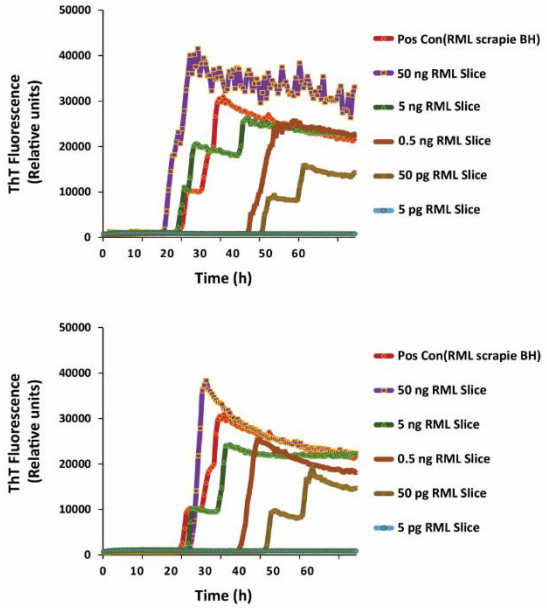

Supplementary Fig 4. Prion seeding kinetics between biological replicates have high reproducibility. RT-QuIC reactions seeded with the slice cultures from two separate experiments show similar seeding kinetics across the wide range of dilutions tested.

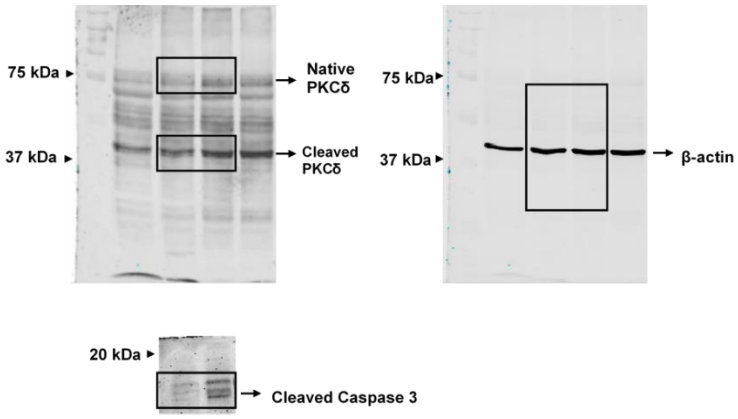

Supplementary Fig 5. Original western blots for the cropped images used in Fig 1G. Regions of Western Blots shown in the figures 1G were highlighted in black boxes.

CHAPTER IV: EX-VIVO BRAIN SLICE CULTURE MODEL FOR CHRONIC WASTING DISEASE

Naveen Kondru,[1] Sireesha Manne,[1] Robyn Kokemuller,[1,2] Justin Greenlee,[2] Heather West Greenlee,[1] Tracy Nichols,[3] Qingzhong Kong,[4] Vellareddy Anantharam,[1] Arthi Kanthasamy,[1] Patrick Halbur,[1] and Anumantha Kanthasamy[1*]

1. Department of Biomedical Sciences, College of Veterinary Medicine, Iowa State University, Ames, IA, USA.
2. Virus and Prion Research Unit, National Animal Disease Center, Agricultural Research Service, United States Department of Agriculture, Ames, IA, USA.
3. Surveillance, Preparedness and Response Services, Veterinary Services, USDA, Fort Collins, CO, USA.
4. Departments of Pathology and Neurology, Case Western Reserve University, Cleveland, OH, USA.
5. Veterinary Diagnostic and Production Animal Medicine, College of Veterinary Medicine, Iowa State University, Ames, IA, USA.

Abstract

Modeling diseases using the *ex-vivo* platform accelerates the study of prions and other protein misfolding diseases (PMDs) that have long incubation times. One manifestation of prion disease is chronic wasting disease (CWD) that has a 2–3 year incubation period in cervids. CWD has been shown to have rapid transmission yet it remains difficult to diagnose, or control and impossible to treat. We have recently developed an integrated organotypic slice culture assay for the detection of scrapie prions using ultrasensitive prion seeding. However, there are

no such *ex-vivo* models to study CWD prions due to the strong transmission barrier from deer to wildtype mice. Therefore, we utilized a cervidized transgenic (Tg12) mouse model to develop and characterize the *ex-vivo* brain slice culture model for CWD. We tested for CWD infectivity in the cultured slices using sensitive seeding assays such as the real-time quaking-induced conversion (RT-QuIC) assay and protein misfolding cyclic amplification (PMCA), along with the conventional methods of western blots and immunohistochemistry. Slice cultures from the Tg12 (elk sequence) $PrP^{+/-}$ genotype tested positive, but the slices from the $PrP^{-/-}$ genotype did not. We also tested the efficiency to propagate *in-vivo* of CWD prions generated in slices. The CWD prions generated in slices were transmitted efficiently back into the Tg12 mice and subsequently passed again with a reduction of incubation periods. Further, we established the activity of anti-prion compounds and the diagnostic utility of this CWD slice culture model. Our results demonstrate this integrated brain slice model of CWD provides a means to study prion propagation, CWD diagnosis to test potential therapeutics as they become available.

Introduction

Chronic Wasting Disease (CWD) is a transmissible spongiform encephalopathy (TSE) or prion disease of cervids, with a natural incubation period in the range of 2–3 years.(Williams *et al.*, 1980, 1993) The first detection of CWD was in a captive mule deer in the Colorado foothills in 1967. Currently, CWD has been reported in 24 states in the United States of America, in 2 provinces in Canada, and in South Korea and Norway.(Hannaoui *et al.*, 2017; Ricci *et al.*, 2018) CWD is a naturally occurring disease in both captive and wild cervids; it spreads rapidly through horizontal(Moore *et al.*, 2016) or vertical transmission(Nalls *et al.*, 2013). CWD prions

have been detected in a variety of tissue samples and biological fluids such as cerebrospinal fluid (CSF) and urine. CWD has been reported as transmissible to a wide host range by experimental inoculation.(Saunders *et al.*, 2012) For example, CWD is transmitted to cattle by intracerebral (IC) inoculation.(Hamir *et al.*, 2001) While there is no absolute species barrier demonstrated between CWD-infected deer and humans, it has been experimentally transmitted to several other species such as ferrets,(Sigurdson *et al.*, 2008) raccoons,(Hamir *et al.*, 2003) small ruminants,(Hamir *et al.*, 2006) domestic cats,(Mathiason *et al.*, 2013; Seelig *et al.*, 2015) pigs,(Moore *et al.*, 2017a) and non-human primates (squirrel monkeys were highly susceptible while Cynomolgus macaques were resistant).(Race *et al.*, 2014) Conversely, human PrP-expressing mice appear to be resilient to CWD infection despite not conclusively demonstrated.(Wilson *et al.*, 2012)

Despite CWD transmission to other species, wild-type (WT) mice have not been shown to support CWD prion infectivity. Therefore, transgenic mice expressing the deer *PRNP* sequence were developed to support the CWD prion *in-vivo* experimentation. These mice typically develop signs of CWD within 230 days following IC inoculation but will show signs in 160 days if they are homozygous for PrP transgene.(Browning *et al.*, 2004) Similarly, Kong and colleagues developed another line of transgenic mice that expresses elk *PRNP* sequence in a prion knockout background and has an incubation period of 118–142 days.(Kong *et al.*, 2005) Another strain of mice termed as VM mice are susceptible to both Bovine Spongiform Encephalopathy and Scrapie are also tested for CWD prion infection. The first passage mice showed low attack rate (~5%) while the second passage mice showed 100% attack rates.(Lee *et al.*, 2013)

The incubation period of CWD in experimental inoculations can exceed up to 3 years in cervids. Studying CWD prions in the laboratory can be time-consuming and requires adequate space equipped for cervid suites with high maintenance costs. Therefore, the purpose of this study is to develop and characterize an *ex-vivo* model of CWD to address some of the challenges in studying CWD prions. We have recently demonstrated that the integrated organotypic slice cultures and RT-QuIC (OSCAR) model using RML scrapie prions is a realistic model to study prion biology in a reduced time. This model utilizes advantages of both *ex-vivo* experimentation and ultrasensitive prion detection. Brain slices maintain a 3D environment with the integration of different cell types in the brain such as: neurons, astrocytes, microglia, and oligodendrocytes. Therefore, we hypothesized that a slice culture model for CWD prions would facilitate the study of the biology of these prions in a reasonable and shorter timescale. In this study, we developed and characterized the brain slice cultures to examine the CWD prions in culture. The slice cultures support CWD prion replication, and the kinetics of the prion seeding was quantified at different time points. Furthermore, we demonstrated that these CWD brain slice culture models could be used to test pharmacological compounds and the diagnostic utility of these slice cultures.

Materials and Methods

Ethics Statement

The experiments were performed according to *Guide for the Care and Use of Laboratory Animals*. All experiments involving animals were done with the approval of Institutional Animal Care and Use Committee (IACUC) at Iowa State University and the National Animal Disease Center under protocol number 3985.

Slice Culture Assays

Organotypic cerebellar slice cultures were done as reported previously.**(Kondru, et al., 2017a)** In brief, organotypic cerebellar slices were prepared from 10- to 12- day-old mouse pups from either transgenic (Tg12) or prion protein knockout ($prnp^{-/-}$) mice. For the cerebellar slices, the cerebellum was dissected out from the whole brain and positioned in the sagittal plane of the specimen tube in a microtome. The cerebellum was held in the specimen tube using 2% low-melting agarose. After positioning the cerebellum, the tube was chilled with an ice-cold chilling block to quickly solidify the agarose. The tube was then inserted into a tank filled with ice-cold Gey's Balanced Salt Solution along with kynurenic acid (GBSSK). Slices of 350 µm thickness were prepared using a medium speed setting on the microtome. After collection, slices were transferred to a plate filled with cold GBSSK. Later, brain homogenates from either uninfected deer or CWD infected deer obex were used to infect a pool of 20–30 slices. The slices were incubated for 1 hr at 4°C with brain homogenates diluted in the GBSSK solution to a final concentration of 100 µg/ml (W/V). After treatment, slices were washed twice with fresh, ice-cold GBSSK and then transferred onto membrane inserts preloaded in a 6-well plate. The residual buffer was removed, and 1 ml of fresh media was added to the basolateral compartment of the plate, avoiding any air bubbles at the base of the membrane. The slices were maintained in a standard cell culture incubator with 5% CO_2 at 37°C. The slice culture media was replaced on alternate days with pre-warmed media. After the desired length of time, the slices were harvested with ice-cold phosphate buffered saline (PBS) and pelleted. The pellets were stored at -80°C until analysis. For immunohistochemistry (IHC), the slices were washed once in ice-cold PBS, and 4% paraformaldehyde was added for overnight treatment at 4°C. For testing the activity of anti-prion drugs on the slices, 1000X stock concentrations of

drugs were used for treatments. The treatments were started at day 15 and followed up by the addition of fresh media with compounds on every alternate day up to 35 days. For testing rectoanal mucosa-associated lymphoid tissue (RAMALT) samples, the RAMALT homogenate was filtered through a 0.22 µ filter, and 100 µg/ml of the homogenate was exposed to 7-day old slices for 24 hours in the media, followed by replacement with fresh media and cultures for an additional 28 days in regular media.

Animal Inoculations

The slice culture lysates were injected into 6–8-week-old Tg12 mice that express the elk prion protein sequence. The lysates were prepared from a pool of 6–7 slices washed with ice-cold PBS twice, pelleted and frozen in -80^{o}C until injection. The pellets were homogenized in 60 µl of PBS with a fine needle and inoculated to the brain slice culture homogenate at 30 µl/mouse via intracranial injection into the right cerebral hemisphere at the level of the temporal bone. Samples were collected after animals exhibiting clinical signs had died. For immunohistochemistry evaluation, various regions of the brain were fixed in formalin, later changed to 10% neutral buffered formalin, and then embedded in paraffin wax. Sections of 4 µm thickness were affixed to slides for immunolabelling with antibodies. Anti-PrP 6H4 antibody was used to visualize the PrP^{CWD} in the sections.

Western Blot Analysis

Proteinase K digestion and western blot analysis were done according to previously published protocols.**(Anantharam, et al., 2008; Kondru, et al., 2017a; Nichols *et al.*, 2012; Orru *et al.*, 2015c)** In brief, after washing the slices with ice-cold PBS twice, they were harvested using PBS. Equal amounts of protein were loaded on 15% sodium dodecyl sulfate polyacrylamide gel electrophoresis SDS-PAGE gels after determining the concentrations using a Bradford

assay. Proteins were separated using electrophoresis and later transferred onto a nitrocellulose membrane. These membranes were blocked with LI-COR blocking buffer (LBB) for an hour. They were then incubated with the primary antibodies overnight, followed by a secondary antibody incubation using an Alexa Fluor-conjugated anti-mouse antibody. LI-COR's Odyssey IR imaging system was used to capture the images. For Proteinase K digestion experiments, 25 µg/ml of Proteinase K was used to digest 200 µg of protein for 30 minutes at 37°C followed by boiling samples for 10 minutes. These samples were used to separate the proteins using electrophoresis after transferring the proteins onto nitrocellulose membranes conjugated with POM1 PrP antibody at 1:5,000 concentration (Prionatis, AG) overnight at 4°C. Secondary antibodies were added after washing with 0.1% Tween in 1X PBS three times. Images were captured with an Odyssey IR imaging system.

Immunohistochemistry

Paraffin-embedded tissues were analyzed using immunohistochemistry for the detection of PrP^{CWD}. In brief, brain slices were deparaffinized and rehydrated prior to a 20-minute autoclave cycle in an antigen retrieval solution (Dako Target Retrieval Solution, Dako Corp., Carpinteria, CA). Tissues were then blocked with 3% hydrogen peroxide and Background Buster (Innovex Biosciences Inc., Richmond, CA) for 20 minutes each at room temperature. The primary antibody, Anti PrP mAb 6H4 (1:200; Prionics, Zurich, CH), at a concentration of 0.9 mg/ml, was diluted in Dako Antibody Diluent and incubated for 96 hours at 4°C. Mouse brain tissues were incubated for 15 minutes in 98% formic acid prior to a 30-minute autoclave cycle. Tissues were then incubated with primary antibody overnight at 4°C (6C2; CVI-WUR, Lelystad, NL). The secondary antibody, Dako EnVision^{+} Dual Link System HRP, was incubated at room temperature for 45 minutes. Tissues were then washed with Tris-buffered saline and .05%

Tween 20 (TBS-T). A DAB Peroxidase Substrate Kit (Vector Laboratories Inc., Burlingame, CA) was used to stain the slides for three minutes followed by a counterstain of hematoxylin and eosin (Leica Microsystems Inc., Wetzlar, DE) for two minutes. Tissues were then dehydrated, and coverslipped. Images for the figures were captured using a Nikon DS camera on a Nikon Eclipse 55i microscope.

Recombinant Prion Protein Purification

Truncated Syrian hamster recombinant prion protein (SHrPrP) amino acid residues 90–231 was expressed and purified as per previously published protocols.(Kondru, et al., 2017a; Moore *et al.*, 2017b; West Greenlee *et al.*, 2016) In brief, SHrPrP (90–231) was expressed in the Rosetta™(DE3) strain of *E.coli* with kanamycin and chloramphenicol as the antibiotics of selection. Overnight autoinduction supplements were added to express the protein. Since SHrPrP is associated with inclusion bodies, BugBuster (Millipore) was used to lyse the bacterial cells and isolate inclusion bodies. These inclusion bodies were denatured in 8M guanidine hydrochloride (GuHCl) for about an hour and later preequilibrated with nickel-nitrilotriacetic acid (Ni-NTA Superflow) resin for 50 minutes on a rotator. After equilibration with Ni-NTA beads, the bodies were loaded into the AKTA#XK26 column and purified using affinity chromatography on a Bio-Rad DuoFlow system at 4°C. On-column refolding was done from 100% denaturing to 100% refolding conditions. Elution of pure rPrP was due to the competitive binding between imidazole and rPrP to Ni-NTA resin. After elution, peak fractions of the pure rPrP were collected in a pre-chilled dialysis buffer (10mM Sodium phosphate buffer, pH 5.8) and dialyzed in two exchanges of 3.6 L of dialysis buffer. Finally, pure rPrP was filtered and the concentration of protein was determined using the absorbance at 280 nm. The absorbance at 280 nm was multiplied by the extinction coefficient to get the final rPrP

concentration in mg/ml. Protein was aliquoted and stored at -80°C until being used for experiments. Each batch of purified protein was tested for quality using a western blot analysis and test plates before being subjected to a seeding assay.

Real-Time Quaking-Induced Conversion (RT-QuIC) Assay

The RT-QuIC analysis was done as per previously published protocols.(Haley *et al.*, 2016; Henderson, et al., 2015; Kondru, et al., 2017a; Orru, et al., 2015b) Briefly, assay was done in either Cytation 3 (BioTek) or CLARIOstar (BMG), and the reaction mixture consisted of 350 mM NaCl, 0.1 M EDTA, 10 µM ThT, 0.1 mg/ml rPrP, along with 0.0025% SDS in PBS. 95 µl of the reaction mixture was loaded in each well of a 96-well plate with 5 µl of seed coming from either CWD or normal brain homogenates (NBH) and either slices infected with CWD or NBH. The reaction was carried out in a Nunc 96-well plate with a sealer and the plates were incubated at 42°C in the plate reader with alternating 1-min. shake and rest cycles. ThT fluorescence readings were taken every 30 min. with a 450±15 nm excitation and 480±10 nm emission, and data analysis was performed using MARS V5.2 R8 and Gen 5 version 2.07.17 software for CLARIOstar and Cytation 3 respectively. After exporting the fluorescence readings, graphs were plotted with GraphPad Prism 7.0 (GraphPad Software, Inc., La Jolla, CA). A sample was determined as positive when it crossed the fluorescence threshold, which is defined as the average mean fluorescence of control samples plus 10 standard deviations. Each sample was tested in triplicates or quadruplicates.

Protein Misfolding Cyclic Amplification (PMCA)

The slice culture samples were diluted and blinded. PMCA was performed as described previously.(Nichols *et al.*, 2009) In brief, the brains from 4–6-week-old mice expressing the cervid *PRNP* sequence were harvested after perfusion and homogenized into a 10% w/v

solution by placing brain tissue in a tube with 2.5 mm glass beads (BioSpec), PBS with 150 mM NaCl, and 4 mM EDTA (PMCA buffer). Then the solution was homogenized in a Blue Bullet homogenizer (Next Advance) for 4 min. Once homogenized, samples were clarified from debris by centrifugation. The supernatant was removed and stored at -80°C to be used as the substrate for PMCA reaction. A pool of 7 slices was homogenized in 100 µl of lysis buffer and was homogenized as described previously.(Kondru, et al., 2017a) The lysates were subjected to three 10-fold dilutions in PBS and used to seed the PMCA reactions. After PMCA, the amplified samples were visualized by western blot as described in the previous report.(Nichols *et al.*, 2015)

Dihydroethidium (DHE) Conversion Assay

To determine the reactive oxygen species (ROS) generated by CWD prions, DHE conversion assay was performed as described previously.(Herrmann *et al.*, 2015b) The adherent slices in the culture at 42 days post-inoculation (dpi) were washed twice in pre-warmed GBSS and incubated with 10 µg/ml DHE for 20 min in GBSS. Fluorescence microscopic imaging was performed on the slices using a 10X objective. The images were captured at 3–4 randomized areas per slice and quantified using ImageJ with similar threshold settings**.**

Results

Brain Slice Cultures from Cervidized Mice Support CWD Infectivity

Organotypic cerebellar slice cultures prepared from 9- to 12-day-old transgenic cervidized (Tg12) and $PrP^{-/-}$ pups were infected with CWD or NBH and maintained in cultures up to 52 dpi. The CWD prions that accumulated in these slices were detected using RT-QuIC assay based on their seeding ability. As hypothesized, the Tg12 slices treated with NBH as

well as $PrP^{-/-}$ slices treated with CWD or NBH did not show the infectivity (Fig. 1A). Prion seeding activity from cerebellar slices was also observed using serial PMCA (sPMCA). Infectious prions were amplified only in slices from Tg12 pups infected with CWD brain homogenate, and not in $PrP^{-/-}$ slices. This reflects similar observations made with the RT-QuIC assay (Fig. 1B). From both RT-QuIC and sPMCA it is evident that only cervidized slices (and not slices derived from $PrP^{-/-}$) were able to maintain the CWD prions and develop PK-resistant bands on the western blot. Next, the slice cultures were stained for deposition of resistant PrP as described in the methods for IHC. Distinct immunoreactivity of PrP^{CWD} was observed in the slices infected with CWD but not in any controls (Fig. 1C). For the electrophoresis profile, the lysates of the slices were digested with Proteinase K. The slices infected with CWD brain homogenate have shown a distinct pattern of di-, mono-, and unglycosylated PK-resistant bands of PrP^{CWD} on immunoblots, with bands, shifted lower than those from slices not treated with Proteinase K. This indicates a lower molecular mass of fragments after treating with Proteinase-K, along with the characteristic banding pattern of misfolded prions (Fig. 1D). Finally, we measured the ROS production from the slice cultures using the DHE conversion assay and the fluorescence was quantified. The cervidized slices infected with CWD demonstrated significantly higher ROS reactivity when compared to controls (Figure 1E). Taken together, these results suggest the CWD prions have the ability to infect and propagate in the slice cultures when cervidized PrP sequence transgene is introduced.

Kinetics of CWD Prion Propagation in *Ex-Vivo* Cerebellar Slice Cultures

Tg12 slices infected with CWD brain homogenate were cultured for various periods and harvested after 1, 21, 28, 35, 42, and 48 days post-infection (dpi). The slice cultures

demonstrated a low seeding ability at 21 dpi (Fig. 2A) and continued to increase at later time points. To further delineate the seeding dose (SD) required for the RT-QuIC assay, we tested serial 10-fold dilutions of 52 dpi slice culture homogenates from 50 ng to 50 fg; initial seeding activity was observed from the 50 ng dose up to 50 fg (Fig. 2B). To compare the seeding activity of prions in slice cultures with CWD brain homogenate, we tested different 10-fold dilutions of a CWD brain homogenate in the RT-QuIC assay. The seeding kinetics of the brain homogenates was compared to the cultured slices (Fig. 2C). A time-dependent increase in the accumulation of prions was observed from the SD_{50} (seeding activity, 50%) values and reached the maximum by 7 weeks post-infection in the slices, after which, the infectivity peaks 7 weeks (Fig. 2D) and suggesting that the seeding kinetics are comparable to the CWD brain homogenate.

Slice Cultures as Models for Transmission Assays and Screening Therapeutics

The slice cultures were treated with three anti-prion compounds and assayed at various doses to determine the prion seeding activity (Fig. 3A). Congo red reduced the amplification kinetics of misfolded prions, which was evident at 5 ng and 0.5 ng seeding doses of CWD-infected slices. Likewise, at a seeding dose of 50 pg Congo red completely inhibited the seeding activity (Fig. 3A). To test the diagnostic ability of slices from clinical samples, the infectivity of recto-anal mucosa-associated lymphoid tissue (RAMALT) samples were used. The 100 µg RAMALT sample was homogenized and exposed to the slices in culture media for 24 hours on day 7 and were cultured for 3 weeks. Subsequently, the slices were harvested, and lysates of different concentrations (50 ng to 50 pg) were used to compare the seeding ability of these slices with the CWD RAMALT sample as a positive control. Prion amplification kinetics suggested a concentration and *PRNP* expression dependent seeding activity. The slices

exposed to 50 ng of the CWD-infected RAMALT sample had the highest seeding ability, followed by other seeding doses of slices, when compared to the slices of the control RAMALT sample (Fig. 3B).

Infectivity of Prions Generated in Slice Culture Models

To test whether prions generated in slice cultures were biologically active, we intracerebrally inoculated Tg12 mice with CWD-infected slices (passage 1). The animals were euthanized when clinical signs became apparent and had a median survival time of 208 days. NBH treated brain slices were inoculated in a similar way, but had a prolonged lifespan reaching up to ~500 days. Brain homogenate from a passage 1 mouse was subsequently passaged by intracerebral inoculation to other Tg12 mice (passage 2) and the mice were observed for clinical signs. The second passage had earlier clinical signs with a median survival of 139.5 days (Fig. 4A). The seeding activity of the passage 1 brain homogenates were tested in serial 10-fold dilutions using the RT-QuIC assay and the misfolded prions that accumulated were comparable to the CWD brain homogenate (Fig. 4B). Immunohistochemistry was used to detect PrP^{CWD} in various brain regions of mice inoculated with the slice cultures. PrP^{CWD} immunoreactivity was observed in all of the brain regions of animals inoculated with CWD-infected slices, but not in control animals (Fig. 4C).

Discussion

The nature of CWD prions in *ex-vivo* brain slice cultures has not been characterized. In the current study, we extended the brain slice culture model by coupling it with sensitive seeding assays like RT-QuIC and PMCA for detection of the CWD prions. CWD prions are reluctant to propagate in Wild-type (WT) mice or slice cultures from WT mice. Therefore, we prepared the slice cultures from a transgenic mouse model that express a cervidized sequence of PrP.

The slices were cultured for 35 days and tested for seeding activity using the RT-QuIC assay (Fig. 1A). The $PrP^{-/-}$ slices treated with CWD and slices treated with NBH did not show amplification in both assays, indicating that prions replicate in cerebellar slice cultures. Next, we characterized seeding ability using PMCA with a similar profile of prion amplification that is specific to the PrP expression and in agreement with the RT-QuIC results (Fig. 1B). Unlike the RML scrapie strain that reached maximum titers by 42 dpi in WT slices, CWD prions took ~23% longer to reach maximum titers in slice cultures from Tg12 mice. One possible explanation for this long incubation period may be lower amplification kinetics of CWD prions in the heterozygous PrP genotype for Tg12 mice compared to RML scrapie. Brain samples from CWD-infected captive mule deer have PrP^{CWD} deposition mostly in the medulla and basal ganglia with lowest accumulations in the cerebral cortex and mild cerebellar involvement.(Liberski *et al.*, 2001) Therefore, utilizing the slice cultures from brain regions where CWD prion preferentially attack can be speculated as a good substitute. Additionally, the slice cultures were also tested for immunoreactivity of PrP^{CWD} in the sections and PK-resistant prions on western blot. We tested the accumulation of misfolded prions in slices at 3 weeks and reached maximum titers by 7 weeks. Dihydroethidium (DHE) is a specific adduct of reactive oxygen species and forms a product 2-hydroxyethidium that can be captured using fluorescence. CWD prions cause oxidative stress in the slices at 42 dpi and the slices with $PrP^{+/-}$ show significantly higher DHE reactivity when compared to all the controls.

Characterizing the seeding activity at various time points reveals a steady increase in the prion titers, suggesting a time-dependent amplification of CWD prions in the slice cultures. A slice culture at 52 dpi was tested for seeding ability and is comparable to a terminally ill CWD brain homogenate. PrP misfolding was evaluated for each dilution based on seeding ability of log

dilutions at each time point. An example of 52 dpi slices is shown in Fig. 2B. To quantify the seeding activity of slice cultures, the Spearman-Kärber method was used to determine the SD_{50} (seeding activity, 50%) values as described previously.(Henderson, et al., 2015; Kondru, et al., 2017a) The seeding activity quantified at 21 dpi was lower and reached a maximum after 7 weeks in culture (Fig. 2D). Overall, the quantification of slice culture prions had a time-dependent increase in the accumulation. Anti-prion compounds have been shown to have distinct effects with respect to different strains. To determine the activity of anti-prion compounds on the CWD prions in the slice cultures, we tested different known anti-prion compounds: Astemizole, Congo red, and Quinacrine. While Astemizole did not show any reduction in the prion titers, Quinacrine promoted the seeding ability of CWD prions (Fig. 3A). This phenomenon is similar to previously reported studies in transgenic mice that demonstrated how quinacrine promotes the resistance of CWD prions through conformational changes.(Bian *et al.*, 2014) However, congo red reduced the seeding activity of the CWD prions in the slice cultures. The slice cultures were also tested for transmission efficiency of the infectivity from the RAMALT rectal biopsies of deer.(Monello *et al.*, 2013) These results suggest slice culture models would be suitable for picking up infectivity from the exposed biological material. The utility of this model may be valuable if it can be extended to experimental testing of the transmissible prions from a variety of biological fluids that are known to harbor infective prions. However, the experimental range of infectivity is yet to be discerned. Although it remains to be tested, this model may be explored to determine strain characteristics based on the genotype of cervid PrP sequence as new animal models emerge.(Duque Velasquez *et al.*, 2015) The broader dynamic range of seeding assays enables for a more sensitive and accurate measurement of infectivity from slice cultures with a minimum protein requirement.

Acknowledgments

NIH supported this work under grant number ES19267, ISU Presidential Wildlife initiative, and the Iowa State University Veterinary Diagnostic Laboratory. The W. Eugene and Linda Lloyd Chair Endowment for AGK is also acknowledged. We thank the Dr. Byron Caughey lab at NIH for providing constructs and protocols. We also thank Gary Zenitsky for assistance in preparing this manuscript and Jordan Gongora and Kayla Guthals for assistance with figures. We thank Kevin Hassall and the LAR staff for animal husbandry.

Contributions

NK and AGK conceived the idea and designed the experiments. NK, SM, RK, HG, JG, and TN performed the experiments. JG, HG, and QK contributed transgenic cervidized mice. AK and PH provided helpful recommendations. NK and SM performed data analysis. NK, SM, and AGK wrote the manuscript and all authors reviewed the manuscript. AGK supervised and coordinated the entire study.

Conflicts of Interest

The authors declare no potential conflicts of interest.

References

1 Williams, E. S. & Young, S. Chronic wasting disease of captive mule deer: a spongiform encephalopathy. *Journal of wildlife diseases* **16**, 89-98 (1980).

2 Williams, E. S. & Young, S. Neuropathology of chronic wasting disease of mule deer (Odocoileus hemionus) and elk (Cervus elaphus nelsoni). *Vet Pathol* **30**, 36-45, doi:10.1177/030098589303000105 (1993).

3 Ricci, A. *et al.* Scientific opinion on chronic wasting disease (II). *EFSA Journal* **16**, e05132, doi:doi:10.2903/j.efsa.2018.5132 (2018).

4 Hannaoui, S., Schatzl, H. M. & Gilch, S. Chronic wasting disease: Emerging prions and their potential risk. *PLOS Pathogens* **13**, e1006619, doi:10.1371/journal.ppat.1006619 (2017).

5 Moore, S. J. *et al.* Horizontal Transmission of Chronic Wasting Disease in Reindeer. *Emerg Infect Dis* **22**, 2142-2145, doi:10.3201/eid2212.160635 (2016).

6 Nalls, A. V. *et al.* Mother to offspring transmission of chronic wasting disease in reeves' muntjac deer. *PloS one* **8**, e71844, doi:10.1371/journal.pone.0071844 (2013).

7 Saunders, S. E., Bartelt-Hunt, S. L. & Bartz, J. C. Occurrence, transmission, and zoonotic potential of chronic wasting disease. *Emerg Infect Dis* **18**, 369-376, doi:10.3201/eid1803.110685 (2012).

8 Hamir, A. N. *et al.* Preliminary findings on the experimental transmission of chronic wasting disease agent of mule deer to cattle. *J Vet Diagn Invest* **13**, 91-96, doi:10.1177/104063870101300121 (2001).

9 Sigurdson, C. J. *et al.* Experimental chronic wasting disease (CWD) in the ferret. *J Comp Pathol* **138**, 189-196, doi:10.1016/j.jcpa.2008.01.004 (2008).

10 Hamir, A. N. *et al.* Experimental inoculation of scrapie and chronic wasting disease agents in raccoons (Procyon lotor). *Vet Rec* **153**, 121-123 (2003).

11 Hamir, A. N. *et al.* Transmission of chronic wasting disease of mule deer to Suffolk sheep following intracerebral inoculation. *J Vet Diagn Invest* **18**, 558-565, doi:10.1177/104063870601800606 (2006).

12 Seelig, D. M. *et al.* Lesion profiling and subcellular prion localization of cervid chronic wasting disease in domestic cats. *Vet Pathol* **52**, 107-119, doi:10.1177/0300985814524798 (2015).

13 Mathiason, C. K. *et al.* Susceptibility of domestic cats to chronic wasting disease. *J Virol* **87**, 1947-1956, doi:10.1128/JVI.02592-12 (2013).

14 Moore, S. J. *et al.* Experimental transmission of the chronic wasting disease agent to swine after oral or intracranial inoculation. *J Virol*, doi:10.1128/jvi.00926-17 (2017).

15 Race, B. *et al.* Chronic wasting disease agents in nonhuman primates. *Emerg Infect Dis* **20**, 833-837, doi:10.3201/eid2005.130778 (2014).

16 Wilson, R. *et al.* Chronic wasting disease and atypical forms of bovine spongiform encephalopathy and scrapie are not transmissible to mice expressing wild-type levels of human prion protein. *J Gen Virol* **93**, 1624-1629, doi:10.1099/vir.0.042507-0 (2012).

17 Browning, S. R. *et al.* Transmission of prions from mule deer and elk with chronic wasting disease to transgenic mice expressing cervid PrP. *J Virol* **78**, 13345-13350, doi:10.1128/JVI.78.23.13345-13350.2004 (2004).

18 Kong, Q. *et al.* Chronic wasting disease of elk: transmissibility to humans examined by transgenic mouse models. *The Journal of neuroscience : the official journal of the Society for Neuroscience* **25**, 7944-7949, doi:10.1523/jneurosci.2467-05.2005 (2005).

19 Lee, Y. H. *et al.* Experimental chronic wasting disease in wild type VM mice. *J Vet Med Sci* **75**, 1107-1110 (2013).

20 Kondru, N. *et al.* Integrated Organotypic Slice Cultures and RT-QuIC (OSCAR) Assay: Implications for Translational Discovery in Protein Misfolding Diseases. *Sci Rep* **7**, 43155, doi:10.1038/srep43155 (2017).

21 Anantharam, V. *et al.* Opposing roles of prion protein in oxidative stress- and ER stress-induced apoptotic signaling. *Free radical biology & medicine* **45**, 1530-1541, doi:10.1016/j.freeradbiomed.2008.08.028 (2008).

22 Orru, C. D. *et al.* Bank Vole Prion Protein As an Apparently Universal Substrate for RT-QuIC-Based Detection and Discrimination of Prion Strains. *PLoS pathogens* **11**, e1004983, doi:10.1371/journal.ppat.1004983 (2015).

23 Nichols, T. A. *et al.* Detection of prion protein in the cerebrospinal fluid of elk (Cervus canadensis nelsoni) with chronic wasting disease using protein misfolding cyclic amplification. *J Vet Diagn Invest* **24**, 746-749, doi:10.1177/1040638712448060 (2012).

24 Moore, S. J. *et al.* Experimental Transmission of the Chronic Wasting Disease Agent to Swine after Oral or Intracranial Inoculation. *J. Virol.* **91**, doi:10.1128/jvi.00926-17 (2017).

25 West Greenlee, M. H. *et al.* Temporal Resolution of Misfolded Prion Protein Transport, Accumulation, Glial Activation, and Neuronal Death in the Retinas of Mice Inoculated with Scrapie. *The American journal of pathology* **186**, 2302-2309, doi:10.1016/j.ajpath.2016.05.018 (2016).

26 Haley, N. J. *et al.* Seeded Amplification of Chronic Wasting Disease Prions in Nasal Brushings and Recto-anal Mucosa-Associated Lymphoid Tissues from Elk by Real-Time Quaking-Induced Conversion. *Journal of clinical microbiology* **54**, 1117-1126, doi:10.1128/jcm.02700-15 (2016).

27 Orru, C. D. *et al.* Rapid and sensitive RT-QuIC detection of human Creutzfeldt-Jakob disease using cerebrospinal fluid. *MBio* **6**, doi:10.1128/mBio.02451-14 (2015).

28 Henderson, D. M. *et al.* Quantitative assessment of prion infectivity in tissues and body fluids by real-time quaking-induced conversion. *J Gen Virol* **96**, 210-219, doi:10.1099/vir.0.069906-0 (2015).

29 Nichols, T. A. *et al.* Detection of protease-resistant cervid prion protein in water from a CWD-endemic area. *Prion* **3**, 171-183 (2009).

30 Nichols, T. A., Fischer, J. W., Spraker, T. R., Kong, Q. & VerCauteren, K. C. CWD prions remain infectious after passage through the digestive system of coyotes (Canis latrans). *Prion* **9**, 367-375, doi:10.1080/19336896.2015.1086061 (2015).

31 Herrmann, U. S. *et al.* Prion Infections and Anti-PrP Antibodies Trigger Converging Neurotoxic Pathways. *PLoS Pathogens* **11**, e1004662, doi:10.1371/journal.ppat.1004662 (2015).

32 Liberski, P. P., Guiroy, D. C., Williams, E. S., Walis, A. & Budka, H. Deposition patterns of disease-associated prion protein in captive mule deer brains with chronic wasting disease. *Acta Neuropathol* **102**, 496-500 (2001).

33 Bian, J., Kang, H. E. & Telling, G. C. Quinacrine promotes replication and conformational mutation of chronic wasting disease prions. *Proc Natl Acad Sci U S A* **111**, 6028-6033, doi:10.1073/pnas.1322377111 (2014).

34 Monello, R. J. *et al.* Efficacy of antemortem rectal biopsies to diagnose and estimate prevalence of chronic wasting disease in free-ranging cow elk (Cervus elaphus nelsoni). *Journal of wildlife diseases* **49**, 270-278, doi:10.7589/2011-12-362 (2013).

35 Duque Velasquez, C. *et al.* Deer Prion Proteins Modulate the Emergence and Adaptation of Chronic Wasting Disease Strains. *J Virol* **89**, 12362-12373, doi:10.1128/JVI.02010-15 (2015).

Figures:

Fig 1A

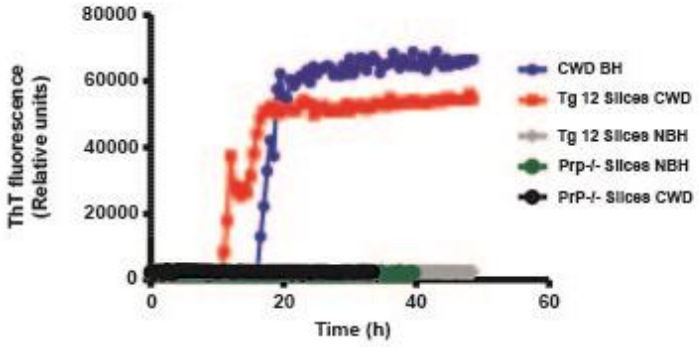

Fig 1B

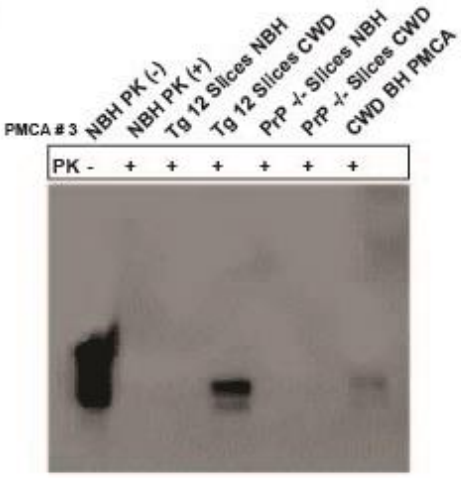

Fig 1C

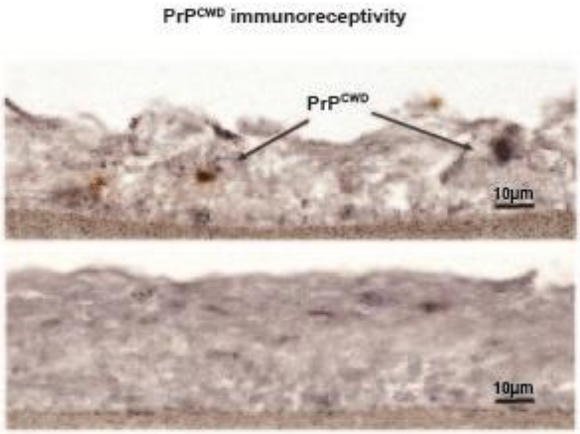

Fig 1D

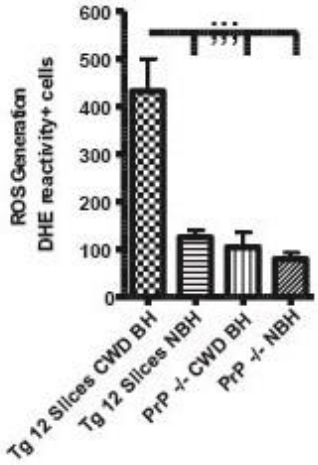

Fig 1E

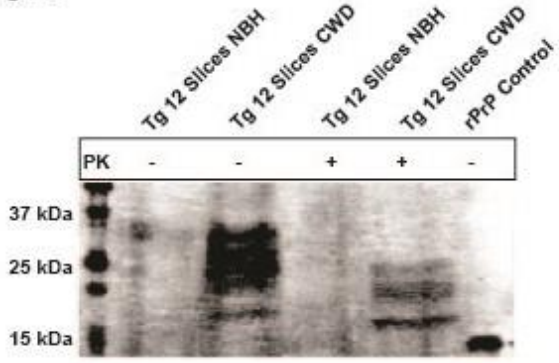

Fig. 1. *In-vitro* seeded amplification of CWD prions from organotypic slice cultures using RT-QuIC assay and PMCA (A) Slice cultures from Tg12 (PrP +/-) efficiently seed the RT-QuIC assay. PrP -/- slices prepared in the blinded fashion with the genotypes blinded. Representative RT-QuIC traces were shown for the reactions seeded with 5 ng of slice culture homogenates from either CWD BH infected slice cultures (42 dpi) or brain homogenates from CWD-infected deer showed strong positive peaks. However, the slices treated with NBH or PrP -/- slices infected and cultured with CWD BH did not show seeding activity and stayed at the baseline throughout the reaction period. (n>15 independent batches of slice cultures). Cultured slices from PrP-/- did not show seeding activity (both NBH and RML scrapie groups) at any seed concentration. Quantification of average ThT fluorescence values obtained over 60-hour period for each seed concentration tested from slice cultures shows the similar activity of the CWD BH seed. Each trace is a combined average of 3 technical replicates and 2 biological replicates from a pool of 7-10 slices. (B) Immunohistochemistry of PrP^{CWD} using 6H4 antibody was performed. Representative image of the cross-section of the slice was shown from a 42 dpi slices. (C)The PK-resistant prion show immunoreactivity from the slice cultures obtained from PrP +/- slice cultures but not from the PrP -/- slices infected and cultured at 42 dpi. Similarly, NBH slices do not show immunoreactivity for PK-resistant prions (image not is shown). Membranes were probed with anti-PrP mouse monoclonal antibody, POM1. Representative western blot was shown. (E) CWD prions induced oxidative stress was measured using DHE conversion assay and quantified using ImageJ. CWD BH infected cerebellar slices showed significantly higher ROS generation when compared to NBH treated brain slice cultures or PrP -/- slice cultures. Data were analyzed using one-way ANOVA; n = 4 biological replicates. Data are mean ± SEM (*$p<0.05$, **$p<0.01$, ***$P<0.001$).

Fig 2A

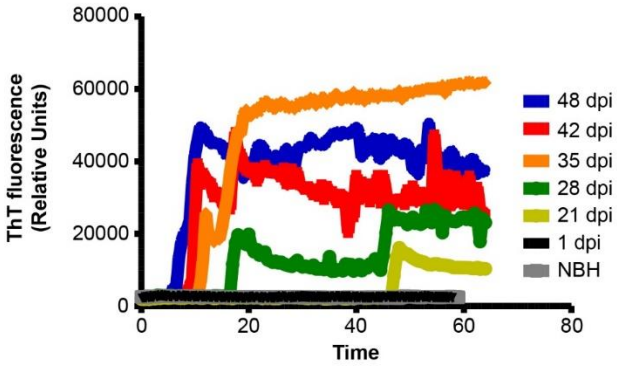

Fig 2B

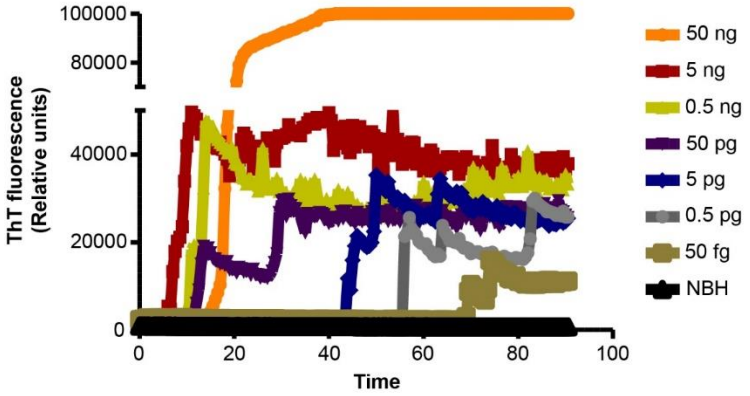

Fig 2C

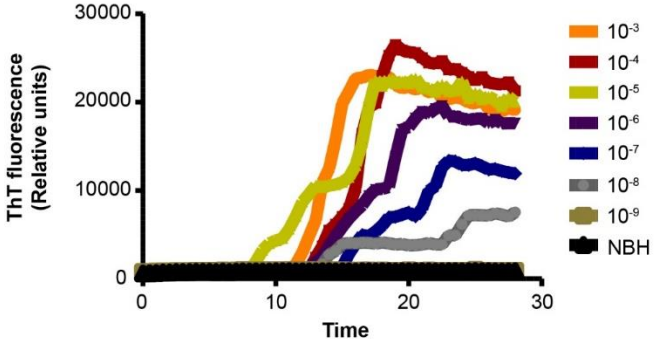

Fig 2D

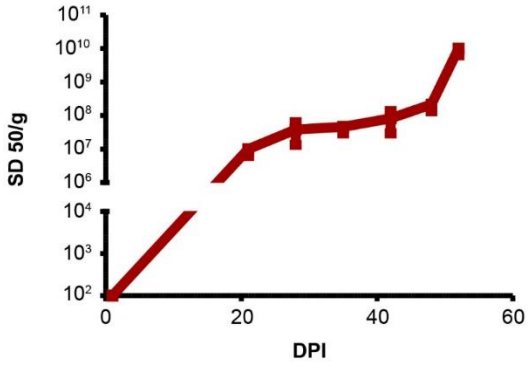

Fig. 2. Seeding profile of CWD prions from the organotypic slice cultures

(A) Slices were infected with either normal deer brain homogenate (NBH) or CWD-infected deer brain homogenates and cultured up to 52 dpi. Representative traces from an average of triplicate reactions were shown for each time points tested (1, 21, 28, 35, 42 and 48 dpi). (B) The lysates were prepared from slices at 52 dpi and serially diluted 10-fold ranging from 50 ng to 50 fg. Reactions consisted of 5ul of these dilutions as seed and tested in triplicate in the RT-QuIC assay. (C) A representative western blot demonstrating the PK-resistant prion, a biochemical hallmark accumulating in the organotypic cerebellar slices present only in CWD-infected Tg12 slices while PrP is digested completely in the cultures with NBH treatment.

Fig 3A

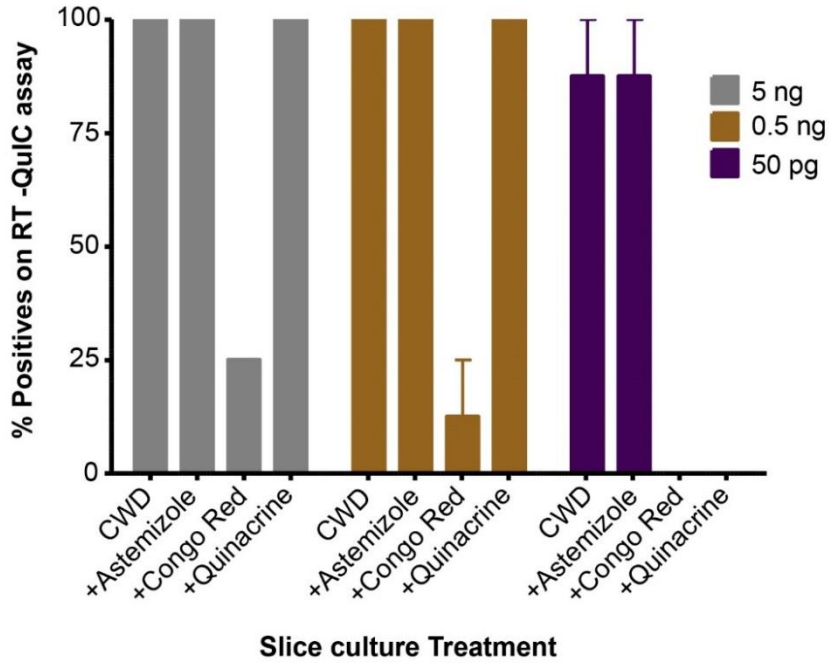

Fig 3B

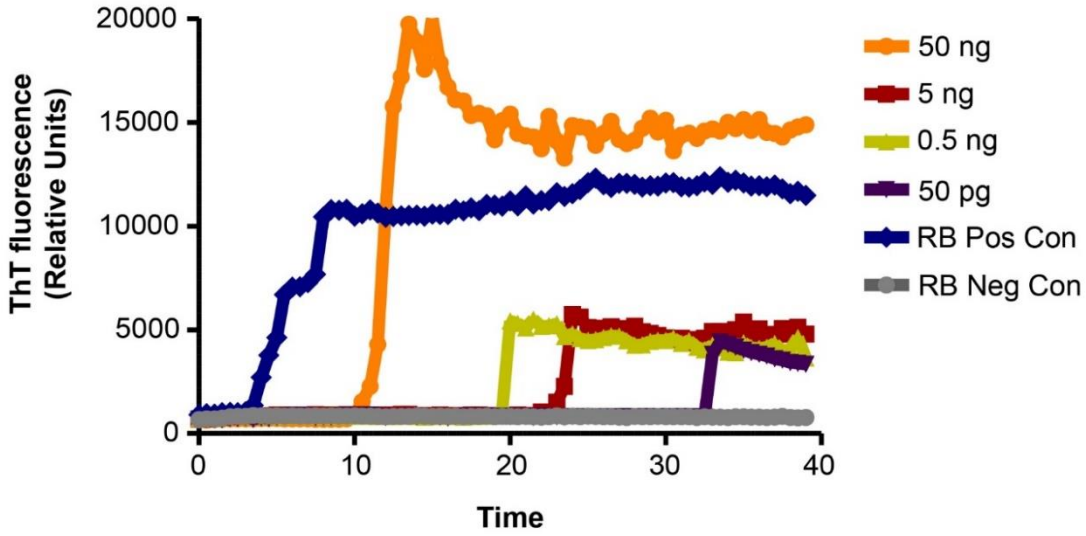

Fig. 3. Anti-prion activity of compounds and capture of CWD prions from biological samples using slice cultures

(A) The anti-prion activity of compounds Astemizole, Congo red and Quinacrine. The percent

seeding ratios for CWD prions were tested in log dilutions (5ng, 0.5 ng, 50 pg shown as Grey orange and purple bars respectively). When the reactions were seeded with 5ng of seed, Congo red was able to reduce the seeding by 75% of the wells while Astemizole and Quinacrine treated slices have similar seeding ability like CWD infected controls. A similar trend is observed when the reactions were seeded with 0.5ng of the lysate. Inhibitory activity was observed for Quinacrine and Congo red when the reactions seeded contain 50pg of the seed while Astemizole has no apparent effect on the seeding activity of CWD prion-infected slice cultures. (B) CWD slices were exposed to recto-anal mucosa associated lymphoid tissue (RAMALT) samples to determine the prion propagation. The RAMALT homogenates were sterile filtered and 100 µg of this lysate is exposed to the 7-day old slices in culture media. The media was replaced with fresh media after 24 hours and cultured the slices for another 21 days. Traces represent the average seeding ability of these slices at different dilutions (50ng to 50pg) along with the CWD RAMALT sample. 50ng of the slices exposed to CWD infected RAMLAT sample had the highest seeding ability when followed by other seeding doses of slices (Fig. 3B).

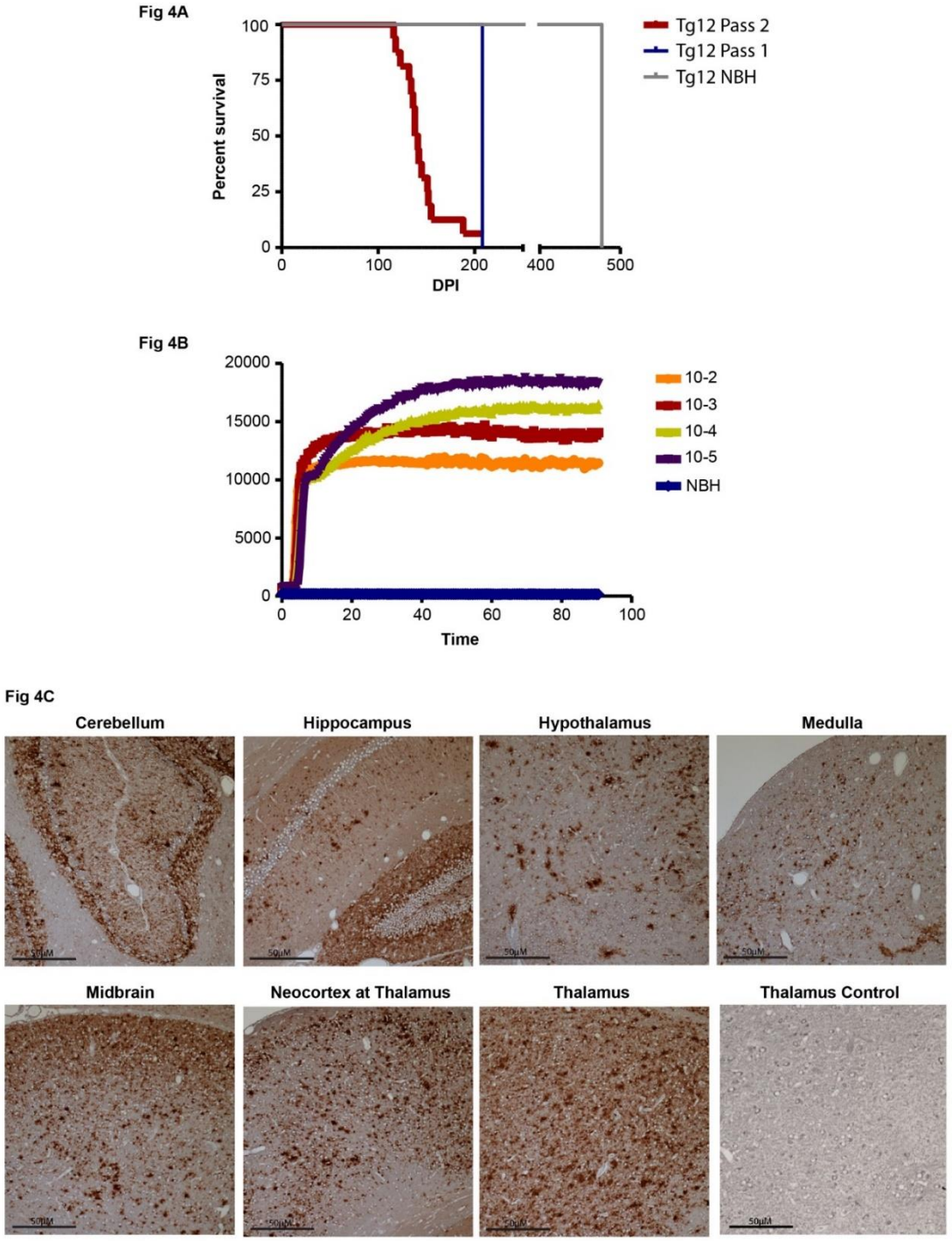

Fig. 4. Transmission of CWD prions from slice cultures to mice inoculation

(A) The 7-10 cerebellar slices from 42 dpi CWD infected and control cultures were pooled and washed twice in PBS. The pellet was resuspended in 60 µl of PBS by multiple and passages

through a 20-gauge needle and injected 30 µl into Tg12 mice. The CWD slices injected with had a lifespan of 208 days and displayed clinical signs before death. The mice infected with NBH slices had a lifespan of 477 days with no clinical signs before the endpoint. The brain homogenate from these mice were passaged again into Tg12 with an average lifespan of 139.5 days demonstrating a reduced incubation period. (B) Traces represent the average of 4 replicates from the reactions seeded with 5 µl the brain homogenate from the CWD slices infected Tg12 mice. (C) Immunohistochemistry of the paraffin-embedded tissue sections from multiple brain regions suggests neuropathology and CWD prion plaques. The sections of a negative control slice from thalamus devoid of such plaques were shown for comparison. Plaques were more abundant at the granular layer of the cerebellum, hippocampal formation. A diffuse pattern was observed in hypothalamus and medulla while a mixed pattern was manifested in midbrain and thalamus. Scale bars: 50 µm.

/CHAPTER V: α-SYNUCLEIN AND MANGANESE ELICIT DISTINCT TRANSCRIPTOMIC ALTERATIONS THAT DISRUPT MICROGLIAL HOMEOSTASIS

A manuscript to be submitted to Glia

Naveen Kondru[1], Sireesha Manne[1], Emir Malovic[1], Souvarish Sarkar, Huajin Jin[1] Vellareddy Anantharam[1], Arthi Kanthasamy[1], and Anumantha Kanthasamy[1*]

1. Department of Biomedical Sciences, College of Veterinary Medicine, Iowa State University, Ames, IA 50011, USA.

* Corresponding author: akanthas@iastate.edu

Abstract

Converging evidence suggests that microglial dysfunction is a central player in the pathogenesis of neurodegenerative diseases such as Alzheimer's disease (AD), Parkinson's disease (PD), Amyotrophic Lateral Sclerosis (ALS) and Frontotemporal dementia (FTD). Risk factors such as metal exposure, pesticides, and peripheral inflammation (gut & lungs) have been implicated in the etiology of PD. The divalent metal Manganese (Mn) can cross the blood-brain barrier and is linked to Parkinsonism. We hypothesized that Mn interacts synergistically with α-synuclein (α-syn) to trigger destructive neuroinflammatory processes. Therefore, we performed transcriptome analysis of microglia in response to Mn and α-syn and their co-treatments to identify the key genes and signaling pathways underpinning the inflammatory response. We further validated the identified targets using quantitative real-time PCR and immunoblots. The α-syn treatment predominately activated innate immune response-related

genes involving cytokine and chemokine imbalances and their associated signaling pathways (TNF, NF-kB, and TLR signaling). In contrast, Mn caused distinct changes to pathways related to cellular senescence, NOD-like receptor signaling, apoptosis, HIF-1 signaling, and pyrimidine metabolism. Mn and α-syn co-treatment caused major perturbations in Rho GTPase signaling and inflammasome activation. Co-treatment also caused profound changes in transcripts that triggered microglia to switch to their more cytotoxic, M1 phenotype. Top upregulated genes were *Il6*, *Urah*, *Nos2*, *Lcn2*, and *Csf3*, while *Slc14a1* transcripts were down-regulated. Overall, our study identifies distinct genes and pathways elicited by α-syn and Mn that perturb microglial homeostasis. These findings also suggest that environmental factors can induce neuroimmune transformations that possibly alter the course of neurodegenerative processes. (Funding acknowledgment: NIH grants ES026892, NS088206, and W. Eugene Linda Lloyd Endowed Chair)

Introduction

Microglia play a pivotal role in maintaining protein homeostasis in neurodegenerative such as Parkinson's and Alzheimer's disease. Microglia are immune cells that reside in the central nervous system (CNS) and represent about 10% of cells. They have a key role in immune responses along with astrocytes that are typically triggered by receptor and ligand interaction. Despite their role in inflammation, microglial cells have been implicated in a variety of functions such as synaptic pruning, neuronal programmed cell death, synaptic plasticity and immunity in several CNS disorders. See this review for genes of interest (Salter *et al.*, 2017). Unlike peripheral immune cells, microglia are traced to have originated from myeloid progenitors (RUNX1+/CD45-/C-Kit+) in the yolk-sac, then migrate to CNS. Since their early

embryonic development (E8.5 in mouse), they participate in CNS homeostasis. Microglia have unique ability to phagocytose and clear the protein aggregates, thus several studies are currently under investigation for therapeutic development. Growing evidence from genome-wide association study GWAS studies from clinically confirmed FTD samples identified the immune function related genes (such as HLA on chromosome 6 are enriched) are increased (Broce *et al.*, 2018). Mn neurotoxicity also termed as "manganism" has a resemblance to motor aspects of Parkinson's disease. Mn is also shown to induce dopaminergic neurodegeneration and microglial activation. Additionally, maternal exposure to Mn induces activation of macrophages and microglia in the offspring rats. When dams were exposed at a dose of 800 ppm, these rats have sustained inflammatory process as evidenced by the significant increase in the pro-inflammatory cytokines, *Il1a*, *Il6*, *Nos2*, and *Tnf* in the hippocampus when examined at 21 days after birth.(Abe *et al.*, 2015) In a different study, postnatal (days 21–34) exposure to Mn (100 mg/Kg) by oral gavage and observed, reduction in the striatal dopamine, activation of NF-kB signaling and increased Nitrosative stress (*Nos2* and *3NT*) expression (Moreno *et al.*, 2011). Microglia scavenge extracellular α-syn, thus making them an attractive target to develop therapeutic targets and to maintain protein homeostasis in CNS diseases (Lee *et al.*, 2008). For example, MHCII signaling complex was shown to be required for activation of microglia in immune response to α-syn aggregates and was reported as a potential target for the development of neuroprotective therapies (Harms *et al.*, 2013). Additionally, neuroinflammation and microglial response have been implicated in psychiatric disorders such as depression, bipolar disorder, schizophrenia, and autism (Reus *et al.*, 2015). Metabolic reprogramming has been linked to the phenotypic classification of microglial polarity. The shift in the mode of energy production from oxidative phosphorylation to aerobic glycolysis is

linked to M1 phenotype suggesting mitochondrial metabolites drives the polarization state of microglia (Orihuela *et al.*, 2016). Microglial activation induced by Mn was shown to precede and is responsible for preferential cell death in dopaminergic cells when compared to other neurons (Zhang *et al.*, 2009). Another study demonstrates M1 state is responsible for detrimental effects on recovery in the injured CNS. This study also demonstrates that TNF prevents M1 to M2 state in spinal cord injury. The effect of another metal ion, Iron is known to create unfavorable inflammation as it switches cells from M2 to M1 phenotype (Kroner *et al.*, 2014). Microglial senescence leads to impaired ability to clear the myelin debris by phagocytic dysfunction and preventing this can be a promising target. Cell culture models and primary cells have improved understanding of the microglial biology and remain to be the major neurodegenerative models to study CNS diseases. In this study, we used RNA-Sequencing to characterize changes in the mRNA profile of microglial response when treated with Mn, α-syn and their co-treatment. Based on expression levels of these transcriptome-wide analysis, we provide key mechanisms or pathways that alters microglial homeostasis in clearing aggregates or counter neurotoxicity.

Results

Innate immune response leading to cytokine signaling in microglia is triggered by misfolded α-syn

Microglial cells were exposed to misfolded α-syn for 24 hours and the transcriptome analysis was performed to identify the differentially expressed mRNAs. Genes are grouped based on the differential expression of genes. Fig. 1A shows volcano plots of the genes that are differentially expressed in response to misfolded α-syn treatment. A total of 840 genes were upregulated and 890 genes were downregulated. The genes shown in red dots were

upregulated. Some of these top increased gene changes were *Il6, Lcn2, Fpr1, Il1b, Slfn1*(>300 fold); *Csf3, Bcl2a1a, Il1a, Nos2* (>150 fold); *Adh7, Cxcl3, Gstt4, Urah* (>150 fold); Most of these genes are implicated in cytokine signaling, release, and receptor binding event that triggers a typical innate immune response. The genes shown in green dots were downregulated genes. The top genes that are downregulated are *Cecr6* (>150 fold); Ocstamp, *Serpinb1a, Tspan10, Sema4g* (>20 fold); *Klhl38, Hpgd, Slc14a1, Gm5086, Camk2b, Cd24a, Asb10, Lifr, Cx3cr1* (>10 fold); The genes with top changes and their associated p-values are listed under supplementary Table 1. Fig. 1B&C shows heat maps of the top 50 genes that are differentially expressed and major pathways in response to α-syn treatment. Genes that are upregulated are shown in red and the genes that are downregulated are shown in green.

Manganese treatment alters transcriptomic changes in microglial cells that lead to microglial senescence.

Manganese has been implicated in the microglia-mediated neurodegeneration. Microglia were exposed to 100 μM Mn for 24 hours and the transcriptome analysis identifies differentially expressed genes that are unique to Manganese neurotoxicity. Based on the differential expression of genes, volcano plots of the genes that are differentially expressed in response to Mn treatment were shown in Fig. 2A. A total of 2236 gene were upregulated, and 2196 genes were downregulated. The genes shown in red dots were upregulated. Some of the top gene changes were *Gsta2, Sstr5, Adh7, H2-Q9* (~200-250-fold increase); *Vat1l, Car6, Tnfsf4, Agpat9, Dio2, Spta1*(~100-fold increase); *Rtn4r, Cd207, Osbp2, Calcb, Rhpn2, Wnt9a, Ptgs2, Avil, Mmp13, Il6, Mmp10* (>50-fold increase). The genes that were downregulated are represented as shown in green dots. The top genes that are downregulated are *Cx3cr1, Asb10, Kmo, Ttn, Abca9, Sema4g, Ankle1, Tlr2, Pif1, Hist1h2ao* (7-15-fold decrease). However, there

is a profound downregulation in haptoglobin gene (78 fold) that has been implicated in neuroprotection following intracerebral hemorrhage (Garton *et al.*, 2017a). The genes with top fold changes and least p-values are listed under supplementary Table 2. Fig. 2B&C shows heat maps of the top 50 genes that are differentially expressed and major pathways in response to misfolded α-syn treatment. Genes that are upregulated are shown is red and the genes that are downregulated are shown in green.

Manganese and misfolded α-syn synergistically alters transcriptomic landscape of the microglial cells to promote cytotoxic signaling

α-syn interacts with Mn both *in-vitro* and in *in-vivo.* To determine the precise effects of the Mn binding to misfolded α-syn, microglia were co-treated, and the transcriptome profile is analyzed. The differential expression of genes was plotted and shown in Fig. 3A. A total of 2237 gene were significantly upregulated but over half of the transcripts are unique to the co-treatment when compared to individual treatments alone. The genes shown in red dots were upregulated. We found some of the top gene changes were associated with activation of microglia that leads to subsequent cytotoxic signaling. A striking increase was noted in the following genes - *Il6* (3400 fold), *Urah* (1450 fold), *Nos2, Lcn2 Csf3* (> 1000-fold); Other genes that were upregulated are *Il12b, Adh7, Il1b, Mmp3, Il1f6* (> 500-fold); *Slfn1, Ptgs2os, Serpinb2, Cxcl3, Il1a, Bcl2a1a, H2-Q9, Ptgs2, Sstr5* (> 200-fold increase); Transcripts of the genes that are involved in chemokine and cytokine signaling are abundantly increased (>100 fold). Mn caused major perturbations in the transcripts of Rho-GTPases signaling, their effectors, and cell cycle regulation (Fig.2C). Some of these top genes are *Ccl5, Cxcl2, Mmp13, Ifnb1, Cemip, Plagl1, Traf1, Tmc7, Dio2, Pydc4, Mmp10, Rsad2, Ggt1, Upp1*. Transcripts related to innate defense such as Interferon signaling are also abundantly expressed. *Pgf, Lif,*

Rgs9, Tpbg, Gpr126, Procr, Zbp1, Tnn, Rtn4r, Isg15, Car6, Spta1, Osbp2, Agpat9, Ifit3 showed > 50-fold increased. In addition to the upregulated genes, misfolded α-syn and Mn co-treatment caused some dramatic change in the transcripts that are down-regulated. Slc14a1, (a solute carrier family 14 - urea transporter), has 110-fold decrease suggesting proteins for neural transmitter recycling are decreased. Other genes that are downregulated are Serpinb1a, Hp, Abca9, Armc2, Ppfia4, Kmo, *Hpgd, Asb10, Xkr5, Kcne3*. Fig. 3B shows a heat map of top 50 transcripts that are upregulated (red) and downregulated (green) upon co-treatment of Mn and misfolded α-syn while Fig. 3C represents major pathways and biological process affected. The genes with top fold changes are listed under Table 1.

Mn and misfolded α-syn alter distinct pathways that alter microglial function

M1 and M2 phenotypic alteration in the microglia contributing either to a cytotoxic function or immunomodulatory roles respectively are increasingly being accepted for functional description. We have examined the transcripts to determine if there is any functional alteration. Interestingly, we observed that Mn and misfolded α-syn co-treatment caused a profound activation of M1-Cytotoxic phenotype (Fig. 4B). Such unanimous changes in the pro-inflammatory genes were not profound when either of the treatments was done alone. Top upregulated genes based on the magnitude of fold changes in the transcripts with respect to either of the treatments was shown in Table 1. Majority of pathways are related to innate immunity and stress response pathways in microglia. The Venn diagram (Fig. 4A) shows significantly different genes that are either converging and unique to each treatment. When microglial cells were treated with misfolded α-syn, a total of 232 genes are significantly different that are unique to this treatment. Other significantly different genes, 85 genes related to Mn treatment only group and 399 genes are overlapping with the co-treatment group and

1014 genes that are significantly different in all three treatments. Similarly, 914 genes differentially expressed and unique Mn treatment alone and 1024 for co-treatment. However about 2419 genes that are differentially expressed overlap for Mn and co-treatment.

Discussion

We have systemically characterized the transcriptome of microglia in response to the neurotoxicant Manganese, misfolded α-syn, and their co-treatment. While microglia are shown to play important role in tackling the misfolded α-syn, and Mn neurotoxicity, how microglia responds to these stimuli are not characterized. Microglia have been shown to efficiently clear extracellular α-syn with concurrent activation of TLR signaling and CX3CL1– CX3CR1 signaling deficits (Thériault *et al.*, 2016). This inherent ability of microglia to protect CNS in neurodegeneration as a phenomenon being explored as druggable target (Sanchez-Guajardo *et al.*, 2015). Using RNA sequencing, we identified pathways and genes involved in this context. We corroborated the sequencing data using a panel of key genes involved using qRT-PCR, Immunoblotting (dot blots), and immunocytochemistry. A comprehensive study characterized the transcripts that are enriched in microglia and other cell types in the brain (Zhang *et al.*, 2014). The current transcriptome analysis identified majority of the transcripts are expressed (32/34 genes matched). Transcriptome profiling of misfolded α-syn responsive genes are associated with major biological perturbations related to cellular responses to cytokines and their receptors, inflammation, positive response to cell motility, protein trafficking, DNA binding, reactive oxygen species and activation of pathways such as MAPK cascade leading to a phagocytic phenotype. On the other hand, Mn-induced major changes in biological pathways related to cell cycle, cytokine response, transferase activity, regulation of cellular protein localization, protein serine/threonine kinase activity, phase separation, oxidative stress,

intrinsic apoptosis, cell adhesion. Interestingly, RNA processing such as RNP complex biogenesis, protein and nitrogen catabolism and innate immune responses were altered. The co-treatment of Mn and misfolded α-syn resulted in changes in the much larger pool of transcripts related to innate immunity, cytokine signaling, modification-dependent protein catabolic process, activation of protein kinases, oxidative stress, and DNA replication. Additionally, TNF signaling appears to be a major player in the co-treatment as evidenced by immunoblots. Similarly, elevated levels of TNF-alpha2 have been reported to be a principal feature of CSF from FTD patients(Broce, et al., 2018). Another study demonstrated IFN milieu downregulates microglial myocyte-specific enhancer factor 2C (Mef2C) (Deczkowska *et al.*, 2017) that leads to inflated microglial response and subsequent adverse behavior in mice. Mn caused downregulation of Mef2C and thus might be contributing to the hostile microglial response to α-syn. IFN gamma is known to restrict innate, protective cells thereby increasing the susceptibility to influenza virus (Califano *et al.*, 2018). We observed misfolded α-syn activated IFN gamma signaling may play a detrimental role in the pathogenesis that may lead to microglial dysfunction and neuronal damage. Another report suggested glial activation in the neuroinflammatory process is mediated by NOS2 expression during Mn exposure (Streifel *et al.*, 2012). Similarly, we find striking upregulation in the RNA and protein levels of NOS2 suggesting Mn exacerbates the 3-nitrotyrosine protein adducts. Mn also triggered profound changes in signaling by Rho-GTPases (Fig. 2C). This effect is even exacerbated with the misfolded α-syn co-treatment (Fig. 3C). Rho signaling has a major link to cell motility, actin dynamics, and vesicular trafficking (Ridley). Therefore, we speculate that Mn may affect microglial motility, membrane protrusions, thereby altering the microglial phagocytic ability to clear protein aggregates.

Despite our efforts to obtain a clear picture of transcriptome from microglia in culture, the brain remains to be the more complex environment. For example, *Pu.1* and *Irf8* genes, that are lineage-specific differentiate microglia from tissue-resident macrophages. In the current study, *Irf8* but not *Pu.1* transcripts are detected in the current transcriptome dataset. However, based on the transcriptome profiling of different brain cell types in another study (Mathys *et al.*, 2017; Zhang, et al., 2014), most transcripts that are enriched specifically in the microglia are detected in our transcriptome analysis (see Supplementary Table 8). Further, we list the major changes associated with genes (at least 5-fold changes) were listed in supplementary tables 2-6. Developing novel tools such as organotypic models such as OSCAR model (Kondru *et al.*, 2017b) would be a superior advantage to study misfolded α-syn induced neurotoxicity. We are currently investigating the some of these findings in the slice culture model of α-syn prions. Overall, our findings provide novel insights into global transcriptome responses with microglia that open the door for identifying targets governing microglial homeostasis.

Materials and Methods

Cell culture and treatments

Mouse microglial cell line was a gift from Douglas T Golenbock (U Mass) and cultured as described previously**.** (Halle *et al.*, 2008). These immortalized microglial cells showed absolute purity and resembled primary microglia in both morphology and surface expression markers such as CD11b+ and CD14+, CD45+, MHCII, CD11c, and F4/80. (See supplementary fig 1 in the cited paper). Further, these cells responded to ATP and amyloid beta with larger soma and amoeboid morphology and expression of Nitric oxide, TNF and IL-1beta expression levels that match primary microglia**.** Cells were maintained in DMEM:F12 media supplemented with 9%

FBS, penicillin/streptomycin, glutamine, and sodium pyruvate and treatments were done with serum excluded.

RNA seq and analysis

Total RNA was extracted using the Trizol reagent (Ambion) from three biological replicates of mouse microglia that are in 4-6th passage. The RNA concentration was measured with Nanodrop (Thermo Fisher Scientific, Waltham, MA). RNA-Seq was performed with poly-A enrichment method. Next, the cDNA libraries for RNA-seq samples were constructed and sequenced. Before library construction, samples were spiked with Ex-Fold External RNA Consortium controls (Ambion, Foster City, CA). Libraries then underwent deep sequencing to 20 million reads of length 150 base pairs, paired-end sequencing.

Quantitative real-time PCR (qRT-PCR)

qRT-PCR was performed as described previously (Ay *et al.*, 2017) (Kim *et al.*, 2017). Total RNA from the cells was extracted using Trizol reagent (Invitrogen). RNA was quantified using Nanodrop and converted to cDNA using the High Capacity cDNA Synthesis kit (Life Technologies). PCR was performed according to the manufacturer's protocol. Validated primers (Qiagen) were used for detecting the mRNA of target genes. For housekeeping gene controls, Validated primers of 18S rRNA and GAPDH were used. The threshold cycle (Ct) result was adjusted and fold change in gene expression was calculated using the delta-delta Ct method.

Dot Blot

Immunoreactivity of samples was determined by dot-blot using Bio-Dot® Microfiltration System using manufacturer's protocol as described previously (Sun, et al., 2005). In brief, microglial lysates were prepared, and protein concentrations were determined as described

above. Next, 0.5 µg of lysates were mixed with 200 µl of Tris-buffered saline (1X TBS) having 0.1% Tween-20. After incubation, samples were allowed to adsorb onto a nitrocellulose membrane for 1 h. The membrane was washed twice with 200 µl of 1X TBS using a gentle vacuum, blocked with 1X LBB for 30 min, incubated with primary and secondary antibodies as described previously (Kondru, et al., 2017a).

Recombinant protein expression and purification

Recombinant alpha-α-syn and prion proteins were expressed and purified using previously reported protocols (Atarashi, et al., 2008; Orru, et al., 2011; Vascellari, et al., 2012; West Greenlee, et al.; Wilham, et al., 2010). Recombinant alpha-α-syn was prepared using size exclusion followed by anion exchange chromotography. Step by step protocols are provided in the supplemental info. Each batch was routinely tested for quality and activity using Coomassie and Western blot.

Acknowledgements

(Funding acknowledgment: NIH grants ES026892, NS088206, and W. Eugene Linda Lloyd Endowed Chair). We thank Monica Hepker and Griffin Clabaugh for assistance with Dot Blots.

Conflicts of interest

A.G.K. and V.A. are shareholders of PK Biosciences Corporation (Ames, IA), which is interested in developing therapeutic strategies for protein misfolding diseases including prion disease. Other authors declare no potential conflicts of interest.

Table 1. Top differentially expressed and upregulated genes when microglial cells when exposed to Manganese and misfolded α-syn and functional implications

		Fold change				
Gene	**Name**	**α-syn**	**Mn**	**Syn+ Mn**	**Implications**	**Ref**
Il6	interleukin 6	714	52	3407	Pro-inflammatory cytokine	(Petković *et al.*, 2016)
Urah	urate (5-hydroxyiso-) hydrolase	103	22	1453	Activation by inflamogen	(Horiuchi *et al.*, 2015)
Il12b	interleukin 12b	4	6	788	p40 subunit activates NF-κB leading to iNOS expression	(Pahan *et al.*, 2001)
Nos2	nitric oxide synthase 2, inducible	180	25	1141	Proinflammatory, Oxidative stress, Neurobehaviour	(Kurland *et al.*, 2016; Straccia *et al.*, 2011; Streifel, et al., 2012)
Csf3	colony stimulating factor 3 (granulocyte)	237	8	1099	Proinflammatory, Jak-STAT signaling, proliferation	(Gonzalez-Pena *et al.*, 2016)
Mmp3	matrix metallopeptidase 3	7	6	629	Pro-inflammatory activation, Correlates with Huntington disease severity	(Connolly *et al.*, 2016)
Il1f6	interleukin 1 family, member 6	37	6	513	inflammasome activation, Stress induced deficits and inflammation	(Giulian *et al.*, 1986; Kaushal *et al.*, 2015)
Ptgs2os	prostaglandin-endoperoxide synthase 2, opposite strand	53	14	319	lincRNA-Cox2, TLR signaling mediated inflammatory response	(Carpenter *et al.*, 2013)
Serpinb2	serine (or cysteine) peptidase inhibitor, clade B, member 2	46	40	293	Proteostasis during protein misfolding, Cryoprotection	(Lee *et al.*, 2015)
Ccl5	chemokine (C-C motif) ligand 5	43	4	181	Calcium influx, Pro-inflammatory, Microglial growth factor	(Shideman *et al.*, 2006; Solga *et al.*, 2015)
Gm5483	predicted gene 5483	14	16	138	Unknown	

	Table 1. (continued)					
Cxcl2	chemokine (C-X-C motif) ligand 2	37	13	174	P2X7 receptor stimulation and PKC AMPK signaling activation	(Shiratori *et al.*, 2010)
Gm5416	predicted gene 5416	11	10	102	Unknown	
Ptgs2	prostaglandin-endoperoxide synthase 2	25	58	222	Inflammation, Cox-2/Ptgs2 activation leads to cytotoxic (M1-like) phenotype	(Hellmann *et al.*, 2015)
Rsad2	radical S-adenosyl methionine domain containing 2	14	15	110	late response activation gene in neurodegeneration; Defense response to virus; Essential for Golgi trafficking of TNF-α	(Chung *et al.*, 2011; Mathys, et al., 2017)
Cemip	cell migration inducing protein	23	17	128	Unknown	
Lcn2	lipocalin 2	510	34	1134	M1 polarization of activated microglia is amplified; autocrine signal in ramification and apoptosis	(Jang *et al.*, 2013; Lee *et al.*, 2007)
Traf1	TNF receptor-associated factor 1	36	5	123	Apoptosis, FADD to the TNFR1 complex mediates apoptosis	(Hsu *et al.*, 1995; Liu *et al.*, 1996)
Upp1	uridine phosphorylase 1	22	13	100	Microglial activation by P2Y receptors. Increased phagocytotic activity in microglia	(Haynes *et al.*, 2006; Ransohoff *et al.*, 2009)
Plagl1	pleiomorphic adenoma gene-like 1	12	36	125	Unknown	
Mmp13	matrix metallopeptidase 13	9	56	156	Inflammation resulting neuronal loss, Protease with broad substrate specificity	(Hugenberg *et al.*, 2017; Ito *et al.*, 2007)
Ifnb1	interferon beta 1, fibroblast	7	52	132	Cognitive performance is impaired	(Deczkowska, et al., 2017)
Mmp10	matrix metallopeptidase 10	5	48	110	Stromelysin-2	(Konnecke *et al.*, 2013)
Cxcl3	chemokine (C-X-C motif) ligand 3	125	17	278	Chemokine binds to CXCR2, migration, and adhesion	(Farioli-Vecchioli *et al.*, 2012)
Ggt1	gamma-glutamyltransferase 1	-1	63	108	Glutathione metabolism, Superoxide generation,	(Roy *et al.*, 2012; Smith *et al.*, 1995)

Table 1. (continued)

Il1b	interleukin 1 beta	345	4	664	Proinflammatory, Inflammasome	(Sanchez-Guajardo, et al., 2015; Stojakovic *et al.*, 2017)
Tmc7	transmembrane channel-like gene family 7	9	71	121	Unknown	
Pydc4	pyrin domain containing 4	50	41	119	Inflammasome	(Ratsimandresey *et al.*, 2013)
Adh7	alcohol dehydrogenase 7 (class IV), mu or sigma polypeptide	133	247	672	Unknown	
Dio2	deiodinase, iodothyronine, type II	12	95	121	Unknown	
Il1a	interleukin 1 alpha	190	6	269	Pro-inflammatory	(Das *et al.*, 2016; Madeddu *et al.*, 2015)
Bcl2a1a	B cell leukemia/lymphoma 2 related protein A1a	229	6	242	Apoptosis, Prion mediated neurodegeneration	(Xiang *et al.*, 2004)
H2-Q9	histocompatibility 2, Q region locus 9	67	191	231	Unknown, Speculated for Microglial activation.	(Imamura *et al.*, 2003)
Slfn1	schlafen 1	317	68	465	Unknown, Microglial activation?	(Boutej *et al.*)
Sstr5	somatostatin receptor 5	15	260	202	Phagocytosis of amyloid aggregates, inhibition of cAMP, tyrosine phosphorylation	(Carniglia *et al.*, 2017; Fleisher-Berkovich *et al.*, 2010)

Table 2. Top differentially expressed and downregulated genes when microglial cells when exposed to Manganese and A-syn and microglial function

		Fold change				
Gene	**Name**	**α-syn**	**Mn**	**Syn+ Mn**	**Implications**	**Ref**
Kcne3	potassium voltage-gated channel, Isk-related subfamily, gene 3	-5	-3	-108	Modulates Kv3.1 and Kv2.1channel activity	(McCrossan *et al.*, 2003)
Nptxr	neuronal pentraxin receptor	-4	-1	-91	Removal of debris from the synaptic space, downregulated in oxidative stress and PD	(Anantharam *et al.*, 2007; Thomas *et al.*, 2006)
Xkr5	X Kell blood group precursor-related family, member 5	-2	-6	-85	Unknown	
Asb10	ankyrin repeat and SOCS box-containing 10	-16	-12	-81	Unknown	
Pira4	paired-Ig-like receptor A4	-2	-2	-81	Unknown	
Hpgd	hydroxyprostaglandin dehydrogenase 15 (NAD)	-12	-7	-75	General function in prostaglandin inactivation	
Naaladl1	N-acetylated alpha-linked acidic dipeptidase-like 1	-1	-11	-73	NMDA antagonist, metabolic inhibition	(Thomas *et al.*, 2000)
Kmo	kynurenine 3-monooxygenase (kynurenine 3-hydroxylase)	-1	-12	-45	tryptophan metabolism	(Zwilling *et al.*, 2011)
Ppfia4	protein tyrosine phosphatase, receptor type, f polypeptide (PTPRF), interacting protein (liprin), alpha 4	-6	-6	-42	trafficking of LAR subfamily PTPases, AMPA-type glutamate receptors	(Katoh *et al.*, 2003)
Armc2	armadillo repeat containing 2	-9	-6	-41	unknown	
Abca9	ATP-binding cassette, sub-family A (ABC1), member 9	-3	-8	-36	monocyte differentiation into macrophages, cholesterol-responsive	(Piehler *et al.*, 2002)
Hp	haptoglobin	-2	-79	-36	Neuroprotection	(Deuel *et al.*, 2015; Garton *et al.*, 2017b)
Serpinb1a	serine (or cysteine) peptidase inhibitor, clade B, member 1a	-25	-2	-35	leukocyte elastase inhibitor	(Cologna *et al.*, 2012)

References

Abe, H., Ohishi, T., Nakane, F., Shiraki, A., Tanaka, T., Yoshida, T., and Shibutani, M. (2015). Exposure to MnCl2 . 4H2O during development induces activation of microglial and perivascular macrophage populations in the hippocampal dentate gyrus of rats. *J Appl Toxicol* **35**(5), 529-35.

Adamchik, Y., Frantseva, M. V., Weisspapir, M., Carlen, P. L., and Perez Velazquez, J. L. (2000). Methods to induce primary and secondary traumatic damage in organotypic hippocampal slice cultures. *Brain Res Brain Res Protoc* **5**(2), 153-8.

Aguzzi, A., and Falsig, J. (2012). Prion propagation, toxicity and degradation. *Nat Neurosci* **15**(7), 936-9.

Anantharam, V., Kanthasamy, A., Choi, C. J., Martin, D. P., Latchoumycandane, C., Richt, J. A., and Kanthasamy, A. G. (2008). Opposing roles of prion protein in oxidative stress- and ER stress-induced apoptotic signaling. *Free Radic Biol Med* **45**(11), 1530-41.

Anantharam, V., Kitazawa, M., Latchoumycandane, C., Kanthasamy, A., and Kanthasamy, A. G. (2004). Blockade of PKCdelta proteolytic activation by loss of function mutants rescues mesencephalic dopaminergic neurons from methylcyclopentadienyl manganese tricarbonyl (MMT)-induced apoptotic cell death. *Annals of the New York Academy of Sciences* **1035**, 271-89.

Anantharam, V., Lehrmann, E., Kanthasamy, A., Yang, Y., Banerjee, P., Becker, K. G., Freed, W. J., and Kanthasamy, A. G. (2007). Microarray Analysis of Oxidative Stress Regulated Genes in Mesencephalic Dopaminergic Neuronal Cells: Relevance to Oxidative Damage in Parkinson's Disease. *Neurochemistry international* **50**(6), 834-847.

Anderson, M. E., Postupna, N., and Ruffo, M. (2003). Effects of High-Frequency Stimulation in the Internal Globus Pallidus on the Activity of Thalamic Neurons in the Awake Monkey. *Journal of neurophysiology* **89**(2), 1150-1160.

Atarashi, R., Wilham, J. M., Christensen, L., Hughson, A. G., Moore, R. A., Johnson, L. M., Onwubiko, H. A., Priola, S. A., and Caughey, B. (2008). Simplified ultrasensitive prion detection by recombinant PrP conversion with shaking. *Nature methods* **5**(3), 211-2.

Ay, M., Luo, J., Langley, M., Jin, H., Anantharam, V., Kanthasamy, A., and Kanthasamy, A. G. (2017). Molecular mechanisms underlying protective effects of quercetin against mitochondrial dysfunction and progressive dopaminergic neurodegeneration in cell culture and MitoPark transgenic mouse models of Parkinson's Disease. *J Neurochem* **141**(5), 766-782.

Ayers, J. I., Diamond, J., Sari, A., Fromholt, S., Galaleldeen, A., Ostrow, L. W., Glass, J. D., Hart, P. J., and Borchelt, D. R. (2016). Distinct conformers of transmissible misfolded SOD1 distinguish human SOD1-FALS from other forms of familial and sporadic ALS. *Acta Neuropathol* **132**(6), 827-840.

Bernis, M. E., Babila, J. T., Breid, S., Wusten, K. A., Wullner, U., and Tamguney, G. (2015). Prion-like propagation of human brain-derived alpha-synuclein in transgenic mice expressing human wild-type alpha-synuclein. *Acta Neuropathol Commun* **3**, 75.

Berry, D. B., Lu, D., Geva, M., Watts, J. C., Bhardwaj, S., Oehler, A., Renslo, A. R., DeArmond, S. J., Prusiner, S. B., and Giles, K. (2013). Drug resistance confounding prion therapeutics. *Proc Natl Acad Sci U S A* **110**(44), E4160-9.

Bian, J., Kang, H. E., and Telling, G. C. (2014). Quinacrine promotes replication and conformational mutation of chronic wasting disease prions. *Proc Natl Acad Sci U S A* **111**(16), 6028-33.

Boutej, H., Rahimian, R., Thammisetty, S. S., Béland, L.-C., Lalancette-Hébert, M., and Kriz, J. Diverging mRNA and Protein Networks in Activated Microglia Reveal SRSF3 Suppresses Translation of Highly Upregulated Innate Immune Transcripts. *Cell reports* **21**(11), 3220-3233.

Brana, C., Biggs, T. E., Mann, D. A., and Sundstrom, L. E. (1999). A macrophage hippocampal slice co-culture system: application to the study of HIV-induced brain damage. *J Neurosci Methods* **90**(1), 7-11.

Broce, I., Karch, C. M., Wen, N., Fan, C. C., Wang, Y., Hong Tan, C., Kouri, N., Ross, O. A., Höglinger, G. U., Muller, U., *et al.* (2018). Immune-related genetic enrichment in frontotemporal dementia: An analysis of genome-wide association studies. *PLOS Medicine* **15**(1), e1002487.

Browning, S. R., Mason, G. L., Seward, T., Green, M., Eliason, G. A., Mathiason, C., Miller, M. W., Williams, E. S., Hoover, E., and Telling, G. C. (2004). Transmission of prions from mule deer and elk with chronic wasting disease to transgenic mice expressing cervid PrP. *J Virol* **78**(23), 13345-50.

Brundin, P., Melki, R., and Kopito, R. (2010). Prion-like transmission of protein aggregates in neurodegenerative diseases. *Nat Rev Mol Cell Biol* **11**(4), 301-7.

Butler, D. A., Scott, M. R., Bockman, J. M., Borchelt, D. R., Taraboulos, A., Hsiao, K. K., Kingsbury, D. T., and Prusiner, S. B. (1988). Scrapie-infected murine neuroblastoma cells produce protease-resistant prion proteins. *J Virol* **62**(5), 1558-64.

Bywood, P. T., and Johnson, S. M. (2000). Differential vulnerabilities of substantia nigra catecholamine neurons to excitatory amino acid-induced degeneration in rat midbrain slices. *Exp Neurol* **162**(1), 180-8.

Califano, D., Furuya, Y., Roberts, S., Avram, D., McKenzie, A. N. J., and Metzger, D. W. (2018). IFN-gamma increases susceptibility to influenza A infection through suppression of group II innate lymphoid cells. *Mucosal immunology* **11**(1), 209-219.

Camenzind, R. S., Chip, S., Gutmann, H., Kapfhammer, J. P., Nitsch, C., and Bendfeldt, K. (2010). Preservation of transendothelial glucose transporter 1 and P-glycoprotein transporters in a cortical slice culture model of the blood-brain barrier. *Neuroscience* **170**(1), 361-71.

Campeau, J. L., Wu, G., Bell, J. R., Rasmussen, J., and Sim, V. L. (2013). Early increase and late decrease of purkinje cell dendritic spine density in prion-infected organotypic mouse cerebellar cultures. *PLoS One* **8**(12), e81776.

Carniglia, L., Ramírez, D., Durand, D., Saba, J., Turati, J., Caruso, C., Scimonelli, T. N., and Lasaga, M. (2017). Neuropeptides and Microglial Activation in Inflammation, Pain, and Neurodegenerative Diseases. *Mediators of Inflammation* **2017**, 5048616.

Carpenter, S., Aiello, D., Atianand, M. K., Ricci, E. P., Gandhi, P., Hall, L. L., Byron, M., Monks, B., Henry-Bezy, M., Lawrence, J. B., *et al.* (2013). A long noncoding RNA mediates both activation and repression of immune response genes. *Science (New York, N.Y.)* **341**(6147), 789-92.

Caspi, S., Halimi, M., Yanai, A., Sasson, S. B., Taraboulos, A., and Gabizon, R. (1998). The anti-prion activity of Congo red. Putative mechanism. *J Biol Chem* **273**(6), 3484-9.

Caughey, B., Brown, K., Raymond, G. J., Katzenstein, G. E., and Thresher, W. (1994). Binding of the protease-sensitive form of PrP (prion protein) to sulfated glycosaminoglycan and congo red [corrected]. *J Virol* **68**(4), 2135-41.

Caughey, B., Race, R. E., Ernst, D., Buchmeier, M. J., and Chesebro, B. (1989). Prion protein biosynthesis in scrapie-infected and uninfected neuroblastoma cells. *J Virol* **63**(1), 175-81.

Chadwick, E. J., Yang, D. P., Filbin, M. G., Mazzola, E., Sun, Y., Behar, O., Pazyra-Murphy, M. F., Goumnerova, L., Ligon, K. L., Stiles, C. D., *et al.* (2015). A Brain Tumor/Organotypic Slice Co-culture System for Studying Tumor Microenvironment and Targeted Drug Therapies. *J Vis Exp* doi: 10.3791/53304(105), e53304.

Chesebro, B., Striebel, J., Rangel, A., Phillips, K., Hughson, A., Caughey, B., and Race, B. (2015). Early Generation of New PrPSc on Blood Vessels after Brain Microinjection of Scrapie in Mice. *mBio* **6**(5).

Choi, C. J., Anantharam, V., Martin, D. P., Nicholson, E. M., Richt, J. A., Kanthasamy, A., and Kanthasamy, A. G. (2010). Manganese upregulates cellular prion protein and contributes to altered stabilization and proteolysis: relevance to role of metals in pathogenesis of prion disease. *Toxicol Sci* **115**(2), 535-46.

Chung, E. S., Chung, H., and Bae, H. (2011). RSAD2 is a key requirement for Golgi trafficking of TNF-α in activated microglia (117.26). *The Journal of Immunology* **186**(1 Supplement), 117.26-117.26.

Clapp-Lilly, K. L., Smith, M. A., Perry, G., Harris, P. L., Zhu, X., and Duffy, L. K. (2001). Melatonin acts as antioxidant and pro-oxidant in an organotypic slice culture model of Alzheimer's disease. *Neuroreport* **12**(6), 1277-80.

Cologna, S. M., Jiang, X.-S., Backlund, P. S., Cluzeau, C. V. M., Dail, M. K., Yanjanin, N. M., Siebel, S., Toth, C. L., Jun, H.-s., Wassif, C. A., *et al.* (2012). Quantitative Proteomic Analysis of Niemann-Pick Disease, Type C1 Cerebellum Identifies Protein Biomarkers and Provides Pathological Insight. *PLoS ONE* **7**(10), e47845.

Connolly, C., Magnusson-Lind, A., Lu, G., Wagner, P. K., Southwell, A. L., Hayden, M. R., Bjorkqvist, M., and Leavitt, B. R. (2016). Enhanced immune response to MMP3 stimulation in microglia expressing mutant huntingtin. *Neuroscience* **325**, 74-88.

Cramm, M., Schmitz, M., Karch, A., Mitrova, E., Kuhn, F., Schroeder, B., Raeber, A., Varges, D., Kim, Y.-S., Satoh, K., *et al.* (2015a). Stability and Reproducibility Underscore Utility of RT-QuIC for Diagnosis of Creutzfeldt-Jakob Disease. *Mol Neurobiol* doi: 10.1007/s12035-015-9133-2, 1-9.

Cramm, M., Schmitz, M., Karch, A., Mitrova, E., Kuhn, F., Schroeder, B., Raeber, A., Varges, D., Kim, Y. S., Satoh, K., *et al.* (2015b). Stability and Reproducibility Underscore Utility of RT-QuIC for Diagnosis of Creutzfeldt-Jakob Disease. *Mol Neurobiol* doi: 10.1007/s12035-015-9133-2.

Croft, C. L., Kurbatskaya, K., Hanger, D. P., and Noble, W. (2017). Inhibition of glycogen synthase kinase-3 by BTA-EG4 reduces tau abnormalities in an organotypic brain slice culture model of Alzheimer's disease. *Sci Rep* **7**(1), 7434.

Das, A., Kim, S. H., Arifuzzaman, S., Yoon, T., Chai, J. C., Lee, Y. S., Park, K. S., Jung, K. H., and Chai, Y. G. (2016). Transcriptome sequencing reveals that LPS-triggered transcriptional responses in established microglia BV2 cell lines are poorly representative of primary microglia. *J Neuroinflammation* **13**(1), 182.

Daviaud, N., Garbayo, E., Lautram, N., Franconi, F., Lemaire, L., Perez-Pinzon, M., and Montero-Menei, C. N. (2014). Modeling nigrostriatal degeneration in organotypic cultures, a new ex vivo model of Parkinson's disease. *Neuroscience* **256**, 10-22.

Deczkowska, A., Matcovitch-Natan, O., Tsitsou-Kampeli, A., Ben-Hamo, S., Dvir-Szternfeld, R., Spinrad, A., Singer, O., David, E., Winter, D. R., Smith, L. K., *et al.* (2017). Mef2C restrains microglial inflammatory response and is lost in brain ageing in an IFN-I-dependent manner. *Nat Commun* **8**(1), 717.

Demaimay, R., Chesebro, B., and Caughey, B. (2000). Inhibition of formation of protease-resistant prion protein by Trypan Blue, Sirius Red and other Congo Red analogs. *Arch Virol Suppl*(16), 277-83.

Deuel, J. W., Vallelian, F., Schaer, C. A., Puglia, M., Buehler, P. W., and Schaer, D. J. (2015). Different target specificities of haptoglobin and hemopexin define a sequential protection system against vascular hemoglobin toxicity. *Free Radic Biol Med* **89**, 931-943.

Diekmann, S., Nitsch, R., and Ohm, T. G. (1994). The organotypic entorhinal-hippocampal complex slice culture of adolescent rats. A model to study transcellular changes in a circuit particularly vulnerable in neurodegenerative disorders. *J Neural Transm Suppl* **44**, 61-71.

Doh-Ura, K., Iwaki, T., and Caughey, B. (2000). Lysosomotropic agents and cysteine protease inhibitors inhibit scrapie-associated prion protein accumulation. *J Virol* **74**(10), 4894-7.

Dossi, E., Blauwblomme, T., Nabbout, R., Huberfeld, G., and Rouach, N. (2014). Multi-electrode Array Recordings of Human Epileptic Postoperative Cortical Tissue. *J Vis Exp* doi: doi:10.3791/51870(92), e51870.

Duque Velasquez, C., Kim, C., Herbst, A., Daude, N., Garza, M. C., Wille, H., Aiken, J., and McKenzie, D. (2015). Deer Prion Proteins Modulate the Emergence and Adaptation of Chronic Wasting Disease Strains. *J Virol* **89**(24), 12362-73.

Falsig, J., and Aguzzi, A. (2008a). The prion organotypic slice culture assay--POSCA. *Nat Protoc* **3**(4), 555-62.

Falsig, J., Julius, C., Margalith, I., Schwarz, P., Heppner, F. L., and Aguzzi, A. (2008b). A versatile prion replication assay in organotypic brain slices. *Nat Neurosci* **11**(1), 109-17.

Falsig, J., Sonati, T., Herrmann, U. S., Saban, D., Li, B., Arroyo, K., Ballmer, B., Liberski, P. P., and Aguzzi, A. (2012). Prion pathogenesis is faithfully reproduced in cerebellar organotypic slice cultures. *PLoS Pathog* **8**(11), e1002985.

Farioli-Vecchioli, S., Cina, I., Ceccarelli, M., Micheli, L., Leonardi, L., Ciotti, M. T., De Bardi, M., Di Rocco, C., Pallini, R., Cavallaro, S., *et al.* (2012). Tis21 knock-out enhances the frequency of

medulloblastoma in Patched1 heterozygous mice by inhibiting the Cxcl3-dependent migration of cerebellar neurons. *J Neurosci* **32**(44), 15547-64.

Fleisher-Berkovich, S., Filipovich-Rimon, T., Ben-Shmuel, S., Hülsmann, C., Kummer, M. P., and Heneka, M. T. (2010). Distinct modulation of microglial amyloid β phagocytosis and migration by neuropeptides(i). *Journal of Neuroinflammation* **7**, 61-61.

Fuentealba, P., Timofeev, I., Bazhenov, M., Sejnowski, T. J., and Steriade, M. (2005). Membrane Bistability in Thalamic Reticular Neurons During Spindle Oscillations. *Journal of neurophysiology* **93**(1), 294-304.

Gähwiler, B. H., Capogna, M., Debanne, D., McKinney, R. A., and Thompson, S. M. (1997). Organotypic slice cultures: a technique has come of age. *Trends in Neurosciences* **20**(10), 471-477.

Garton, T., Keep, R. F., Hua, Y., and Xi, G. (2017a). CD163, a Hemoglobin/Haptoglobin Scavenger Receptor, After Intracerebral Hemorrhage: Functions in Microglia/Macrophages Versus Neurons. *Translational Stroke Research* **8**(6), 612-616 (journal article).

Garton, T., Keep, R. F., Hua, Y., and Xi, G. (2017b). CD163, a Hemoglobin/Haptoglobin Scavenger Receptor, After Intracerebral Hemorrhage: Functions in Microglia/Macrophages Versus Neurons. *Transl Stroke Res* **8**(6), 612-616.

Geschwind, M. D., Kuo, A. L., Wong, K. S., Haman, A., Devereux, G., Raudabaugh, B. J., Johnson, D. Y., Torres-Chae, C. C., Finley, R., Garcia, P., *et al.* (2013). Quinacrine treatment trial for sporadic Creutzfeldt-Jakob disease. *Neurology* **81**(23), 2015-23.

Ghaemmaghami, S., Ahn, M., Lessard, P., Giles, K., Legname, G., DeArmond, S. J., and Prusiner, S. B. (2009). Continuous Quinacrine Treatment Results in the Formation of Drug-Resistant Prions. *PLoS Pathogens* **5**(11), e1000673.

Giles, K., Berry, D. B., Condello, C., Dugger, B. N., Li, Z., Oehler, A., Bhardwaj, S., Elepano, M., Guan, S., Silber, B. M., *et al.* (2016). Optimization of aryl amides that extend survival in prion-infected mice. *J Pharmacol Exp Ther* doi: 10.1124/jpet.116.235556.

Giles, K., Berry, D. B., Condello, C., Hawley, R. C., Gallardo-Godoy, A., Bryant, C., Oehler, A., Elepano, M., Bhardwaj, S., Patel, S., *et al.* (2015). Different 2-Aminothiazole Therapeutics Produce Distinct Patterns of Scrapie Prion Neuropathology in Mouse Brains. *J Pharmacol Exp Ther* **355**(1), 2-12.

Giulian, D., Baker, T. J., Shih, L. C., and Lachman, L. B. (1986). Interleukin 1 of the central nervous system is produced by ameboid microglia. *The Journal of Experimental Medicine* **164**(2), 594-604.

Gonzalez-Pena, D., Nixon, S. E., Southey, B. R., Lawson, M. A., McCusker, R. H., Hernandez, A. G., Dantzer, R., Kelley, K. W., and Rodriguez-Zas, S. L. (2016). Differential Transcriptome Networks between IDO1-Knockout and Wild-Type Mice in Brain Microglia and Macrophages. *PLoS One* **11**(6), e0157727.

Gordon, R., Hogan, C. E., Neal, M. L., Anantharam, V., Kanthasamy, A. G., and Kanthasamy, A. (2011). A simple magnetic separation method for high-yield isolation of pure primary microglia. *J Neurosci Methods* **194**(2), 287-96.

Haley, N. J., and Hoover, E. A. (2015). Chronic wasting disease of cervids: current knowledge and future perspectives. *Annual review of animal biosciences* **3**, 305-25.

Haley, N. J., Siepker, C., Hoon-Hanks, L. L., Mitchell, G., Walter, W. D., Manca, M., Monello, R. J., Powers, J. G., Wild, M. A., Hoover, E. A., *et al.* (2016). Seeded Amplification of Chronic Wasting Disease Prions in Nasal Brushings and Recto-anal Mucosa-Associated Lymphoid Tissues from Elk by Real-Time Quaking-Induced Conversion. *Journal of clinical microbiology* **54**(4), 1117-26.

Halle, A., Hornung, V., Petzold, G. C., Stewart, C. R., Monks, B. G., Reinheckel, T., Fitzgerald, K. A., Latz, E., Moore, K. J., and Golenbock, D. T. (2008). The NALP3 inflammasome is involved in the innate immune response to amyloid-beta. *Nature immunology* **9**(8), 857-65.

Hamir, A. N., Cutlip, R. C., Miller, J. M., Williams, E. S., Stack, M. J., Miller, M. W., O'Rourke, K. I., and Chaplin, M. J. (2001). Preliminary findings on the experimental transmission of chronic wasting disease agent of mule deer to cattle. *J Vet Diagn Invest* **13**(1), 91-6.

Hamir, A. N., Kunkle, R. A., Cutlip, R. C., Miller, J. M., Williams, E. S., and Richt, J. A. (2006). Transmission of chronic wasting disease of mule deer to Suffolk sheep following intracerebral inoculation. *J Vet Diagn Invest* **18**(6), 558-65.

Hamir, A. N., Miller, J. M., Cutlip, R. C., Stack, M. J., Chaplin, M. J., Jenny, A. L., and Williams, E. S. (2003). Experimental inoculation of scrapie and chronic wasting disease agents in raccoons (Procyon lotor). *Vet Rec* **153**(4), 121-3.

Hannaoui, S., Schatzl, H. M., and Gilch, S. (2017). Chronic wasting disease: Emerging prions and their potential risk. *PLOS Pathogens* **13**(11), e1006619.

Harischandra, D. S., Kondru, N., Martin, D. P., Kanthasamy, A., Jin, H., Anantharam, V., and Kanthasamy, A. G. (2014). Role of proteolytic activation of protein kinase Cdelta in the pathogenesis of prion disease. *Prion* **8**(1), 143-53.

Harms, A. S., Cao, S., Rowse, A. L., Thome, A. D., Li, X., Mangieri, L. R., Cron, R. Q., Shacka, J. J., Raman, C., and Standaert, D. G. (2013). MHCII is required for alpha-synuclein-induced activation of microglia, CD4 T cell proliferation, and dopaminergic neurodegeneration. *J Neurosci* **33**(23), 9592-600.

Haynes, S. E., Hollopeter, G., Yang, G., Kurpius, D., Dailey, M. E., Gan, W. B., and Julius, D. (2006). The P2Y12 receptor regulates microglial activation by extracellular nucleotides. *Nature neuroscience* **9**(12), 1512-9.

Hellmann, J., Tang, Y., Zhang, M. J., Hai, T., Bhatnagar, A., Srivastava, S., and Spite, M. (2015). Atf3 negatively regulates Ptgs2/Cox2 expression during acute inflammation. *Prostaglandins & other lipid mediators* **116-117**, 49-56.

Henderson, D. M., Davenport, K. A., Haley, N. J., Denkers, N. D., Mathiason, C. K., and Hoover, E. A. (2015). Quantitative assessment of prion infectivity in tissues and body fluids by real-time quaking-induced conversion. *J Gen Virol* **96**(Pt 1), 210-9.

Henderson, D. M., Manca, M., Haley, N. J., Denkers, N. D., Nalls, A. V., Mathiason, C. K., Caughey, B., and Hoover, E. A. (2013). Rapid antemortem detection of CWD prions in deer saliva. *PloS one* **8**(9), e74377.

Herms, J. W., Tings, T., Dunker, S., and Kretzschmar, H. A. (2001). Prion protein affects Ca2+-activated K+ currents in cerebellar purkinje cells. *Neurobiol Dis* **8**(2), 324-30.

Herrmann, U. S., Sonati, T., Falsig, J., Reimann, R. R., Dametto, P., O'Connor, T., Li, B., Lau, A., Hornemann, S., Sorce, S., *et al.* (2015a). Prion infections and anti-PrP antibodies trigger converging neurotoxic pathways. *PLoS Pathog* **11**(2), e1004662.

Herrmann, U. S., Sonati, T., Falsig, J., Reimann, R. R., Dametto, P., O'Connor, T., Li, B., Lau, A., Hornemann, S., Sorce, S., *et al.* (2015b). Prion Infections and Anti-PrP Antibodies Trigger Converging Neurotoxic Pathways. *PLoS Pathogens* **11**(2), e1004662.

Hogue, M. J. (1947). Human fetal brain cells in tissue cultures; their identification and motility. *The Journal of experimental zoology* **106**(1), 85-107.

Holmes, C., Jones, S. A., and Greenfield, S. A. (1995). The influence of target and non-target brain regions on the development of mid-brain dopaminergic neurons in organotypic slice culture. *Brain Res Dev Brain Res* **88**(2), 212-9.

Horiuchi, H., Parajuli, B., Wang, Y., Azuma, Y.-T., Mizuno, T., Takeuchi, H., and Suzumura, A. (2015). Interleukin-19 Acts as a Negative Autocrine Regulator of Activated Microglia. *PLOS ONE* **10**(3), e0118640.

Hsu, H., Xiong, J., and Goeddel, D. V. (1995). The TNF receptor 1-associated protein TRADD signals cell death and NF-κB activation. *Cell* **81**(4), 495-504.

Hugenberg, V., Wagner, S., Kopka, K., Schäfers, M., Schuit, R. C., Windhorst, A. D., and Hermann, S. (2017). Radiolabeled Selective Matrix Metalloproteinase 13 (MMP-13) Inhibitors: (Radio)Syntheses and in Vitro and First in Vivo Evaluation. *Journal of Medicinal Chemistry* **60**(1), 307-321.

Imamura, K., Hishikawa, N., Sawada, M., Nagatsu, T., Yoshida, M., and Hashizume, Y. (2003). Distribution of major histocompatibility complex class II-positive microglia and cytokine profile of Parkinson's disease brains. *Acta Neuropathologica* **106**(6), 518-526 (journal article).

Ito, S., Kimura, K., Haneda, M., Ishida, Y., Sawada, M., and Isobe, K. (2007). Induction of matrix metalloproteinases (MMP3, MMP12 and MMP13) expression in the microglia by amyloid-beta stimulation via the PI3K/Akt pathway. *Experimental gerontology* **42**(6), 532-7.

Jang, E., Lee, S., Kim, J. H., Kim, J. H., Seo, J. W., Lee, W. H., Mori, K., Nakao, K., and Suk, K. (2013). Secreted protein lipocalin-2 promotes microglial M1 polarization. *Faseb j* **27**(3), 1176-90.

Jaunmuktane, Z., Mead, S., Ellis, M., Wadsworth, J. D., Nicoll, A. J., Kenny, J., Launchbury, F., Linehan, J., Richard-Loendt, A., Walker, A. S., *et al.* (2015). Evidence for human transmission of amyloid-beta pathology and cerebral amyloid angiopathy. *Nature* **525**(7568), 247-50.

Karapetyan, Y. E., Sferrazza, G. F., Zhou, M., Ottenberg, G., Spicer, T., Chase, P., Fallahi, M., Hodder, P., Weissmann, C., and Lasmezas, C. I. (2013). Unique drug screening approach for prion diseases identifies tacrolimus and astemizole as antiprion agents. *Proc Natl Acad Sci U S A* **110**(17), 7044-9.

Katoh, M., and Katoh, M. (2003). Identification and characterization of human PPFIA4 gene in silico. *International journal of molecular medicine* **12**(6), 1009-14.

Kaushal, V., Dye, R., Pakavathkumar, P., Foveau, B., Flores, J., Hyman, B., Ghetti, B., Koller, B. H., and LeBlanc, A. C. (2015). Neuronal NLRP1 inflammasome activation of Caspase-1 coordinately regulates inflammatory interleukin-1-beta production and axonal degeneration-associated Caspase-6 activation. *Cell death and differentiation* **22**(10), 1676-86.

Kim, D. S., Jin, H., Anantharam, V., Gordon, R., Kanthasamy, A., and Kanthasamy, A. G. (2017). p73 gene in dopaminergic neurons is highly susceptible to manganese neurotoxicity. *Neurotoxicology* **59**, 231-239.

Klohn, P. C., Stoltze, L., Flechsig, E., Enari, M., and Weissmann, C. (2003). A quantitative, highly sensitive cell-based infectivity assay for mouse scrapie prions. *Proc Natl Acad Sci U S A* **100**(20), 11666-71.

Kondru, N., Manne, S., Greenlee, J., West Greenlee, H., Anantharam, V., Halbur, P., Kanthasamy, A., and Kanthasamy, A. (2017a). Integrated Organotypic Slice Cultures and RT-QuIC (OSCAR) Assay: Implications for Translational Discovery in Protein Misfolding Diseases. *Sci Rep* **7**, 43155.

Kondru, N., Manne, S., Greenlee, J., West Greenlee, H., Anantharam, V., Halbur, P., Kanthasamy, A., and Kanthasamy, A. (2017b). Integrated Organotypic Slice Cultures and RT-QuIC (OSCAR) Assay: Implications for Translational Discovery in Protein Misfolding Diseases. *Scientific Reports* **7**, 43155.

Kong, Q., Huang, S., Zou, W., Vanegas, D., Wang, M., Wu, D., Yuan, J., Zheng, M., Bai, H., Deng, H., *et al.* (2005). Chronic wasting disease of elk: transmissibility to humans examined by transgenic mouse models. *The Journal of neuroscience : the official journal of the Society for Neuroscience* **25**(35), 7944-9.

Konnecke, H., and Bechmann, I. (2013). The role of microglia and matrix metalloproteinases involvement in neuroinflammation and gliomas. *Clinical & developmental immunology* **2013**, 914104.

Kotake, Y., Ohta, S., Kanazawa, I., and Sakurai, M. (2003). Neurotoxicity of an endogenous brain amine, 1-benzyl-1,2,3,4-tetrahydroisoquinoline, in organotypic slice co-culture of mesencephalon and striatum. *Neuroscience* **117**(1), 63-70.

Kroner, A., Greenhalgh, A. D., Zarruk, J. G., Passos Dos Santos, R., Gaestel, M., and David, S. (2014). TNF and increased intracellular iron alter macrophage polarization to a detrimental M1 phenotype in the injured spinal cord. *Neuron* **83**(5), 1098-116.

Kurland, D. B., Gerzanich, V., Karimy, J. K., Woo, S. K., Vennekens, R., Freichel, M., Nilius, B., Bryan, J., and Simard, J. M. (2016). The Sur1-Trpm4 channel regulates NOS2 transcription in TLR4-activated microglia. *J Neuroinflammation* **13**(1), 130.

Lee, H. J., Suk, J. E., Bae, E. J., and Lee, S. J. (2008). Clearance and deposition of extracellular alpha-synuclein aggregates in microglia. *Biochem Biophys Res Commun* **372**(3), 423-8.

Lee, J. A., Yerbury, J. J., Farrawell, N., Shearer, R. F., Constantinescu, P., Hatters, D. M., Schroder, W. A., Suhrbier, A., Wilson, M. R., Saunders, D. N., *et al.* (2015). SerpinB2 (PAI-2) Modulates

Proteostasis via Binding Misfolded Proteins and Promotion of Cytoprotective Inclusion Formation. *PLOS ONE* **10**(6), e0130136.

Lee, S., Lee, J., Kim, S., Park, J. Y., Lee, W. H., Mori, K., Kim, S. H., Kim, I. K., and Suk, K. (2007). A dual role of lipocalin 2 in the apoptosis and deramification of activated microglia. *J Immunol* **179**(5), 3231-41.

Lee, Y. H., Sohn, H. J., Kim, M. J., Kim, H. J., Park, K. J., Lee, W. Y., Yun, E. I., Tark, D. S., Choi, Y. P., Cho, I. S., *et al.* (2013). Experimental chronic wasting disease in wild type VM mice. *J Vet Med Sci* **75**(8), 1107-10.

Liberski, P. P., Guiroy, D. C., Williams, E. S., Walis, A., and Budka, H. (2001). Deposition patterns of disease-associated prion protein in captive mule deer brains with chronic wasting disease. *Acta Neuropathol* **102**(5), 496-500.

Liu, Z.-g., Hsu, H., Goeddel, D. V., and Karin, M. (1996). Dissection of TNF Receptor 1 Effector Functions: JNK Activation Is Not Linked to Apoptosis While NF-κB Activation Prevents Cell Death. *Cell* **87**(3), 565-576.

Madeddu, S., Woods, T. A., Mukherjee, P., Sturdevant, D., Butchi, N. B., and Peterson, K. E. (2015). Identification of Glial Activation Markers by Comparison of Transcriptome Changes between Astrocytes and Microglia following Innate Immune Stimulation. *PLoS One* **10**(7), e0127336.
Mallucci, G., and Collinge, J. (2005). Rational targeting for prion therapeutics. *Nat Rev Neurosci* **6**(1), 23-34 (10.1038/nrn1584).

Martin, D. P., Anantharam, V., Jin, H., Witte, T., Houk, R., Kanthasamy, A., and Kanthasamy, A. G. (2011). Infectious prion protein alters manganese transport and neurotoxicity in a cell culture model of prion disease. *Neurotoxicology* **32**(5), 554-62.

Mathiason, C. K., Nalls, A. V., Seelig, D. M., Kraft, S. L., Carnes, K., Anderson, K. R., Hayes-Klug, J., and Hoover, E. A. (2013). Susceptibility of domestic cats to chronic wasting disease. *J Virol* **87**(4), 1947-56.

Mathys, H., Adaikkan, C., Gao, F., Young, J. Z., Manet, E., Hemberg, M., De Jager, P. L., Ransohoff, R. M., Regev, A., and Tsai, L. H. (2017). Temporal Tracking of Microglia Activation in Neurodegeneration at Single-Cell Resolution. *Cell reports* **21**(2), 366-380.

McCrossan, Z. A., Lewis, A., Panaghie, G., Jordan, P. N., Christini, D. J., Lerner, D. J., and Abbott, G. W. (2003). MinK-related peptide 2 modulates Kv2.1 and Kv3.1 potassium channels in mammalian brain. *J Neurosci* **23**(22), 8077-91.

McGuire, L. I., Peden, A. H., Orru, C. D., Wilham, J. M., Appleford, N. E., Mallinson, G., Andrews, M., Head, M. W., Caughey, B., Will, R. G., *et al.* (2012). Real time quaking-induced conversion analysis of cerebrospinal fluid in sporadic Creutzfeldt-Jakob disease. *Annals of neurology* **72**(2), 278-85.

Monello, R. J., Powers, J. G., Hobbs, N. T., Spraker, T. R., O'Rourke, K. I., and Wild, M. A. (2013). Efficacy of antemortem rectal biopsies to diagnose and estimate prevalence of chronic wasting disease in free-ranging cow elk (Cervus elaphus nelsoni). *Journal of wildlife diseases* **49**(2), 270-8.

Moore, S. J., Kunkle, R., Greenlee, M. H., Nicholson, E., Richt, J., Hamir, A., Waters, W. R., and Greenlee, J. (2016). Horizontal Transmission of Chronic Wasting Disease in Reindeer. *Emerg Infect Dis* **22**(12), 2142-2145.

Moore, S. J., West Greenlee, M. H., Kondru, N., Manne, S., Smith, J. D., Kunkle, R. A., Kanthasamy, A., and Greenlee, J. J. (2017a). Experimental transmission of the chronic wasting disease agent to swine after oral or intracranial inoculation. *J Virol* doi: 10.1128/jvi.00926-17.

Moore, S. J., West Greenlee, M. H., Kondru, N., Manne, S., Smith, J. D., Kunkle, R. A., Kanthasamy, A., and Greenlee, J. J. (2017b). Experimental Transmission of the Chronic Wasting Disease Agent to Swine after Oral or Intracranial Inoculation. *J. Virol.* **91**(19).

Moreno, J. A., Streifel, K. M., Sullivan, K. A., Hanneman, W. H., and Tjalkens, R. B. (2011). Manganese-induced NF-kappaB activation and nitrosative stress is decreased by estrogen in juvenile mice. *Toxicol Sci* **122**(1), 121-33.

Morrison, B., 3rd, Cater, H. L., Benham, C. D., and Sundstrom, L. E. (2006). An in vitro model of traumatic brain injury utilising two-dimensional stretch of organotypic hippocampal slice cultures. *J Neurosci Methods* **150**(2), 192-201.

Morrison, B., 3rd, Eberwine, J. H., Meaney, D. F., and McIntosh, T. K. (2000). Traumatic injury induces differential expression of cell death genes in organotypic brain slice cultures determined by complementary DNA array hybridization. *Neuroscience* **96**(1), 131-9.

Nalls, A. V., McNulty, E., Powers, J., Seelig, D. M., Hoover, C., Haley, N. J., Hayes-Klug, J., Anderson, K., Stewart, P., Goldmann, W., *et al.* (2013). Mother to offspring transmission of chronic wasting disease in reeves' muntjac deer. *PloS one* **8**(8), e71844.

Nguyen, T., Sakasegawa, Y., Doh-Ura, K., and Go, M. L. (2011). Anti-prion activities and drug-like potential of functionalized quinacrine analogs with basic phenyl residues at the 9-amino position. *Eur J Med Chem* **46**(7), 2917-29.

Nichols, T. A., Fischer, J. W., Spraker, T. R., Kong, Q., and VerCauteren, K. C. (2015). CWD prions remain infectious after passage through the digestive system of coyotes (Canis latrans). *Prion* **9**(5), 367-75.

Nichols, T. A., Pulford, B., Wyckoff, A. C., Meyerett, C., Michel, B., Gertig, K., Hoover, E. A., Jewell, J. E., Telling, G. C., and Zabel, M. D. (2009). Detection of protease-resistant cervid prion protein in water from a CWD-endemic area. *Prion* **3**(3), 171-83.

Nichols, T. A., Spraker, T. R., Gidlewski, T., Powers, J. G., Telling, G. C., VerCauteren, K. C., and Zabel, M. D. (2012). Detection of prion protein in the cerebrospinal fluid of elk (Cervus canadensis nelsoni) with chronic wasting disease using protein misfolding cyclic amplification. *J Vet Diagn Invest* **24**(4), 746-9.

Noraberg, J., Kristensen, B. W., and Zimmer, J. (1999). Markers for neuronal degeneration in organotypic slice cultures. *Brain Res Brain Res Protoc* **3**(3), 278-90.

Ohnishi, T., Matsumura, H., Izumoto, S., Hiraga, S., and Hayakawa, T. (1998). A novel model of glioma cell invasion using organotypic brain slice culture. *Cancer Res* **58**(14), 2935-40.

Orihuela, R., McPherson, C. A., and Harry, G. J. (2016). Microglial M1/M2 polarization and metabolic states. *British journal of pharmacology* **173**(4), 649-65.

Orru, C. D., Bongianni, M., Tonoli, G., Ferrari, S., Hughson, A. G., Groveman, B. R., Fiorini, M., Pocchiari, M., Monaco, S., Caughey, B., *et al.* (2014). A test for Creutzfeldt-Jakob disease using nasal brushings. *The New England journal of medicine* **371**(6), 519-29.

Orru, C. D., Favole, A., Corona, C., Mazza, M., Manca, M., Groveman, B. R., Hughson, A. G., Acutis, P. L., Caramelli, M., Zanusso, G., *et al.* (2015a). Detection and discrimination of classical and atypical L-type bovine spongiform encephalopathy by real-time quaking-induced conversion. *Journal of clinical microbiology* **53**(4), 1115-20.

Orru, C. D., Groveman, B. R., Hughson, A. G., Zanusso, G., Coulthart, M. B., and Caughey, B. (2015b). Rapid and sensitive RT-QuIC detection of human Creutzfeldt-Jakob disease using cerebrospinal fluid. *mBio* **6**(1).

Orru, C. D., Groveman, B. R., Raymond, L. D., Hughson, A. G., Nonno, R., Zou, W., Ghetti, B., Gambetti, P., and Caughey, B. (2015c). Bank Vole Prion Protein As an Apparently Universal Substrate for RT-QuIC-Based Detection and Discrimination of Prion Strains. *PLoS pathogens* **11**(6), e1004983.

Orrú, C. D., Groveman, B. R., Raymond, L. D., Hughson, A. G., Nonno, R., Zou, W., Ghetti, B., Gambetti, P., and Caughey, B. (2015). Bank Vole Prion Protein As an Apparently Universal Substrate for RT-QuIC-Based Detection and Discrimination of Prion Strains. *PLoS Pathog* **11**(6), e1004983.

Orru, C. D., Wilham, J. M., Raymond, L. D., Kuhn, F., Schroeder, B., Raeber, A. J., and Caughey, B. (2011). Prion disease blood test using immunoprecipitation and improved quaking-induced conversion. *mBio* **2**(3), e00078-11.

Ostergaard, K., Finsen, B., and Zimmer, J. (1995). Organotypic slice cultures of the rat striatum: an immunocytochemical, histochemical and in situ hybridization study of somatostatin, neuropeptide Y, nicotinamide adenine dinucleotide phosphate-diaphorase, and enkephalin. *Exp Brain Res* **103**(1), 70-84.

Pahan, K., Sheikh, F. G., Liu, X., Hilger, S., McKinney, M., and Petro, T. M. (2001). Induction of Nitric-oxide Synthase and Activation of NF-κB by Interleukin-12 p40 in Microglial Cells. *Journal of Biological Chemistry* **276**(11), 7899-7905.

Petković, F., and Castellano, B. (2016). The role of interleukin-6 in central nervous system demyelination. *Neural Regeneration Research* **11**(12), 1922-1923.

Piehler, A., Kaminski, W. E., Wenzel, J. J., Langmann, T., and Schmitz, G. (2002). Molecular structure of a novel cholesterol-responsive A subclass ABC transporter, ABCA9. *Biochem Biophys Res Commun* **295**(2), 408-16.

Prusiner, S. B. (1998). Prions. *Proceedings of the National Academy of Sciences of the United States of America* **95**(23), 13363-13383.

Prusiner, S. B., Woerman, A. L., Mordes, D. A., Watts, J. C., Rampersaud, R., Berry, D. B., Patel, S., Oehler, A., Lowe, J. K., Kravitz, S. N., *et al.* (2015). Evidence for α-synuclein prions causing

multiple system atrophy in humans with parkinsonism. *Proceedings of the National Academy of Sciences* **112**(38), E5308-E5317.

Race, B., Meade-White, K. D., Phillips, K., Striebel, J., Race, R., and Chesebro, B. (2014). Chronic wasting disease agents in nonhuman primates. *Emerg Infect Dis* **20**(5), 833-7.
Ransohoff, R. M., and Perry, V. H. (2009). Microglial physiology: unique stimuli, specialized responses. *Annual review of immunology* **27**, 119-45.

Ratsimandresey, R. A., Dorfleutner, A., and Stehlik, C. (2013). An Update on PYRIN Domain-Containing Pattern Recognition Receptors: From Immunity to Pathology. *Frontiers in immunology* **4**, 440.
Ren, B., Yu, S., Chen, C., Wang, L., Liu, Z., Wu, Q., Wang, L., Zhao, K., and Yang, X. (2015). Invasion and anti-invasion research of glioma cells in an improved model of organotypic brain slice culture. *Tumori* **101**(4), 390-7.

Reus, G. Z., Fries, G. R., Stertz, L., Badawy, M., Passos, I. C., Barichello, T., Kapczinski, F., and Quevedo, J. (2015). The role of inflammation and microglial activation in the pathophysiology of psychiatric disorders. *Neuroscience* **300**, 141-54.

Ricci, A., Allende, A., Bolton, D., Chemaly, M., Davies, R., Escámez, P. S. F., Gironés, R., Herman, L., Koutsoumanis, K., Lindqvist, R., *et al.* (2018). Scientific opinion on chronic wasting disease (II). *EFSA Journal* **16**(1), e05132.

Ridley, A. J. Rho GTPases and actin dynamics in membrane protrusions and vesicle trafficking. *Trends in Cell Biology* **16**(10), 522-529.

Roy, A., Ghosh, A., Jana, A., Liu, X., Brahmachari, S., Gendelman, H. E., and Pahan, K. (2012). Sodium Phenylbutyrate Controls Neuroinflammatory and Antioxidant Activities and Protects Dopaminergic Neurons in Mouse Models of Parkinson's Disease. *PLOS ONE* **7**(6), e38113.

Salter, M. W., and Stevens, B. (2017). Microglia emerge as central players in brain disease. *Nat Med* **23**(9), 1018-1027.

Sanchez-Guajardo, V., Tentillier, N., and Romero-Ramos, M. (2015). The relation between α-synuclein and microglia in Parkinson's disease: Recent developments. *Neuroscience* **302**, 47-58.

Saunders, S. E., Bartelt-Hunt, S. L., and Bartz, J. C. (2012). Occurrence, transmission, and zoonotic potential of chronic wasting disease. *Emerg Infect Dis* **18**(3), 369-76.

Seelig, D. M., Nalls, A. V., Flasik, M., Frank, V., Eaton, S., Mathiason, C. K., and Hoover, E. A. (2015). Lesion profiling and subcellular prion localization of cervid chronic wasting disease in domestic cats. *Vet Pathol* **52**(1), 107-19.

Shi, S., Mitteregger-Kretzschmar, G., Giese, A., and Kretzschmar, H. A. (2013). Establishing quantitative real-time quaking-induced conversion (qRT-QuIC) for highly sensitive detection and quantification of PrPSc in prion-infected tissues. *Acta Neuropathol Commun* **1**(1), 44.

Shideman, C. R., Hu, S., Peterson, P. K., and Thayer, S. A. (2006). CCL5 evokes calcium signals in microglia through a kinase-, phosphoinositide-, and nucleotide-dependent mechanism. *Journal of Neuroscience Research* **83**(8), 1471-1484.

Shiratori, M., Tozaki-Saitoh, H., Yoshitake, M., Tsuda, M., and Inoue, K. (2010). P2X7 receptor activation induces CXCL2 production in microglia through NFAT and PKC/MAPK pathways. *J Neurochem* **114**(3), 810-9.

Sigurdson, C. J., Mathiason, C. K., Perrott, M. R., Eliason, G. A., Spraker, T. R., Glatzel, M., Manco, G., Bartz, J. C., Miller, M. W., and Hoover, E. A. (2008). Experimental chronic wasting disease (CWD) in the ferret. *J Comp Pathol* **138**(4), 189-96.

Smith, T. K., Ikeda, Y., Fujii, J., Taniguchi, N., and Meister, A. (1995). Different sites of acivicin binding and inactivation of gamma-glutamyl transpeptidases. *Proceedings of the National Academy of Sciences of the United States of America* **92**(6), 2360-4.

Solga, A. C., Pong, W. W., Kim, K. Y., Cimino, P. J., Toonen, J. A., Walker, J., Wylie, T., Magrini, V., Griffith, M., Griffith, O. L., *et al.* (2015). RNA Sequencing of Tumor-Associated Microglia Reveals Ccl5 as a Stromal Chemokine Critical for Neurofibromatosis-1 Glioma Growth. *Neoplasia (New York, N.Y.)* **17**(10), 776-88.

Solomon, I. H., Schepker, J. A., and Harris, D. A. (2010). Prion neurotoxicity: insights from prion protein mutants. *Current issues in molecular biology* **12**(2), 51-61.

Sonati, T., Reimann, R. R., Falsig, J., Baral, P. K., O'Connor, T., Hornemann, S., Yaganoglu, S., Li, B., Herrmann, U. S., Wieland, B., *et al.* (2013). The toxicity of antiprion antibodies is mediated by the flexible tail of the prion protein. *Nature* **501**(7465), 102-6.

Stojakovic, A., Paz-Filho, G., Arcos-Burgos, M., Licinio, J., Wong, M.-L., and Mastronardi, C. A. (2017). Role of the IL-1 Pathway in Dopaminergic Neurodegeneration and Decreased Voluntary Movement. *Molecular Neurobiology* **54**(6), 4486-4495 (journal article).

Stoppini, L., Buchs, P. A., and Muller, D. (1991). A simple method for organotypic cultures of nervous tissue. *Journal of Neuroscience Methods* **37**(2), 173-182.

Straccia, M., Gresa-Arribas, N., Dentesano, G., Ejarque-Ortiz, A., Tusell, J. M., Serratosa, J., Solà, C., and Saura, J. (2011). Pro-inflammatory gene expression and neurotoxic effects of activated microglia are attenuated by absence of CCAAT/enhancer binding protein β. *Journal of Neuroinflammation* **8**(1), 156 (journal article).

Streifel, K. M., Moreno, J. A., Hanneman, W. H., Legare, M. E., and Tjalkens, R. B. (2012). Gene deletion of nos2 protects against manganese-induced neurological dysfunction in juvenile mice. *Toxicol Sci* **126**(1), 183-92.

Sun, F., Anantharam, V., Latchoumycandane, C., Kanthasamy, A., and Kanthasamy, A. G. (2005). Dieldrin induces ubiquitin-proteasome dysfunction in alpha-synuclein overexpressing dopaminergic neuronal cells and enhances susceptibility to apoptotic cell death. *The Journal of pharmacology and experimental therapeutics* **315**(1), 69-79.

Suuronen, T., Huuskonen, J., Pihlaja, R., Kyrylenko, S., and Salminen, A. (2003). Regulation of microglial inflammatory response by histone deacetylase inhibitors. *J Neurochem* **87**(2), 407-16.
Sygnecka, K., Heider, A., Scherf, N., Alt, R., Franke, H., and Heine, C. (2015). Mesenchymal stem cells support neuronal fiber growth in an organotypic brain slice co-culture model. *Stem Cells Dev* **24**(7), 824-35.

Tanvig, M., Blaabjerg, M., Andersen, R. K., Villa, A., Rosager, A. M., Poulsen, F. R., Martinez-Serrano, A., Zimmer, J., and Meyer, M. (2009). A brain slice culture model for studies of endogenous and exogenous precursor cell migration in the rostral migratory stream. *Brain Res* **1295**, 1-12.
Thériault, P., and Rivest, S. (2016). Microglia: Senescence Impairs Clearance of Myelin Debris. *Current Biology* **26**(16), R772-R775.

Thomas, A. G., Vornov, J. J., Olkowski, J. L., Merion, A. T., and Slusher, B. S. (2000). N-Acetylated α-Linked Acidic Dipeptidase Converts N-Acetylaspartylglutamate from a Neuroprotectant to a Neurotoxin. *Journal of Pharmacology and Experimental Therapeutics* **295**(1), 16-22.

Thomas, D. M., Francescutti-Verbeem, D. M., and Kuhn, D. M. (2006). Gene expression profile of activated microglia under conditions associated with dopamine neuronal damage. *The FASEB Journal* **20**(3), 515-517.

Ullrich, C., and Humpel, C. (2009). Rotenone induces cell death of cholinergic neurons in an organotypic co-culture brain slice model. *Neurochem Res* **34**(12), 2147-53.

Vascellari, S., Orru, C. D., Hughson, A. G., King, D., Barron, R., Wilham, J. M., Baron, G. S., Race, B., Pani, A., and Caughey, B. (2012). Prion seeding activities of mouse scrapie strains with divergent PrPSc protease sensitivities and amyloid plaque content using RT-QuIC and eQuIC. *PloS one* **7**(11), e48969.

West Greenlee, M. H., Lind, M., Kokemueller, R., Mammadova, N., Kondru, N., Manne, S., Smith, J., Kanthasamy, A., and Greenlee, J. Temporal Resolution of Misfolded Prion Protein Transport, Accumulation, Glial Activation, and Neuronal Death in the Retinas of Mice Inoculated with Scrapie. *The American Journal of Pathology* doi: 10.1016/j.ajpath.2016.05.018.

West Greenlee, M. H., Lind, M., Kokemuller, R., Mammadova, N., Kondru, N., Manne, S., Smith, J., Kanthasamy, A., and Greenlee, J. (2016). Temporal Resolution of Misfolded Prion Protein Transport, Accumulation, Glial Activation, and Neuronal Death in the Retinas of Mice Inoculated with Scrapie. *The American journal of pathology* **186**(9), 2302-9.

Wilham, J. M., Orru, C. D., Bessen, R. A., Atarashi, R., Sano, K., Race, B., Meade-White, K. D., Taubner, L. M., Timmes, A., and Caughey, B. (2010). Rapid end-point quantitation of prion seeding activity with sensitivity comparable to bioassays. *PLoS Pathog* **6**(12), e1001217.

Williams, E. S., and Young, S. (1980). Chronic wasting disease of captive mule deer: a spongiform encephalopathy. *Journal of wildlife diseases* **16**(1), 89-98.

Williams, E. S., and Young, S. (1993). Neuropathology of chronic wasting disease of mule deer (Odocoileus hemionus) and elk (Cervus elaphus nelsoni). *Vet Pathol* **30**(1), 36-45.

Wilson, R., Plinston, C., Hunter, N., Casalone, C., Corona, C., Tagliavini, F., Suardi, S., Ruggerone, M., Moda, F., Graziano, S., *et al.* (2012). Chronic wasting disease and atypical forms of bovine spongiform encephalopathy and scrapie are not transmissible to mice expressing wild-type levels of human prion protein. *J Gen Virol* **93**(Pt 7), 1624-9.

Wolf, H., Hossinger, A., Fehlinger, A., Buttner, S., Sim, V., McKenzie, D., and Vorberg, I. M. (2015). Deposition pattern and subcellular distribution of disease-associated prion protein in cerebellar organotypic slice cultures infected with scrapie. *Front Neurosci* **9**, 410.

Xiang, W., Windl, O., Wunsch, G., Dugas, M., Kohlmann, A., Dierkes, N., Westner, I. M., and Kretzschmar, H. A. (2004). Identification of differentially expressed genes in scrapie-infected mouse brains by using global gene expression technology. *Journal of virology* **78**(20), 11051-60.

Yoon, J. J., Nicholson, L. F., Feng, S. X., Vis, J. C., and Green, C. R. (2010). A novel method of organotypic brain slice culture using connexin-specific antisense oligodeoxynucleotides to improve neuronal survival. *Brain Res* **1353**, 194-203.

Zhang, P., Wong, T. A., Lokuta, K. M., Turner, D. E., Vujisic, K., and Liu, B. (2009). Microglia enhance manganese chloride-induced dopaminergic neurodegeneration: role of free radical generation. *Experimental neurology* **217**(1), 219-230.

Zhang, Y., Chen, K., Sloan, S. A., Bennett, M. L., Scholze, A. R., O'Keeffe, S., Phatnani, H. P., Guarnieri, P., Caneda, C., Ruderisch, N., *et al.* (2014). An RNA-Sequencing Transcriptome and Splicing Database of Glia, Neurons, and Vascular Cells of the Cerebral Cortex. *The Journal of Neuroscience* **34**(36), 11929-11947.

Zwilling, D., Huang, S.-Y., Sathyasaikumar, Korrapati V., Notarangelo, Francesca M., Guidetti, P., Wu, H.-Q., Lee, J., Truong, J., Andrews-Zwilling, Y., Hsieh, Eric W., *et al.* (2011). Kynurenine 3-Monooxygenase Inhibition in Blood Ameliorates Neurodegeneration. *Cell* **145**(6), 863-874.

Supplementary table 1: Misfolded α-Synuclein treatment caused upregulation in the genes in microglia >5 fold

Gene	***Name***	***Fold Change***
Il6	interleukin 6	714
Lcn2	lipocalin 2	510
Fpr1	formyl peptide receptor 1	364
Il1b	interleukin 1 beta	345
Slfn1	schlafen 1	317
Csf3	colony stimulating factor 3 (granulocyte)	237
Bcl2a1a	B cell leukemia/lymphoma 2 related protein A1a	229
Il1a	interleukin 1 alpha	190
Nos2	nitric oxide synthase 2, inducible	180
Adh7	alcohol dehydrogenase 7 (class IV), mu or sigma polypeptide	133
Cxcl3	chemokine (C-X-C motif) ligand 3	125
Gstt4	glutathione S-transferase, theta 4	108
Urah	urate (5-hydroxyiso-) hydrolase	103
Pydc4	pyrin domain containing 4	50
Serpinb2	serine (or cysteine) peptidase inhibitor, clade B, member 2	46
Ccl5	chemokine (C-C motif) ligand 5	43
Fpr2	formyl peptide receptor 2	38
Cxcl2	chemokine (C-X-C motif) ligand 2	37
4921529L05 Rik	RIKEN cDNA 4921529L05 gene	36
Zbp1	Z-DNA binding protein 1	36
Traf1	TNF receptor-associated factor 1	36
Ccl12	chemokine (C-C motif) ligand 12	28
Irg1	immunoresponsive gene 1	26
Ptgs2	prostaglandin-endoperoxide synthase 2	25
Upp1	uridine phosphorylase 1	22
Cxcl10	chemokine (C-X-C motif) ligand 10	20
6530402F18 Rik	RIKEN cDNA 6530402F18 gene	19
Ly6a	lymphocyte antigen 6 complex, locus A	18
Zfp811	zinc finger protein 811	17
Pyhin1	pyrin and HIN domain family, member 1	17
Isg15	ISG15 ubiquitin-like modifier	17
Tarm1	T cell-interacting, activating receptor on myeloid cells 1	16
AA467197	expressed sequence AA467197	16
Saa3	serum amyloid A 3	16
Pydc3	pyrin domain containing 3	15
Gm5483	predicted gene 5483	14
Rsad2	radical S-adenosyl methionine domain containing 2	14

Supplementary table 1 (continued)

Tnn	tenascin N	14
Ccl7	chemokine (C-C motif) ligand 7	13
Gbp5	guanylate binding protein 5	13
Ifit3	interferon-induced protein with tetratricopeptide repeats 3	13
Lipg	lipase, endothelial	12
Hdc	histidine decarboxylase	12
Avil	advillin	12
Ifit1	interferon-induced protein with tetratricopeptide repeats 1	11
Edn1	endothelin 1	11
Isg20	interferon-stimulated protein	11
Pilrb1	paired immunoglobin-like type 2 receptor beta 1	11
Aqp9	aquaporin 9	10
Fam171b	family with sequence similarity 171, member B	10
Apol9b	apolipoprotein L 9b	10
Procr	protein C receptor, endothelial	10
Socs2	suppressor of cytokine signaling 2	10
Mmp13	matrix metallopeptidase 13	9
Tgm1	transglutaminase 1, K polypeptide	9
Lix1	limb expression 1 homolog (chicken)	9
Socs3	suppressor of cytokine signaling 3	9
Gbp7	guanylate binding protein 7	9
Gbp4	guanylate binding protein 4	9
2010005H15 Rik	RIKEN cDNA 2010005H15 gene	9
I830012O16 Rik	NA	9
Osbp2	oxysterol binding protein 2	9
Mx2	MX dynamin-like GTPase 2	9
Apol9a	apolipoprotein L 9a	9
Thbs1	thrombospondin 1	8
9430076C15 Rik	RIKEN cDNA 9430076C15 gene	8
Cish	cytokine inducible SH2-containing protein	8
Gbp2	guanylate binding protein 2	8
Gbp3	guanylate binding protein 3	8
Lif	leukemia inhibitory factor	8
Ifi44	interferon-induced protein 44	8
Gm14446	NA	8
Cmpk2	cytidine monophosphate (UMP-CMP) kinase 2, mitochondrial	8
Irf7	interferon regulatory factor 7	8
Agpat9	1-acylglycerol-3-phosphate O-acyltransferase 9	7
Trim30d	tripartite motif-containing 30D	7
Mnda	myeloid cell nuclear differentiation antigen	7
Serpine1	serine (or cysteine) peptidase inhibitor, clade E, member 1	7

Supplementary table 1 (continued)

Mx1	MX dynamin-like GTPase 1	7
Nfkbiz	nuclear factor of kappa light polypeptide gene enhancer in B cells inhibitor, zeta	7
Ddit3	DNA-damage inducible transcript 3	6
Klra2	killer cell lectin-like receptor, subfamily A, member 2	6
Slamf7	SLAM family member 7	6
Gpr31b	G protein-coupled receptor 31, D17Leh66b region	6
Ifit2	interferon-induced protein with tetratricopeptide repeats 2	6
Il1rn	interleukin 1 receptor antagonist	6
Msr1	macrophage scavenger receptor 1	6
Ccl2	chemokine (C-C motif) ligand 2	6
Angptl3	angiopoietin-like 3	6
Pou2f2	POU domain, class 2, transcription factor 2	6
Pla1a	phospholipase A1 member A	6
Ptpn14	protein tyrosine phosphatase, non-receptor type 14	6
F5	coagulation factor V	6
Gm4070	predicted gene 4070	6
Pilra	paired immunoglobin-like type 2 receptor alpha	6
Hid1	HID1 domain containing	6
Ptger2	prostaglandin E receptor 2 (subtype EP2)	6
Oasl2	2'-5' oligoadenylate synthetase-like 2	6
Ifi204	interferon activated gene 204	6
Lta	lymphotoxin A	6
Oasl1	2'-5' oligoadenylate synthetase-like 1	6
Slc15a3	solute carrier family 15, member 3	6
Wfdc17	WAP four-disulfide core domain 17	6
Cdcp1	CUB domain containing protein 1	5
Zc3h12a	zinc finger CCCH type containing 12A	5
Usp18	ubiquitin specific peptidase 18	5
Trem1	triggering receptor expressed on myeloid cells 1	5
Nox1	NADPH oxidase 1	5
Fcgr1	Fc receptor, IgG, high affinity I	5
Sell	selectin, lymphocyte	5

Supplementary table 2: Misfolded α-Synuclein treatment caused downregulation in the genes in microglia >5 fold

Gene	***Name***	***Fold Change***
Cecr6	cat eye syndrome chromosome region, candidate 6	-179
Sema4g	sema domain, immunoglobulin domain (Ig), transmembrane domain (TM) and short cytoplasmic domain, (semaphorin) 4G	-54
Tspan10	tetraspanin 10	-46
Serpinb1a	serine (or cysteine) peptidase inhibitor, clade B, member 1a	-25
Ocstamp	osteoclast stimulatory transmembrane protein	-22
Cx3cr1	chemokine (C-X3-C motif) receptor 1	-17
Lifr	leukemia inhibitory factor receptor	-16
Asb10	ankyrin repeat and SOCS box-containing 10	-16
Cd24a	CD24a antigen	-14
Camk2b	calcium/calmodulin-dependent protein kinase II, beta	-14
Gm5086	predicted gene 5086	-12
Slc14a1	solute carrier family 14 (urea transporter), member 1	-12
Hpgd	hydroxyprostaglandin dehydrogenase 15 (NAD)	-12
Klhl38	kelch-like 38	-12
Fcrls	Fc receptor-like S, scavenger receptor	-10
Klrd1	killer cell lectin-like receptor, subfamily D, member 1	-9
Srpk3	serine/arginine-rich protein specific kinase 3	-9
Pdk2	pyruvate dehydrogenase kinase, isoenzyme 2	-9
Armc2	armadillo repeat containing 2	-9
Pacsin1	protein kinase C and casein kinase substrate in neurons 1	-8
Mn1	meningioma 1	-8
Gpr162	G protein-coupled receptor 162	-7
Cmbl	carboxymethylenebutenolidase-like (Pseudomonas)	-7
Pianp	PILR alpha associated neural protein	-6
Lsp1	lymphocyte specific 1	-6
Crip1	cysteine-rich protein 1 (intestinal)	-6
Ppfia4	protein tyrosine phosphatase, receptor type, f polypeptide (PTPRF), interacting protein (liprin), alpha 4	-6
Lrrc14b	leucine rich repeat containing 14B	-6
Atp6v0d2	ATPase, H+ transporting, lysosomal V0 subunit D2	-5
Kcne3	potassium voltage-gated channel, Isk-related subfamily, gene 3	-5
9330188P03Rik	RIKEN cDNA 9330188P03 gene	-5
Aif1	allograft inflammatory factor 1	-5

Supplementary table 3: Manganese treatment caused upregulation in the genes in microglia >5 fold

Gene	***Name***	***Fold change***
Gsta2	glutathione S-transferase, alpha 2 (Yc2)	265
Sstr5	somatostatin receptor 5	260
Adh7	alcohol dehydrogenase 7 (class IV), mu or sigma polypeptide	247
H2-Q9	histocompatibility 2, Q region locus 9	191
Vat1l	vesicle amine transport protein 1 homolog-like (T. californica)	151
Car6	carbonic anhydrase 6	145
Tnfsf4	tumor necrosis factor (ligand) superfamily, member 4	113
Agpat9	1-acylglycerol-3-phosphate O-acyltransferase 9	107
Dio2	deiodinase, iodothyronine, type II	95
Spta1	spectrin alpha, erythrocytic 1	92
Rtn4r	reticulon 4 receptor	86
Cd207	CD207 antigen	84
Osbp2	oxysterol binding protein 2	71
Calcb	calcitonin-related polypeptide, beta	66
Rhpn2	rhophilin, Rho GTPase binding protein 2	65
Wnt9a	wingless-type MMTV integration site family, member 9A	62
Ptgs2	prostaglandin-endoperoxide synthase 2	58
Avil	advillin	58
Mmp13	matrix metallopeptidase 13	56
AA467197	expressed sequence AA467197	52
Il6	interleukin 6	52
Mmp10	matrix metallopeptidase 10	48
Myc	myelocytomatosis oncogene	45
Cyp11a1	cytochrome P450, family 11, subfamily a, polypeptide 1	44
Nptx1	neuronal pentraxin 1	44
Myo7b	myosin VIIB	41
Pgf	placental growth factor	41
Ccbe1	collagen and calcium binding EGF domains 1	41
Pydc4	pyrin domain containing 4	41
Serpinb2	serine (or cysteine) peptidase inhibitor, clade B, member 2	40
Rgs9	regulator of G-protein signaling 9	40
Prph	peripherin	39
Spsb1	splA/ryanodine receptor domain and SOCS box containing 1	36
Akap2	A kinase (PRKA) anchor protein 2	36
Lcn2	lipocalin 2	34
Mt3	metallothionein 3	34
Ccdc136	coiled-coil domain containing 136	33
Slc16a14	solute carrier family 16 (monocarboxylic acid transporters), member 14	32
Stbd1	starch binding domain 1	32

Supplementary table 3 (continued)

Cdcp1	CUB domain containing protein 1	30
Dthd1	death domain containing 1	29
Ddit3	DNA-damage inducible transcript 3	27
5031410I06Rik	RIKEN cDNA 5031410I06 gene	26
Efcab6	EF-hand calcium binding domain 6	26
Nyap2	neuronal tyrosine-phophorylated phosphoinositide 3-kinase adaptor 2	26
Procr	protein C receptor, endothelial	26
Rgs16	regulator of G-protein signaling 16	25
Dusp1	dual specificity phosphatase 1	25
A530064D06Rik	RIKEN cDNA A530064D06 gene	25
Dusp8	dual specificity phosphatase 8	25
Nos2	nitric oxide synthase 2, inducible	25
Dusp5	dual specificity phosphatase 5	25
Lif	leukemia inhibitory factor	24
Fam171b	family with sequence similarity 171, member B	24
Mylk2	myosin, light polypeptide kinase 2, skeletal muscle	23
Gpr126	NA	23
Pxdc1	PX domain containing 1	22
Gprc5a	G protein-coupled receptor, family C, group 5, member A	21
Cited1	Cbp/p300-interacting transactivator with Glu/Asp-rich carboxy-terminal domain 1	20
Slc1a1	solute carrier family 1 (neuronal/epithelial high affinity glutamate transporter, system Xag), member 1	20
Itga3	integrin alpha 3	20
Cdkn1c	cyclin-dependent kinase inhibitor 1C (P57)	19
Gadd45a	growth arrest and DNA-damage-inducible 45 alpha	19
Fam83g	family with sequence similarity 83, member G	18
I830012O16Rik	NA	18
Adm	adrenomedullin	18
Gbp8	guanylate-binding protein 8	18
Nox3	NADPH oxidase 3	18
Pira11	paired-Ig-like receptor A11	18
Isg20	interferon-stimulated protein	17
Ifit3	interferon-induced protein with tetratricopeptide repeats 3	17
Pydc3	pyrin domain containing 3	17
Lat	linker for activation of T cells	16
Trib3	tribbles homolog 3 (Drosophila)	16
Gsta3	glutathione S-transferase, alpha 3	16
Gm20594	predicted gene, 20594	16
Ntn1	netrin 1	16
2010005H15Rik	RIKEN cDNA 2010005H15 gene	16

Supplementary table 3 (continued)

Gm5483	predicted gene 5483	16
Rhov	ras homolog gene family, member V	16
Sccpdh	saccharopine dehydrogenase (putative)	15
Jag1	jagged 1	15
Apol9b	apolipoprotein L 9b	15
Lamc2	laminin, gamma 2	15
Bcar1	breast cancer anti-estrogen resistance 1	15
Rsad2	radical S-adenosyl methionine domain containing 2	15
Fam71f2	family with sequence similarity 71, member F2	14
Abcb9	ATP-binding cassette, sub-family B (MDR/TAP), member 9	14
Neurl1a	neuralized E3 ubiquitin protein ligase 1A	14
Gdf15	growth differentiation factor 15	14
Hid1	HID1 domain containing	14
Rph3al	rabphilin 3A-like (without C2 domains)	13
Grb10	growth factor receptor bound protein 10	13
Csn3	casein kappa	13
Pfn2	profilin 2	13
Prkg2	protein kinase, cGMP-dependent, type II	13
Fignl2	fidgetin-like 2	13
Serpine1	serine (or cysteine) peptidase inhibitor, clade E, member 1	13
Plat	plasminogen activator, tissue	13
Cxcl2	chemokine (C-X-C motif) ligand 2	13
Upp1	uridine phosphorylase 1	13
Ndrg1	N-myc downstream regulated gene 1	13
Spns2	spinster homolog 2	12
Rhou	ras homolog gene family, member U	12
B230312C02Rik	RIKEN cDNA B230312C02 gene	12
Epha2	Eph receptor A2	12
Aqp9	aquaporin 9	12
Ptpn14	protein tyrosine phosphatase, non-receptor type 14	12
Fcrlb	Fc receptor-like B	12
Arg1	arginase, liver	12
Tarm1	T cell-interacting, activating receptor on myeloid cells 1	11
Gm13889	predicted gene 13889	11
Wwc1	WW, C2 and coiled-coil domain containing 1	11
Cox6a2	cytochrome c oxidase subunit VIa polypeptide 2	11
Akr1b7	aldo-keto reductase family 1, member B7	11
Pyhin1	pyrin and HIN domain family, member 1	10
P4ha2	procollagen-proline, 2-oxoglutarate 4-dioxygenase (proline 4-hydroxylase), alpha II polypeptide	10
Src	Rous sarcoma oncogene	10
1700030J22Rik	RIKEN cDNA 1700030J22 gene	10

Supplementary table 3 (continued)

Cd22	CD22 antigen	10
Gfod1	glucose-fructose oxidoreductase domain containing 1	10
Ptger2	prostaglandin E receptor 2 (subtype EP2)	10
F2rl2	coagulation factor II (thrombin) receptor-like 2	10
Lrrc32	leucine rich repeat containing 32	10
Apol9a	apolipoprotein L 9a	10
Isg15	ISG15 ubiquitin-like modifier	9
Ifit1	interferon-induced protein with tetratricopeptide repeats 1	9
Mt2	metallothionein 2	9
Cnga3	cyclic nucleotide gated channel alpha 3	9
Rbpms2	RNA binding protein with multiple splicing 2	9
Scg2	secretogranin II	9
Srxn1	sulfiredoxin 1 homolog (S. cerevisiae)	9
Hecw2	HECT, C2 and WW domain containing E3 ubiquitin protein ligase 2	9
Bean1	brain expressed, associated with Nedd4, 1	9
Ccl22	chemokine (C-C motif) ligand 22	9
Sema3e	sema domain, immunoglobulin domain (Ig), short basic domain, secreted, (semaphorin) 3E	9
Mgam	maltase-glucoamylase	9
Acsbg1	acyl-CoA synthetase bubblegum family member 1	9
Ifi44	interferon-induced protein 44	8
Angptl6	angiopoietin-like 6	8
Ccl12	chemokine (C-C motif) ligand 12	8
Sesn3	sestrin 3	8
Nupr1	nuclear protein transcription regulator 1	8
Notch4	notch 4	8
Mmp12	matrix metallopeptidase 12	8
B430306N03Rik	RIKEN cDNA B430306N03 gene	8
Slc35f1	solute carrier family 35, member F1	8
Il1f9	interleukin 1 family, member 9	8
Col20a1	collagen, type XX, alpha 1	8
Smyd1	SET and MYND domain containing 1	8
Gprc5b	G protein-coupled receptor, family C, group 5, member B	8
Plekhg1	pleckstrin homology domain containing, family G (with RhoGef domain) member 1	8
Galnt3	UDP-N-acetyl-alpha-D-galactosamine:polypeptide N-acetylgalactosaminyltransferase 3	8
Ptprn	protein tyrosine phosphatase, receptor type, N	8
Csf3	colony stimulating factor 3 (granulocyte)	8
Lix1	limb expression 1 homolog (chicken)	8
Nyap1	neuronal tyrosine-phosphorylated phosphoinositide 3-kinase adaptor 1	8
Adcy3	adenylate cyclase 3	7
Gm10220	predicted gene 10220	7

Supplementary table 3 (continued)

Cd274	CD274 antigen	7
Stk40	serine/threonine kinase 40	7
Pdlim7	PDZ and LIM domain 7	7
Nfkbiz	nuclear factor of kappa light polypeptide gene enhancer in B cells inhibitor, zeta	7
Slc7a11	solute carrier family 7 (cationic amino acid transporter, y+ system), member 11	7
Cdon	cell adhesion molecule-related/down-regulated by oncogenes	7
Atp13a4	ATPase type 13A4	7
Fgf9	fibroblast growth factor 9	7
Rora	RAR-related orphan receptor alpha	7
Arc	activity regulated cytoskeletal-associated protein	7
Ahr	aryl-hydrocarbon receptor	7
Smad7	SMAD family member 7	7
Rragd	Ras-related GTP binding D	7
Spry4	sprouty homolog 4 (Drosophila)	7
Sh3yl1	Sh3 domain YSC-like 1	7
Ttc12	tetratricopeptide repeat domain 12	7
Hist1h4m	histone cluster 1, H4m	7
Wdr65	NA	7
Acot2	acyl-CoA thioesterase 2	7
Hmcn1	hemicentin 1	7
Hs3st1	heparan sulfate (glucosamine) 3-O-sulfotransferase 1	7
Il1rn	interleukin 1 receptor antagonist	7
Pcdh1	protocadherin 1	7
Dusp10	dual specificity phosphatase 10	6
Ppp1r15a	protein phosphatase 1, regulatory (inhibitor) subunit 15A	6
Coro6	coronin 6	6
Sel1l3	sel-1 suppressor of lin-12-like 3 (C. elegans)	6
Rnf183	ring finger protein 183	6
Dysf	dysferlin	6
Smox	spermine oxidase	6
Il1a	interleukin 1 alpha	6
Zfp462	zinc finger protein 462	6
Bcar3	breast cancer anti-estrogen resistance 3	6
Cmpk2	cytidine monophosphate (UMP-CMP) kinase 2, mitochondrial	6
Serpinb9	serine (or cysteine) peptidase inhibitor, clade B, member 9	6
Pou6f1	POU domain, class 6, transcription factor 1	6
Adamts1	a disintegrin-like and metallopeptidase (reprolysin type) with thrombospondin type 1 motif, 1	6
Ifi204	interferon activated gene 204	6
F3	coagulation factor III	6
Hmox1	heme oxygenase 1	6
Hilpda	hypoxia inducible lipid droplet associated	6

Supplementary table 3 (continued)

Arnt2	aryl hydrocarbon receptor nuclear translocator 2	6
Oasl2	2'-5' oligoadenylate synthetase-like 2	6
Pla2g5	phospholipase A2, group V	6
Ccdc92	coiled-coil domain containing 92	6
Pim1	proviral integration site 1	6
Slc39a2	solute carrier family 39 (zinc transporter), member 2	6
Ankrd50	ankyrin repeat domain 50	6
Epb4.1l1	NA	6
Kdm7a	lysine (K)-specific demethylase 7A	6
Tinagl1	tubulointerstitial nephritis antigen-like 1	6
Klf4	Kruppel-like factor 4 (gut)	6
Smtn	smoothelin	6
Srgn	serglycin	6
Serpinb9b	serine (or cysteine) peptidase inhibitor, clade B, member 9b	6
Chac1	ChaC, cation transport regulator 1	6
Nxph3	neurexophilin 3	6
Aim1	absent in melanoma 1	6
Xaf1	XIAP associated factor 1	6
Ankrd33b	ankyrin repeat domain 33B	6
Mgarp	mitochondria localized glutamic acid rich protein	6
Spry2	sprouty homolog 2 (Drosophila)	6
Slc22a4	solute carrier family 22 (organic cation transporter), member 4	6
Trim30d	tripartite motif-containing 30D	6
Optn	optineurin	6
Zfr2	zinc finger RNA binding protein 2	6
Gm6634	predicted gene 6634	6
Prss50	protease, serine 50	6
Tnfsf18	tumor necrosis factor (ligand) superfamily, member 18	6
Phlda1	pleckstrin homology-like domain, family A, member 1	6
Sqstm1	sequestosome 1	5
Zdhhc18	zinc finger, DHHC domain containing 18	5
Ndst3	N-deacetylase/N-sulfotransferase (heparan glucosaminyl) 3	5
Cx3cl1	chemokine (C-X3-C motif) ligand 1	5
Gata3	GATA binding protein 3	5
Treml4	triggering receptor expressed on myeloid cells-like 4	5
Rasgef1a	RasGEF domain family, member 1A	5
Rab15	RAB15, member RAS oncogene family	5
Thbs1	thrombospondin 1	5
Mapre3	microtubule-associated protein, RP/EB family, member 3	5
Dok7	docking protein 7	5
Ptgir	prostaglandin I receptor (IP)	5
Ppfibp2	PTPRF interacting protein, binding protein 2 (liprin beta 2)	5
Rnf19b	ring finger protein 19B	5
Fam13a	family with sequence similarity 13, member A	5

Supplementary table 3 (continued)

H2-Q8	histocompatibility 2, Q region locus 8	5
Gm7609	predicted pseudogene 7609	5
Plk2	polo-like kinase 2	5
Slc22a18	solute carrier family 22 (organic cation transporter), member 18	5
Perm1	PPARGC1 and ESRR induced regulator, muscle 1	5
Lims2	LIM and senescent cell antigen like domains 2	5
Kdm6b	KDM1 lysine (K)-specific demethylase 6B	5
Mx2	MX dynamin-like GTPase 2	5
Papss2	3'-phosphoadenosine 5'-phosphosulfate synthase 2	5
Slc6a9	solute carrier family 6 (neurotransmitter transporter, glycine), member 9	5
Tgm1	transglutaminase 1, K polypeptide	5
Sema3c	sema domain, immunoglobulin domain (Ig), short basic domain, secreted, (semaphorin) 3C	5
Kpna4	karyopherin (importin) alpha 4	5
Tnfrsf9	tumor necrosis factor receptor superfamily, member 9	5
Rasip1	Ras interacting protein 1	5
Arid3b	AT rich interactive domain 3B (BRIGHT-like)	5
Padi2	peptidyl arginine deiminase, type II	5
Plcl1	phospholipase C-like 1	5
Plk3	polo-like kinase 3	5
Hivep2	human immunodeficiency virus type I enhancer binding protein 2	5
Sez6l2	seizure related 6 homolog like 2	5
Sgk1	serum/glucocorticoid regulated kinase 1	5
Ets1	E26 avian leukemia oncogene 1, 5' domain	5
Plin2	perilipin 2	5
Gpr141	G protein-coupled receptor 141	5
Fzd5	frizzled homolog 5 (Drosophila)	5
Ifit2	interferon-induced protein with tetratricopeptide repeats 2	5

Supplementary table 4: Mn treatment caused downregulation in the genes in microglia >5 fold

Gene	***Name***	***Fold change***
Hp	haptoglobin	-79
Cx3cr1	chemokine (C-X3-C motif) receptor 1	-14
Asb10	ankyrin repeat and SOCS box-containing 10	-12
Kmo	kynurenine 3-monooxygenase (kynurenine 3-hydroxylase)	-12
Ttn	titin	-12
Gm5086	predicted gene 5086	-11
D730005E14Rik	RIKEN cDNA D730005E14 gene	-10
Abca9	ATP-binding cassette, sub-family A (ABC1), member 9	-8
Sema4g	sema domain, immunoglobulin domain (Ig), transmembrane domain (TM) and short cytoplasmic domain, (semaphorin) 4G	-8
4930558J18Rik	RIKEN cDNA 4930558J18 gene	-8
Ankle1	ankyrin repeat and LEM domain containing 1	-8
Tlr2	toll-like receptor 2	-7
Pif1	PIF1 5'-to-3' DNA helicase homolog (S. cerevisiae)	-7
Hist1h2ao	histone cluster 1, H2ao	-7
Hpgd	hydroxyprostaglandin dehydrogenase 15 (NAD)	-7
Ttc30a1	tetratricopeptide repeat domain 30A1	-7
Tmem51	transmembrane protein 51	-7
Ppfia4	protein tyrosine phosphatase, receptor type, f polypeptide (PTPRF), interacting protein (liprin), alpha 4	-6
Gpr34	G protein-coupled receptor 34	-6
Camk2a	calcium/calmodulin-dependent protein kinase II alpha	-6
Cp	ceruloplasmin	-6
Cd24a	CD24a antigen	-6
Saa3	serum amyloid A 3	-6
Csf3r	colony stimulating factor 3 receptor (granulocyte)	-6
AA388235	expressed sequence AA388235	-6
Acat2	acetyl-Coenzyme A acetyltransferase 2	-6
Ms4a6c	membrane-spanning 4-domains, subfamily A, member 6C	-6
Xkr5	X Kell blood group precursor-related family, member 5	-6
Gpr183	G protein-coupled receptor 183	-6
Lrfn1	leucine rich repeat and fibronectin type III domain containing 1	-6
Aspm	asp (abnormal spindle)-like, microcephaly associated (Drosophila)	-6
2810055G20Rik	NA	-6
Armc2	armadillo repeat containing 2	-6
Car9	carbonic anhydrase 9	-6
Klhl23	kelch-like 23	-5

Supplementary table 4 (continued)		
Ccbl2	cysteine conjugate-beta lyase 2	-5
Sesn1	sestrin 1	-5
Rassf4	Ras association (RalGDS/AF-6) domain family member 4	-5
Arhgap19	Rho GTPase activating protein 19	-5
Tha1	threonine aldolase 1	-5
Nrp	NA	-5
F730043M19Rik	RIKEN cDNA F730043M19 gene	-5

Supplementary table 5: Mn and misfolded α-Synuclein co-treatment caused upregulation in the genes in microglia >5 fold

Gene	***Name***	***Fold change***
Il6	interleukin 6	3407
Urah	urate (5-hydroxyiso-) hydrolase	1453
Nos2	nitric oxide synthase 2, inducible	1141
Lcn2	lipocalin 2	1134
Csf3	colony stimulating factor 3 (granulocyte)	1099
Il12b	interleukin 12b	788
Adh7	alcohol dehydrogenase 7 (class IV), mu or sigma polypeptide	672
Il1b	interleukin 1 beta	664
Mmp3	matrix metallopeptidase 3	629
Il1f6	interleukin 1 family, member 6	513
Slfn1	schlafen 1	465
Ptgs2os	prostaglandin-endoperoxide synthase 2, opposite strand	319
Serpinb2	serine (or cysteine) peptidase inhibitor, clade B, member 2	293
Cxcl3	chemokine (C-X-C motif) ligand 3	278
Il1a	interleukin 1 alpha	269
Bcl2a1a	B cell leukemia/lymphoma 2 related protein A1a	242
H2-Q9	histocompatibility 2, Q region locus 9	231
Ptgs2	prostaglandin-endoperoxide synthase 2	222
Sstr5	somatostatin receptor 5	202
Ccl5	chemokine (C-C motif) ligand 5	181
Cxcl2	chemokine (C-X-C motif) ligand 2	174
Mmp13	matrix metallopeptidase 13	156
Gm5483	predicted gene 5483	138
Ifnb1	interferon beta 1, fibroblast	132
Cemip	cell migration inducing protein, hyaluronan binding	128
Plagl1	pleiomorphic adenoma gene-like 1	125
Traf1	TNF receptor-associated factor 1	123
Tmc7	transmembrane channel-like gene family 7	121
Dio2	deiodinase, iodothyronine, type II	121
Pydc4	pyrin domain containing 4	119
AA467197	expressed sequence AA467197	115
Mmp10	matrix metallopeptidase 10	110
Rsad2	radical S-adenosyl methionine domain containing 2	110
Ggt1	gamma-glutamyltransferase 1	108
Gm5416	predicted gene 5416	102
Upp1	uridine phosphorylase 1	100
BC100530	cDNA sequence BC100530	100
Pgf	placental growth factor	96
Lif	leukemia inhibitory factor	94

Supplementary table 5 (continued)

Rgs9	regulator of G-protein signaling 9	94
Tpbg	trophoblast glycoprotein	90
Gpr126	NA	79
Procr	protein C receptor, endothelial	75
Zbp1	Z-DNA binding protein 1	74
Tnn	tenascin N	67
Rtn4r	reticulon 4 receptor	65
Isg15	ISG15 ubiquitin-like modifier	64
Car6	carbonic anhydrase 6	62
Spta1	spectrin alpha, erythrocytic 1	59
Osbp2	oxysterol binding protein 2	56
Agpat9	1-acylglycerol-3-phosphate O-acyltransferase 9	55
Ifit3	interferon-induced protein with tetratricopeptide repeats 3	54
I830012O16Rik	NA	53
Cyp11a1	cytochrome P450, family 11, subfamily a, polypeptide 1	49
Ccl12	chemokine (C-C motif) ligand 12	48
2010005H15Rik	RIKEN cDNA 2010005H15 gene	47
Cmpk2	cytidine monophosphate (UMP-CMP) kinase 2, mitochondrial	47
Cxcl10	chemokine (C-X-C motif) ligand 10	45
Zfp811	zinc finger protein 811	45
Wnt9a	wingless-type MMTV integration site family, member 9A	45
Fam19a2	family with sequence similarity 19, member A2	45
Ifit1	interferon-induced protein with tetratricopeptide repeats 1	44
Irg1	immunoresponsive gene 1	43
Stmn4	stathmin-like 4	43
Isg20	interferon-stimulated protein	43
Dusp1	dual specificity phosphatase 1	42
Pydc3	pyrin domain containing 3	42
Edn1	endothelin 1	41
Gm6460	predicted gene 6460	38
Dusp5	dual specificity phosphatase 5	36
Serpine1	serine (or cysteine) peptidase inhibitor, clade E, member 1	34
Gm13889	predicted gene 13889	33
Gbp5	guanylate binding protein 5	32
Pyhin1	pyrin and HIN domain family, member 1	32
Ccbe1	collagen and calcium binding EGF domains 1	30
Ptpn14	protein tyrosine phosphatase, non-receptor type 14	30
Fam171b	family with sequence similarity 171, member B	30
Myc	myelocytomatosis oncogene	30
Tarm1	T cell-interacting, activating receptor on myeloid cells 1	30
Hdc	histidine decarboxylase	30
Dusp8	dual specificity phosphatase 8	29

Supplementary table 5 (continued)

Il27	interleukin 27	29
Ccr3	chemokine (C-C motif) receptor 3	29
Slc6a19	solute carrier family 6 (neurotransmitter transporter), member 19	28
Apol9b	apolipoprotein L 9b	27
Sh2d2a	SH2 domain containing 2A	27
Lrrc32	leucine rich repeat containing 32	26
Gbp2	guanylate binding protein 2	26
Col4a2	collagen, type IV, alpha 2	25
Mylk2	myosin, light polypeptide kinase 2, skeletal muscle	25
Gbp4	guanylate binding protein 4	25
Cdkn1c	cyclin-dependent kinase inhibitor 1C (P57)	25
Cd274	CD274 antigen	25
Aqp9	aquaporin 9	25
Gprc5a	G protein-coupled receptor, family C, group 5, member A	25
Gpr124	NA	25
Ddit3	DNA-damage inducible transcript 3	25
Rhov	ras homolog gene family, member V	25
Prph	peripherin	23
Ahr	aryl-hydrocarbon receptor	23
Il1f9	interleukin 1 family, member 9	23
Mx2	MX dynamin-like GTPase 2	23
Pxdc1	PX domain containing 1	21
Prkg2	protein kinase, cGMP-dependent, type II	21
Ifit2	interferon-induced protein with tetratricopeptide repeats 2	21
Sdcbp2	syndecan binding protein (syntenin) 2	21
Tgm1	transglutaminase 1, K polypeptide	21
Avil	advillin	20
Hoxa5	homeobox A5	20
Vegfc	vascular endothelial growth factor C	20
Apol9a	apolipoprotein L 9a	20
Fam71f2	family with sequence similarity 71, member F2	19
Ccrl2	chemokine (C-C motif) receptor-like 2	19
Col5a1	collagen, type V, alpha 1	18
B230312C02Rik	RIKEN cDNA B230312C02 gene	18
Thbs1	thrombospondin 1	18
Spsb1	splA/ryanodine receptor domain and SOCS box containing 1	18
Csrnp1	cysteine-serine-rich nuclear protein 1	17
6530402F18Rik	RIKEN cDNA 6530402F18 gene	17
Nfkbiz	nuclear factor of kappa light polypeptide gene enhancer in B cells inhibitor, zeta	17
Cdcp1	CUB domain containing protein 1	17
Ntng2	netrin G2	17

Supplementary table 5 (continued)

Efcab6	EF-hand calcium binding domain 6	17
P4ha2	procollagen-proline, 2-oxoglutarate 4-dioxygenase (proline 4-hydroxylase), alpha II polypeptide	16
Arid3b	AT rich interactive domain 3B (BRIGHT-like)	16
Lta	lymphotoxin A	16
Tnfsf15	tumor necrosis factor (ligand) superfamily, member 15	16
Socs1	suppressor of cytokine signaling 1	16
Il1rn	interleukin 1 receptor antagonist	16
A530032D15Rik	RIKEN cDNA A530032D15Rik gene	16
Adm	adrenomedullin	16
Nyap2	neuronal tyrosine-phophorylated phosphoinositide 3-kinase adaptor 2	16
Gipr	gastric inhibitory polypeptide receptor	15
A530064D06Rik	RIKEN cDNA A530064D06 gene	15
AW011738	expressed sequence AW011738	15
Plat	plasminogen activator, tissue	15
Dusp10	dual specificity phosphatase 10	15
Pim1	proviral integration site 1	14
Src	Rous sarcoma oncogene	14
Mmp12	matrix metallopeptidase 12	14
Rhou	ras homolog gene family, member U	14
Cish	cytokine inducible SH2-containing protein	14
Gadd45a	growth arrest and DNA-damage-inducible 45 alpha	14
Gbp3	guanylate binding protein 3	14
Gdf15	growth differentiation factor 15	13
Arg1	arginase, liver	13
Gbp7	guanylate binding protein 7	13
Lix1	limb expression 1 homolog (chicken)	13
Sema3e	sema domain, immunoglobulin domain (Ig), short basic domain, secreted, (semaphorin) 3E	13
Ptger2	prostaglandin E receptor 2 (subtype EP2)	13
Dok7	docking protein 7	13
Ifi204	interferon activated gene 204	13
Tnfrsf9	tumor necrosis factor receptor superfamily, member 9	13
A1cf	APOBEC1 complementation factor	13
Ccl7	chemokine (C-C motif) ligand 7	13
Mnda	myeloid cell nuclear differentiation antigen	13
Trim30d	tripartite motif-containing 30D	13
Gm14446	NA	13
Pilrb1	paired immunoglobin-like type 2 receptor beta 1	13
Bcar1	breast cancer anti-estrogen resistance 1	13
Hist1h4m	histone cluster 1, H4m	13
Srgn	serglycin	13

Supplementary table 5 (continued)

Ifi202b	interferon activated gene 202B	13
Mgam	maltase-glucoamylase	13
Oasl1	2'-5' oligoadenylate synthetase-like 1	12
Ifi205	interferon activated gene 205	12
Ier3	immediate early response 3	12
Trib3	tribbles homolog 3 (Drosophila)	12
4933432I03 Rik	RIKEN cDNA 4933432I03 gene	12
Ifi44	interferon-induced protein 44	12
Dusp14	dual specificity phosphatase 14	12
Cd83	CD83 antigen	12
Slc15a3	solute carrier family 15, member 3	12
Ppfibp2	PTPRF interacting protein, binding protein 2 (liprin beta 2)	12
Nupr1	nuclear protein transcription regulator 1	11
Syt7	synaptotagmin VII	11
Oasl2	2'-5' oligoadenylate synthetase-like 2	11
Phlda1	pleckstrin homology-like domain, family A, member 1	11
Irf7	interferon regulatory factor 7	11
Xaf1	XIAP associated factor 1	11
Usp18	ubiquitin specific peptidase 18	11
Pfn2	profilin 2	11
Slamf7	SLAM family member 7	11
Slc35f1	solute carrier family 35, member F1	10
Jag1	jagged 1	10
Slc16a14	solute carrier family 16 (monocarboxylic acid transporters), member 14	10
Smad7	SMAD family member 7	10
Socs2	suppressor of cytokine signaling 2	10
Hid1	HID1 domain containing	10
F3	coagulation factor III	10
Ccl3	chemokine (C-C motif) ligand 3	10
Hilpda	hypoxia inducible lipid droplet associated	10
Fignl2	fidgetin-like 2	10
Furin	furin (paired basic amino acid cleaving enzyme)	10
Sdk2	sidekick homolog 2 (chicken)	10
Tnfrsf1b	tumor necrosis factor receptor superfamily, member 1b	10
Ccl22	chemokine (C-C motif) ligand 22	9
Perm1	PPARGC1 and ESRR induced regulator, muscle 1	9
Hecw2	HECT, C2 and WW domain containing E3 ubiquitin protein ligase 2	9
Tnfaip3	tumor necrosis factor, alpha-induced protein 3	9
Mxd1	MAX dimerization protein 1	9
Slc24a1	solute carrier family 24 (sodium/potassium/calcium exchanger), member 1	9
Hist2h2aa1	histone cluster 2, H2aa1	9
Cd69	CD69 antigen	9

Supplementary table 5 (continued)

Lincrna-cox2	NA	9
Arc	activity regulated cytoskeletal-associated protein	9
Rnd3	Rho family GTPase 3	9
Pla1a	phospholipase A1 member A	9
Lat	linker for activation of T cells	9
Acsbg1	acyl-CoA synthetase bubblegum family member 1	9
Pilra	paired immunoglobin-like type 2 receptor alpha	9
Ddit4	DNA-damage-inducible transcript 4	9
Plk2	polo-like kinase 2	9
Ccl2	chemokine (C-C motif) ligand 2	9
Ppp1r15a	protein phosphatase 1, regulatory (inhibitor) subunit 15A	9
Nox3	NADPH oxidase 3	9
Tmem132a	transmembrane protein 132A	8
Cyr61	cysteine rich protein 61	8
Scg2	secretogranin II	8
Mfap3l	microfibrillar-associated protein 3-like	8
Plcl1	phospholipase C-like 1	8
Srxn1	sulfiredoxin 1 homolog (S. cerevisiae)	8
Slc7a11	solute carrier family 7 (cationic amino acid transporter, y+ system), member 11	8
Ndrg1	N-myc downstream regulated gene 1	8
Rapgef5	Rap guanine nucleotide exchange factor (GEF) 5	8
Itga3	integrin alpha 3	8
Cd40	CD40 antigen	8
Rnf19b	ring finger protein 19B	8
Atf3	activating transcription factor 3	8
Ankrd33b	ankyrin repeat domain 33B	8
Smox	spermine oxidase	8
Lamc2	laminin, gamma 2	8
Sqstm1	sequestosome 1	8
Slc22a4	solute carrier family 22 (organic cation transporter), member 4	8
Atp13a4	ATPase type 13A4	8
Hmox1	heme oxygenase 1	8
Gbp6	guanylate binding protein 6	8
Arnt2	aryl hydrocarbon receptor nuclear translocator 2	8
Sccpdh	saccharopine dehydrogenase (putative)	8
Tiparp	TCDD-inducible poly(ADP-ribose) polymerase	8
Mx1	MX dynamin-like GTPase 1	8
Ccdc136	coiled-coil domain containing 136	8
Sema3c	sema domain, immunoglobulin domain (Ig), short basic domain, secreted, (semaphorin) 3C	8
Stk40	serine/threonine kinase 40	8
Rtp4	receptor transporter protein 4	7

Supplementary table 5 (continued)

Ifih1	interferon induced with helicase C domain 1	7
Chac1	ChaC, cation transport regulator 1	7
Dusp13	dual specificity phosphatase 13	7
Gm20594	predicted gene, 20594	7
Moap1	modulator of apoptosis 1	7
9430076C15Rik	RIKEN cDNA 9430076C15 gene	7
Rgag4	retrotransposon gag domain containing 4	7
Tnf	tumor necrosis factor	7
Alas1	aminolevulinic acid synthase 1	7
Sh3yl1	Sh3 domain YSC-like 1	7
Mreg	melanoregulin	7
Slc6a12	solute carrier family 6 (neurotransmitter transporter, betaine/GABA), member 12	7
Gm7609	predicted pseudogene 7609	7
Dnajb9	DnaJ (Hsp40) homolog, subfamily B, member 9	7
Trpm4	transient receptor potential cation channel, subfamily M, member 4	7
Evi2a-evi2b	NA	7
Fcrlb	Fc receptor-like B	7
Pla2g5	phospholipase A2, group V	7
Abcb9	ATP-binding cassette, sub-family B (MDR/TAP), member 9	7
Hist1h4h	histone cluster 1, H4h	7
Nox1	NADPH oxidase 1	7
Rdh12	retinol dehydrogenase 12	7
Slc39a2	solute carrier family 39 (zinc transporter), member 2	7
Osm	oncostatin M	6
Prickle1	prickle homolog 1 (Drosophila)	6
Zc3h12a	zinc finger CCCH type containing 12A	6
B430306N03Rik	RIKEN cDNA B430306N03 gene	6
Mtmr7	myotubularin related protein 7	6
Scimp	SLP adaptor and CSK interacting membrane protein	6
Helz2	helicase with zinc finger 2, transcriptional coactivator	6
Tnnc1	troponin C, cardiac/slow skeletal	6
Mt2	metallothionein 2	6
Herc6	hect domain and RLD 6	6
Trem1	triggering receptor expressed on myeloid cells 1	6
Epha2	Eph receptor A2	6
Acoxl	acyl-Coenzyme A oxidase-like	6
Fam46c	family with sequence similarity 46, member C	6
Plxna4os1	plexin A4, opposite strand 1	6
Lamb3	laminin, beta 3	6
Ptgir	prostaglandin I receptor (IP)	6
Ero1l	ERO1-like (S. cerevisiae)	6

Supplementary table 5 (continued)

Csn3	casein kappa	6
Parp14	poly (ADP-ribose) polymerase family, member 14	6
Col11a2	collagen, type XI, alpha 2	6
Id2	inhibitor of DNA binding 2	6
Jazf1	JAZF zinc finger 1	6
Rgs1	regulator of G-protein signaling 1	6
Lhx2	LIM homeobox protein 2	6
Sp140	Sp140 nuclear body protein	6
Stat2	signal transducer and activator of transcription 2	6
Pilrb2	paired immunoglobin-like type 2 receptor beta 2	6
Tmc3	transmembrane channel-like gene family 3	6
Ccdc92	coiled-coil domain containing 92	6
Kctd12	potassium channel tetramerisation domain containing 12	6
Wfdc17	WAP four-disulfide core domain 17	6
Adcy3	adenylate cyclase 3	6
Marcks	myristoylated alanine rich protein kinase C substrate	6
Btg1	B cell translocation gene 1, anti-proliferative	6
Ntn1	netrin 1	6
Il4ra	interleukin 4 receptor, alpha	6
Plag1	pleiomorphic adenoma gene 1	6
Oas1b	2'-5' oligoadenylate synthetase 1B	6
Gbp9	guanylate-binding protein 9	6
Fndc9	fibronectin type III domain containing 9	6
Gpr31b	G protein-coupled receptor 31, D17Leh66b region	6
Ddx60	DEAD (Asp-Glu-Ala-Asp) box polypeptide 60	6
Pacrg	PARK2 co-regulated	6
Sez6l2	seizure related 6 homolog like 2	6
Rabgef1	RAB guanine nucleotide exchange factor (GEF) 1	6
Gucy2g	guanylate cyclase 2g	6
Hcar2	hydroxycarboxylic acid receptor 2	6
Kpna4	karyopherin (importin) alpha 4	6
Grb10	growth factor receptor bound protein 10	6
Gdnf	glial cell line derived neurotrophic factor	6
Ankrd50	ankyrin repeat domain 50	6
Gfod1	glucose-fructose oxidoreductase domain containing 1	6
Rasip1	Ras interacting protein 1	6
Rbpms2	RNA binding protein with multiple splicing 2	6
Kcnab1	potassium voltage-gated channel, shaker-related subfamily, beta member 1	6
Pdgfa	platelet derived growth factor, alpha	6
Psd2	pleckstrin and Sec7 domain containing 2	6
Ttc39c	tetratricopeptide repeat domain 39C	6
Phf11d	PHD finger protein 11D	5
Socs3	suppressor of cytokine signaling 3	5

Supplementary table 5 (continued)

Casp4	caspase 4, apoptosis-related cysteine peptidase	5
Rora	RAR-related orphan receptor alpha	5
Stx11	syntaxin 11	5
Ccl4	chemokine (C-C motif) ligand 4	5
Gnb4	guanine nucleotide binding protein (G protein), beta 4	5
Dcbld2	discoidin, CUB and LCCL domain containing 2	5
Hivep2	human immunodeficiency virus type I enhancer binding protein 2	5
Trim30a	tripartite motif-containing 30A	5
Dhx58	DEXH (Asp-Glu-X-His) box polypeptide 58	5
Tmem171	transmembrane protein 171	5
Gm6634	predicted gene 6634	5
Zfp703	zinc finger protein 703	5
Cd72	CD72 antigen	5
Atp7b	ATPase, Cu++ transporting, beta polypeptide	5
Bcl2a1d	B cell leukemia/lymphoma 2 related protein A1d	5
Tmem236	transmembrane protein 236	5
Cdc42ep2	CDC42 effector protein (Rho GTPase binding) 2	5
Tnfrsf23	tumor necrosis factor receptor superfamily, member 23	5
Rnf183	ring finger protein 183	5
C130026I21 Rik	RIKEN cDNA C130026I21 gene	5
Rgs12	regulator of G-protein signaling 12	5
Zdhhc18	zinc finger, DHHC domain containing 18	5
Ccr1	chemokine (C-C motif) receptor 1	5
Fam214b	family with sequence similarity 214, member B	5
Slfn4	schlafen 4	5
Rgs16	regulator of G-protein signaling 16	5
Cd22	CD22 antigen	5
Irgm1	immunity-related GTPase family M member 1	5
St3gal1	ST3 beta-galactoside alpha-2,3-sialyltransferase 1	5
Ticam1	toll-like receptor adaptor molecule 1	5
Gadd45b	growth arrest and DNA-damage-inducible 45 beta	5
Glipr2	GLI pathogenesis-related 2	5
Arhgef3	Rho guanine nucleotide exchange factor (GEF) 3	5
Smim3	small integral membrane protein 3	5
11-Mar	membrane-associated ring finger (C3HC4) 11	5
Gimap6	GTPase, IMAP family member 6	5
Cpd	carboxypeptidase D	5
Nckap1	NCK-associated protein 1	5
Lims2	LIM and senescent cell antigen like domains 2	5
Serpinb9	serine (or cysteine) peptidase inhibitor, clade B, member 9	5
Casz1	castor zinc finger 1	5
Zfp36	zinc finger protein 36	5
Galnt3	UDP-N-acetyl-alpha-D-galactosamine:polypeptide N-ag3	5

Supplementary table 6: Mn and misfolded α-Synuclein co-treatment caused downregulation in the genes in microglia >5 fold

Gene	*Name*	*Fold change*
Cecr6	cat eye syndrome chromosome region, candidate 6	-179
Sema4g	sema domain, immunoglobulin domain (Ig), transmembrane domain (TM) and short cytoplasmic domain, (semaphorin) 4G	-54
Tspan10	tetraspanin 10	-46
Serpinb1a	serine (or cysteine) peptidase inhibitor, clade B, member 1a	-25
Ocstamp	osteoclast stimulatory transmembrane protein	-22
Cx3cr1	chemokine (C-X3-C motif) receptor 1	-17
Lifr	leukemia inhibitory factor receptor	-16
Asb10	ankyrin repeat and SOCS box-containing 10	-16
Cd24a	CD24a antigen	-14
Camk2b	calcium/calmodulin-dependent protein kinase II, beta	-14
Gm5086	predicted gene 5086	-12
Slc14a1	solute carrier family 14 (urea transporter), member 1	-12
Hpgd	hydroxyprostaglandin dehydrogenase 15 (NAD)	-12
Klhl38	kelch-like 38	-12
Fcrls	Fc receptor-like S, scavenger receptor	-10
Klrd1	killer cell lectin-like receptor, subfamily D, member 1	-9
Srpk3	serine/arginine-rich protein specific kinase 3	-9
Pdk2	pyruvate dehydrogenase kinase, isoenzyme 2	-9
Armc2	armadillo repeat containing 2	-9
Pacsin1	protein kinase C and casein kinase substrate in neurons 1	-8
Mn1	meningioma 1	-8
Gpr162	G protein-coupled receptor 162	-7
Cmbl	carboxymethylenebutenolidase-like (Pseudomonas)	-7
Pianp	PILR alpha associated neural protein	-6
Lsp1	lymphocyte specific 1	-6
Crip1	cysteine-rich protein 1 (intestinal)	-6
Ppfia4	protein tyrosine phosphatase, receptor type, f polypeptide (PTPRF), interacting protein (liprin), alpha 4	-6
Lrrc14b	leucine rich repeat containing 14B	-6
Atp6v0d2	ATPase, H+ transporting, lysosomal V0 subunit D2	-5
Kcne3	potassium voltage-gated channel, Isk-related subfamily, gene 3	-5
9330188P03Rik	RIKEN cDNA 9330188P03 gene	-5
Aif1	allograft inflammatory factor 1	-5

Supplementary table 7: Expression levels in the genes reported for microglial function and phenotype

Phenotype	*Function*	*Gene*	*Fold Change (Syn)*	*Fold Change (Mn)*	*Fold Change (Syn+Mn)*
M1 classic phenotype (cytotoxic)					
		IL-1b	345	4	664
		IL-6	714	52	3407
		IL-12b	4	6	788
		IFNb1	7	52	132
		CXCL2	37	13	174
		CXCL3	125	17	278
		CXCL10	20	3	45
		IL-1a	190	6	269
		IL-2			
		CCL5 (RANTES)	43	4	181
		Cox-2			
M2a alternate phenotype (repair and regeneration)					
	Anti-inflammatory	*IL-4ra*	3	2	6
		IL-1RA (IL-1Rn)	6	7	16
		CX3CR1 (fractalkine receptor)	-17	-14	-31
		Tab1	-1	-1	-1
		TGF-b1	1	1	1
		Tgfbr1	-2	-2	-2
		Tgfbr2	-2	-1	-1
		Tgfbrap1	-1	-1	-1
		CD40	3	3	8
		CD74	2	-2	2
		Cd209c	1	1	-1
	Repair/Immunomodulatory	YM1			
		Hexa	-1	1	-1
		FIZZ1	-1	-1	-1
		IGF-1r	-1	-2	-2
		IGF-1	-4	-2	-4
		Igf2bp2	3	2	4
		Igfbp4	-2	-2	-5
		Arg1	3	12	13
M2b (c) Type II-deactivating phenotype (immunomodulatory)					
		IL-10	-1	1	-1
		Cox-2			
		SphK2	1	2	3

Supplementary table 8: Expression levels in the genes reported for microglial function and phenotype

		Fold change		
Gene	**Name**	**Syn**	**Mn**	**Mn+ Syn**
Ccrl2	chemokine (C-C motif) receptor-like 2	2.9	1.1	19.1
Cd83	CD83 antigen	-2.6	3.2	11.7
Cd14	CD14 antigen	2.8	2.0	4.8
Itgam	integrin alpha M	2.0	1.7	2.5
H2-K1	histocompatibility 2, K1, K region	1.0	1.4	2.1
B2m	beta-2 microglobulin	1.3	1.6	1.8
Tnfrsf12a	tumor necrosis factor receptor superfamily, member 12a	-1.2	1.3	1.5
Fcer1g	Fc receptor, IgE, high affinity I, gamma polypeptide	1.1	1.2	1.2
Icam1	intercellular adhesion molecule 1	1.1	-1.5	1.2
Fcgr3	Fc receptor, IgG, low affinity III	-1.0	1.2	-1.0
Csf1r	colony stimulating factor 1 receptor	-1.2	-1.6	-1.3
Sirpa	signal-regulatory protein alpha	-1.4	-1.4	-1.5
Tyrobp	TYRO protein tyrosine kinase binding protein	-1.7	-1.5	-1.7
P2ry13	purinergic receptor P2Y, G-protein coupled 13	-1.3	-5.0	-3.2
Trem2	triggering receptor expressed on myeloid cells 2	-2.2	-1.8	-3.8
P2ry12	purinergic receptor P2Y, G-protein coupled 12	-1.2	-2.0	-4.9
Gpr183	G protein-coupled receptor 183	-3.2	-5.9	-17.3
Cx3cr1	chemokine (C-X3-C motif) receptor 1	-17.5	-14.1	-31.0
Ccrl2	chemokine (C-C motif) receptor-like 2	2.9	1.1	19.1
Cd83	CD83 antigen	-2.6	3.2	11.7
Cd14	CD14 antigen	2.8	2.0	4.8
Itgam	integrin alpha M	2.0	1.7	2.5
H2-K1	histocompatibility 2, K1, K region	1.0	1.4	2.1
B2m	beta-2 microglobulin	1.3	1.6	1.8
Tnfrsf12a	tumor necrosis factor receptor superfamily, member 12a	-1.2	1.3	1.5
Fcer1g	Fc receptor, IgE, high affinity I, gamma polypeptide	1.1	1.2	1.2
Icam1	intercellular adhesion molecule 1	1.1	-1.5	1.2
Fcgr3	Fc receptor, IgG, low affinity III	-1.0	1.2	-1.0
Csf1r	colony stimulating factor 1 receptor	-1.2	-1.6	-1.3
Sirpa	signal-regulatory protein alpha	-1.4	-1.4	-1.5
Tyrobp	TYRO protein tyrosine kinase binding protein	-1.7	-1.5	-1.7
P2ry13	purinergic receptor P2Y, G-protein coupled 13	-1.3	-5.0	-3.2
Trem2	triggering receptor expressed on myeloid cells 2	-2.2	-1.8	-3.8

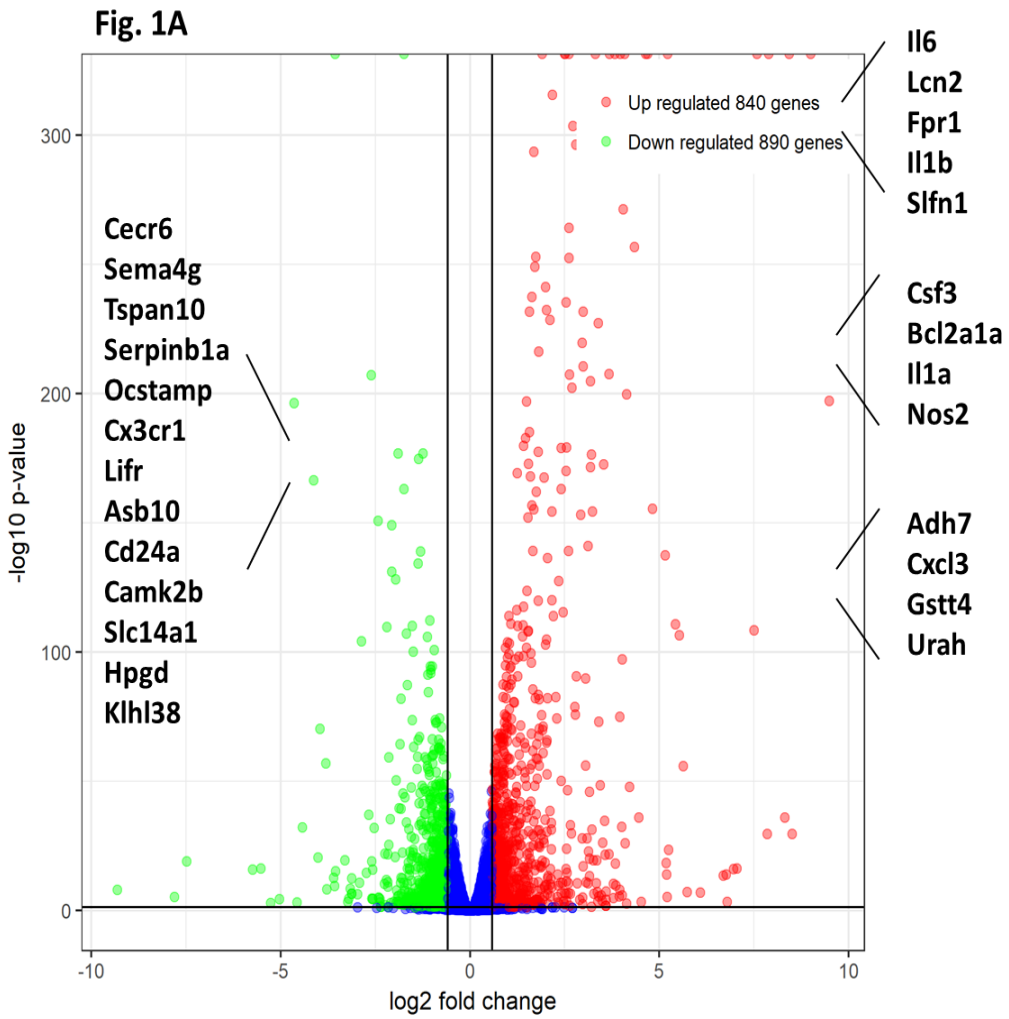

Figure 1: Transcriptomic profiling of microglial responses to misfolded α-Synuclein

(A) differentially expressed microglia transcripts in response to α-syn. Volcano plots of genes that are that are significantly different, upregulated (shown in red) or downregulated (green dots). (B) Hierarchical clustering of top 50 upregulated genes and top 50 down-regulated genes induced αSyn. (C) Reactome enrichment plots illustrating top pathways and biological processes that are altered in response to α-syn treatment.

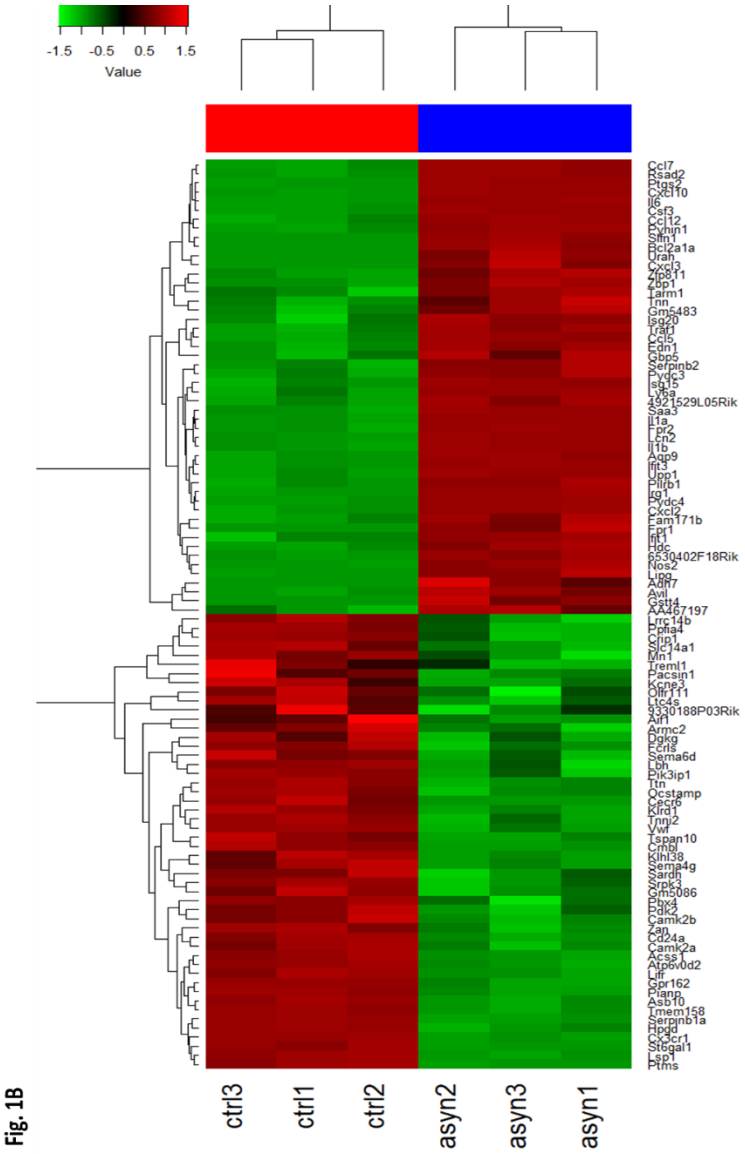

Fig. 1B

Figure 1 (Continued)

Fig. 1C

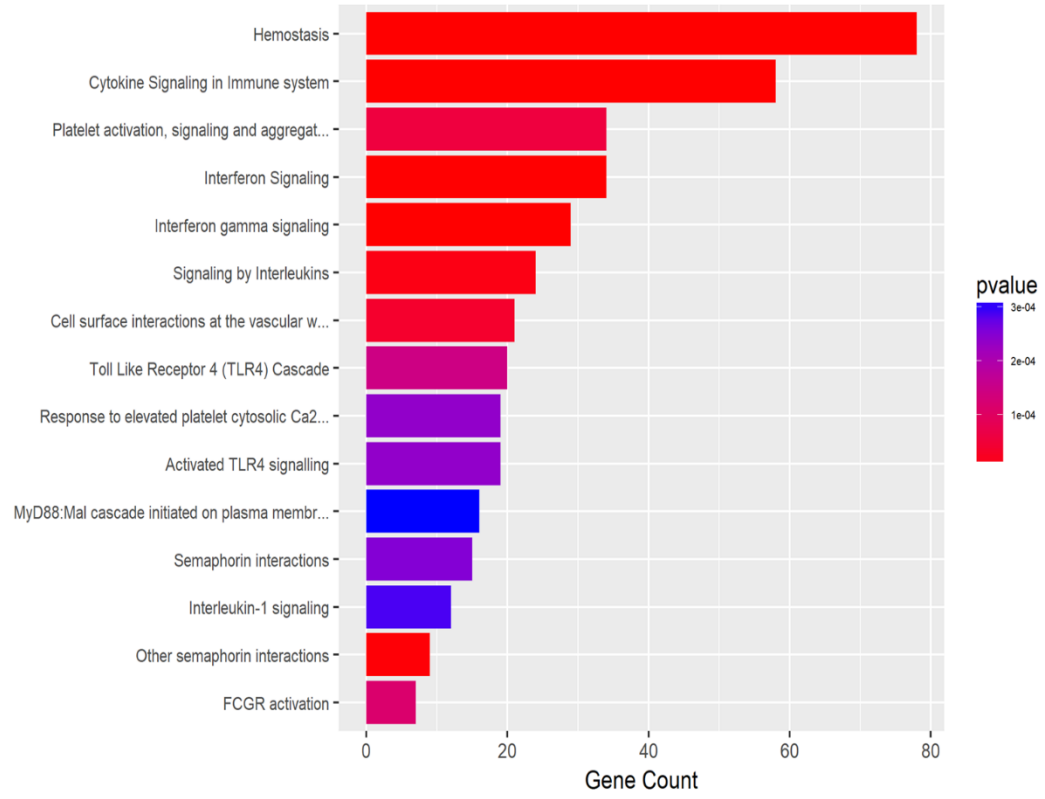

Figure 1 (Continued)

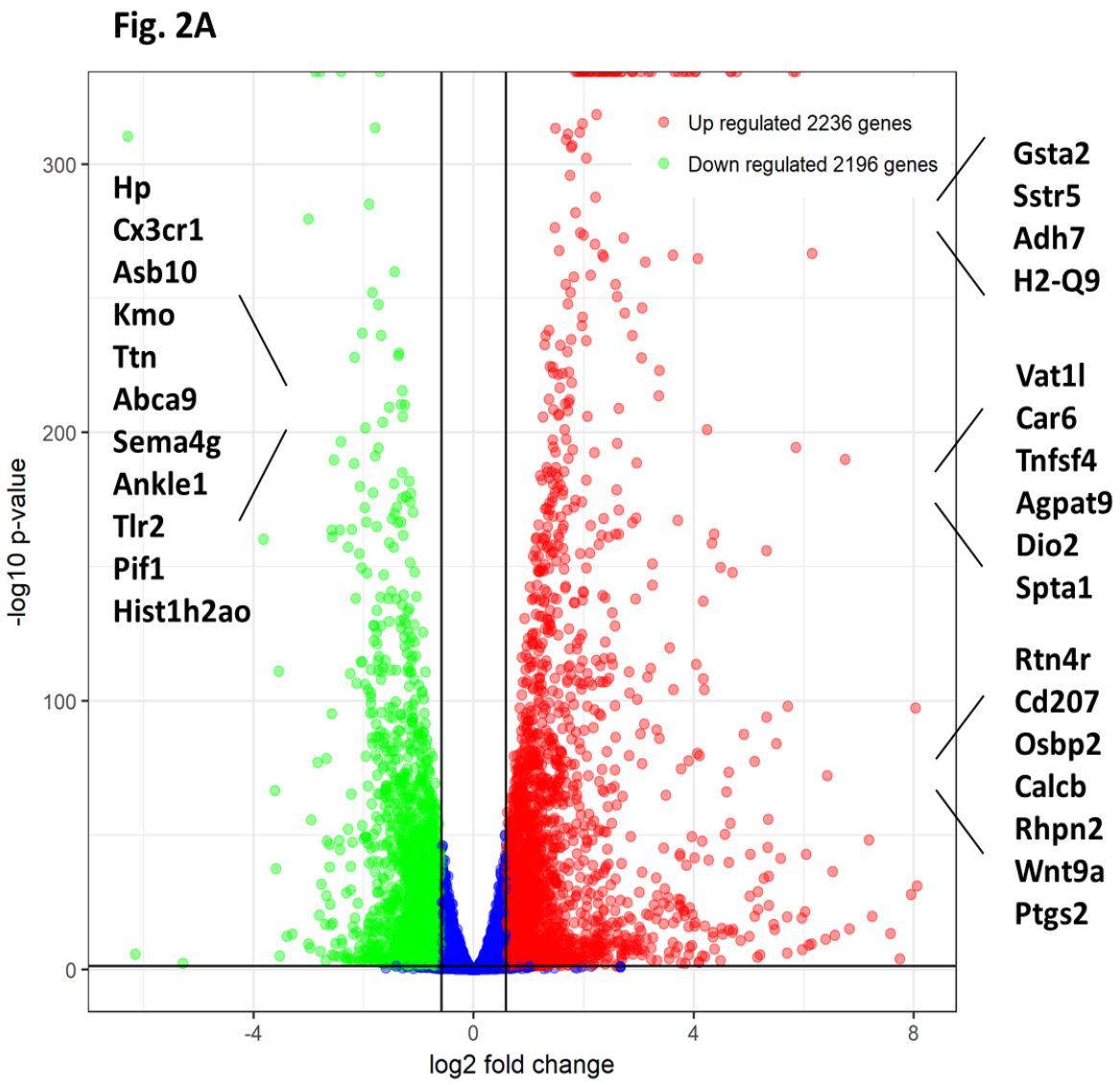

Figure 2: Transcriptomic profiling of microglial responses to Manganese

(A) differentially expressed microglia transcripts in response to Mn. Volcano plots of genes that are that are significantly different, upregulated (shown in red) or downregulated (green dots). (B) Heat maps of top 50 upregulated genes and top 50 down-regulated genes induced Mn. (C) Reactome enrichment plots illustrating top pathways and biological processes that are altered in response to Mn treatment.

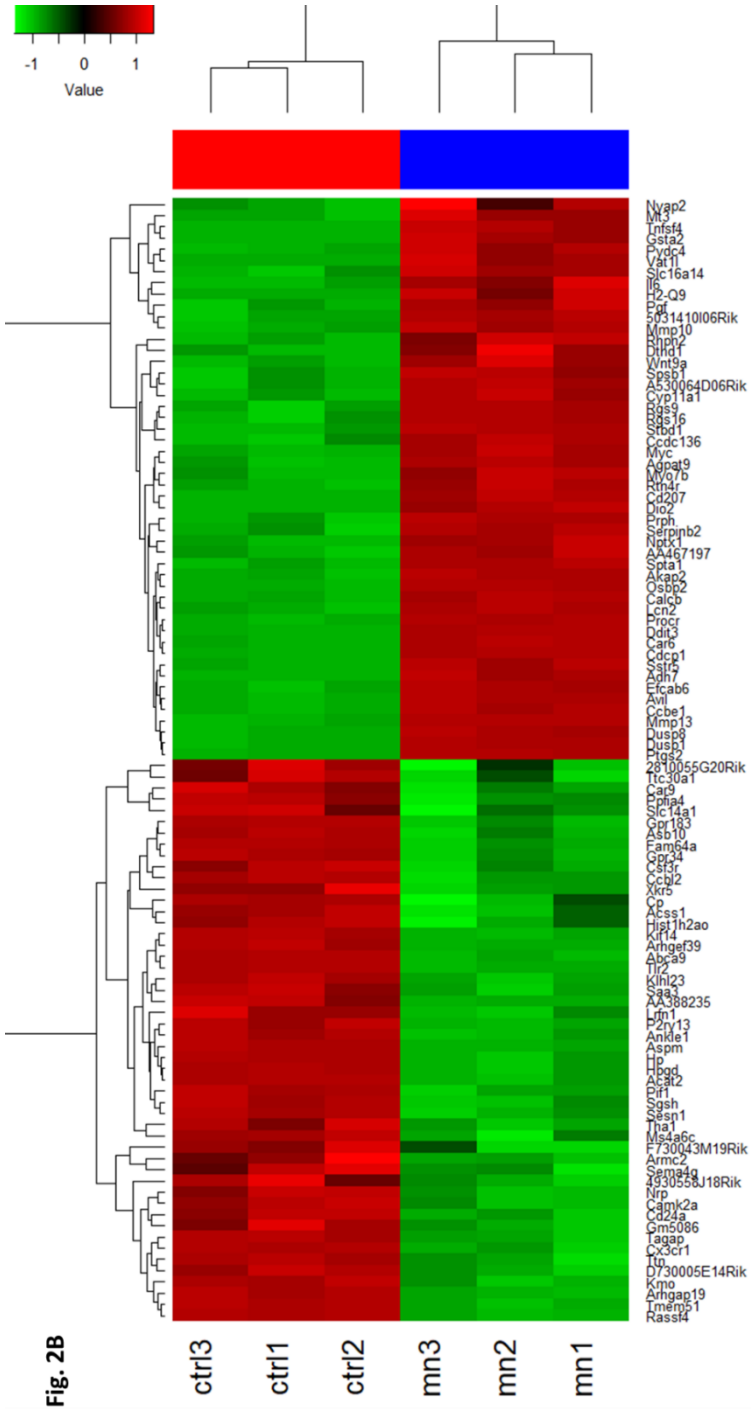

Fig. 2B

Figure 2 (Continued)

Fig. 2C

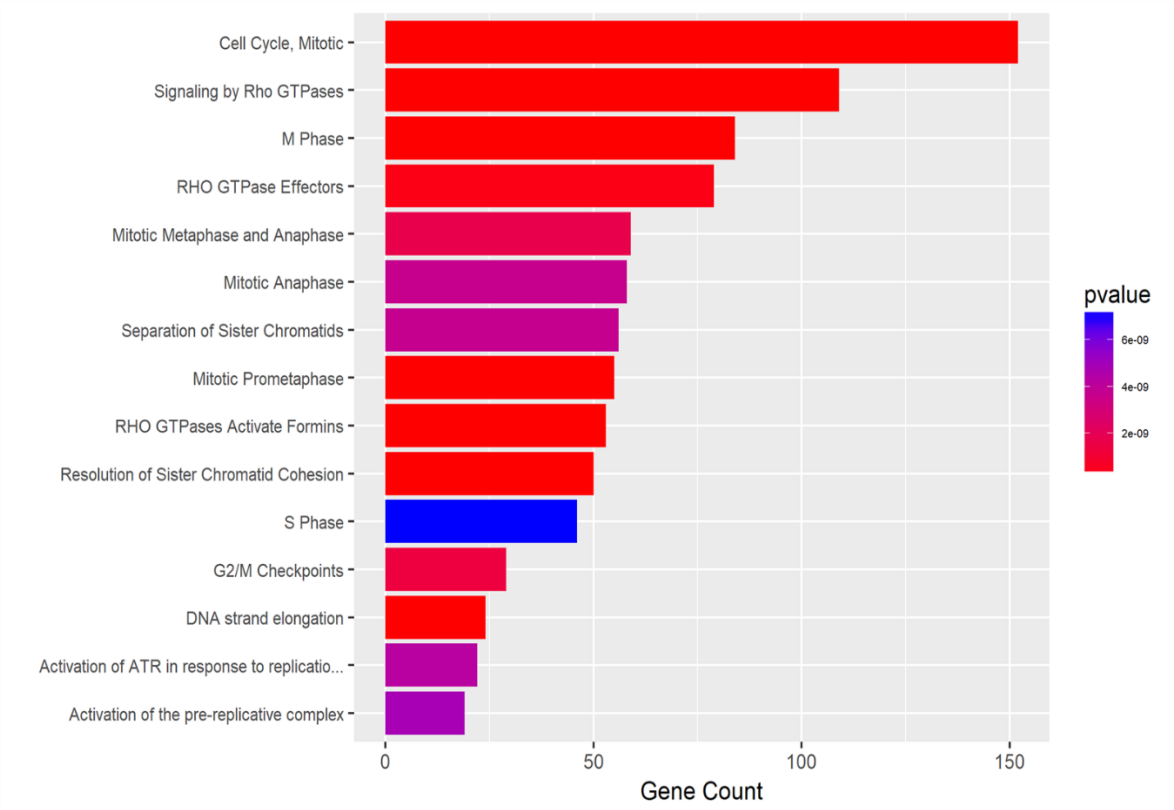

Figure 2 (Continued)

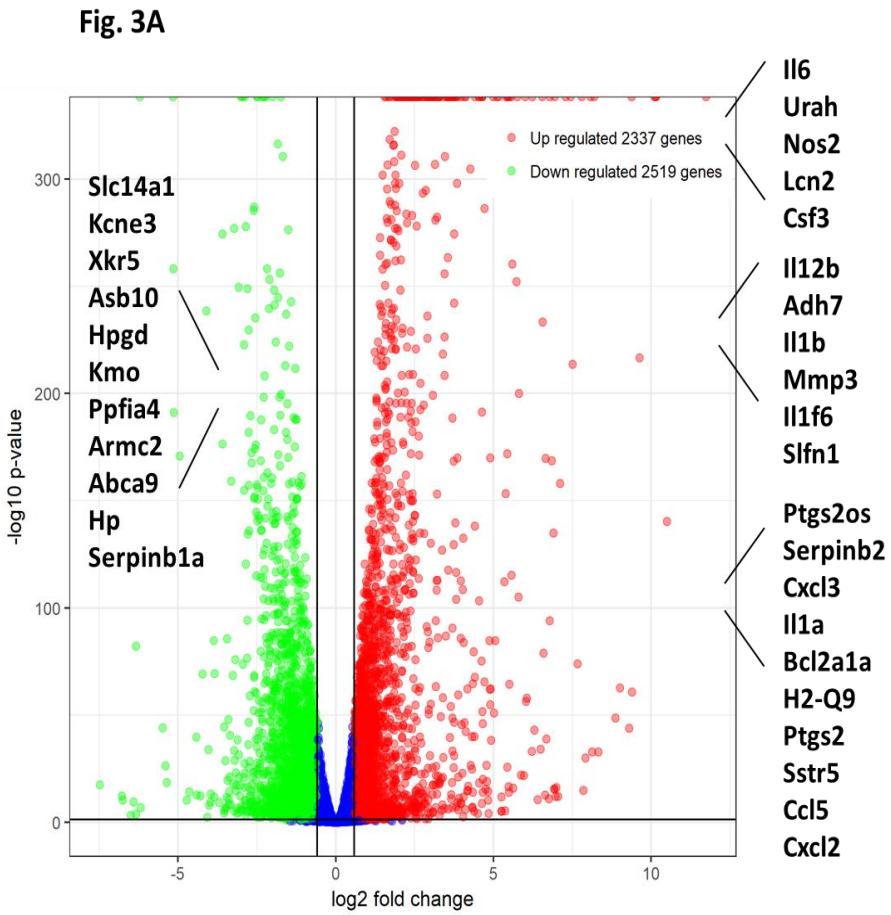

Figure 3: Transcriptomic profiling of microglial responses to Manganese and α-Synuclein co-treatment

(A) differentially expressed microglia transcripts in response to Mn and α-Syn co-treatment. Volcano plots of genes that are that are significantly different, upregulated (shown in red) or downregulated (green dots). (B) Heat maps of top 50 upregulated genes and top 50 down-regulated genes induced Mn and α-Syn co-treatment. (C) Reactome enrichment plots illustrating top pathways and biological processes that are altered in response to Mn and α-Syn co-treatment.

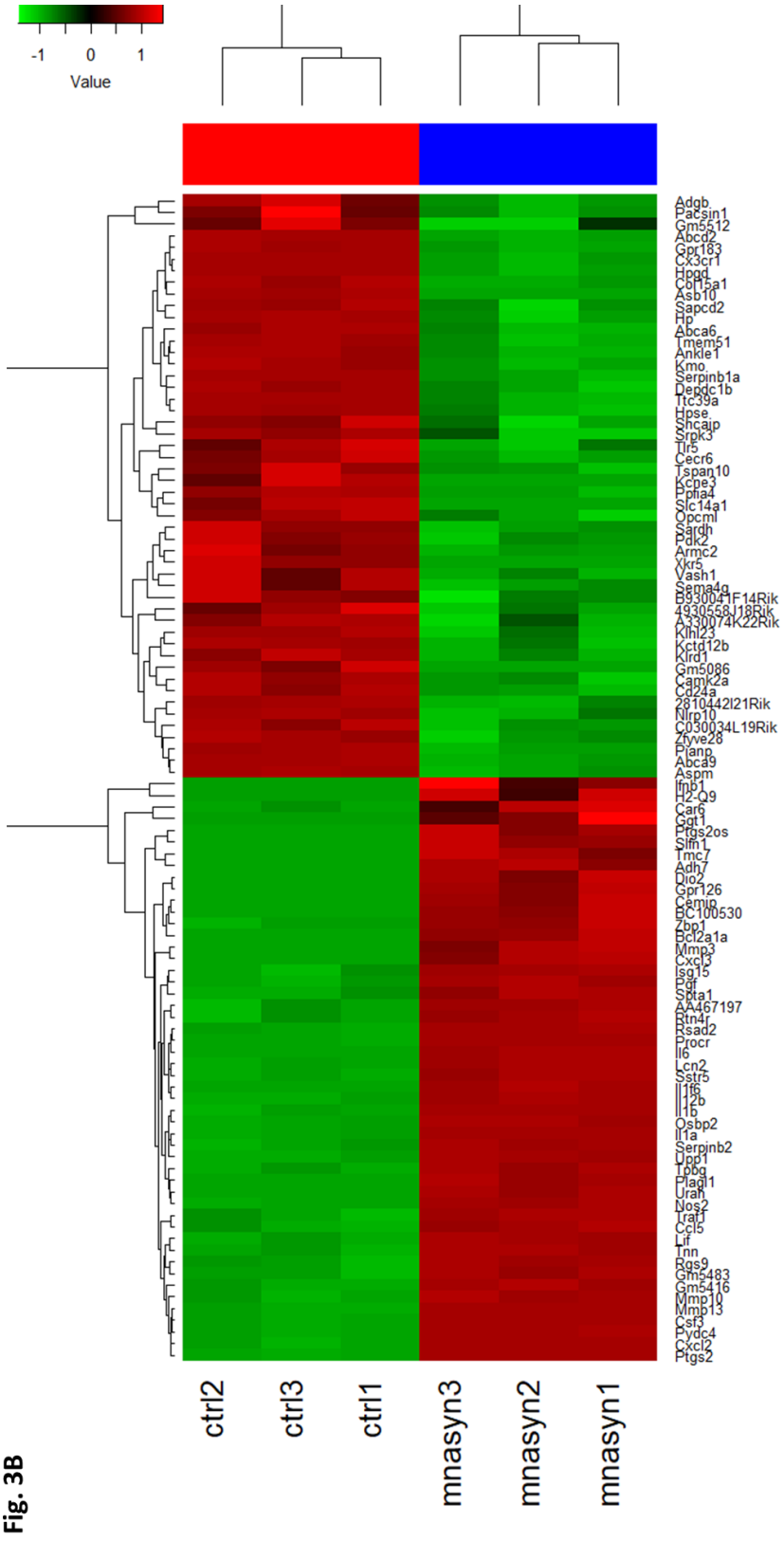

Fig. 3B

Fig. 3 (Continued)

Fig. 3C

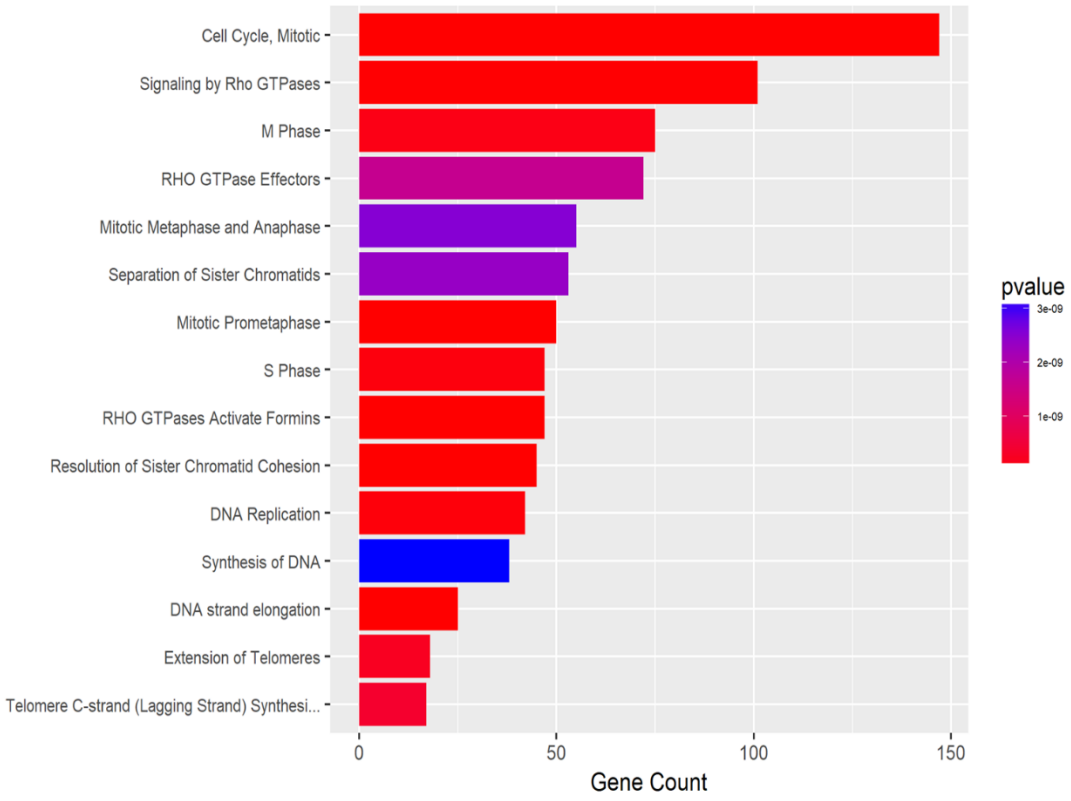

Figure 3 (Continued)

Fig. 4A

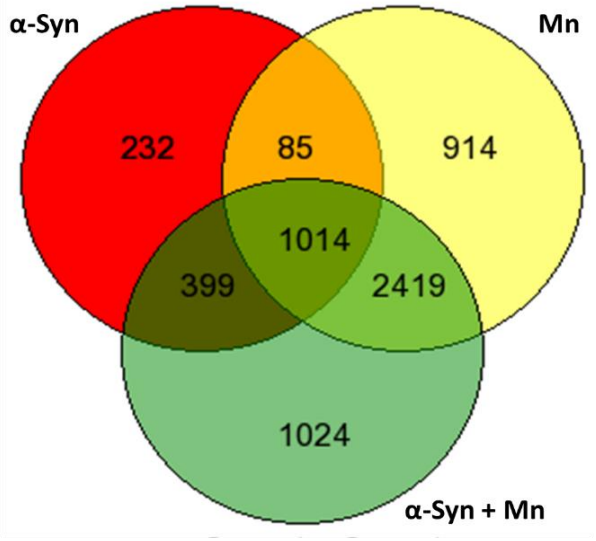

Fig. 4B

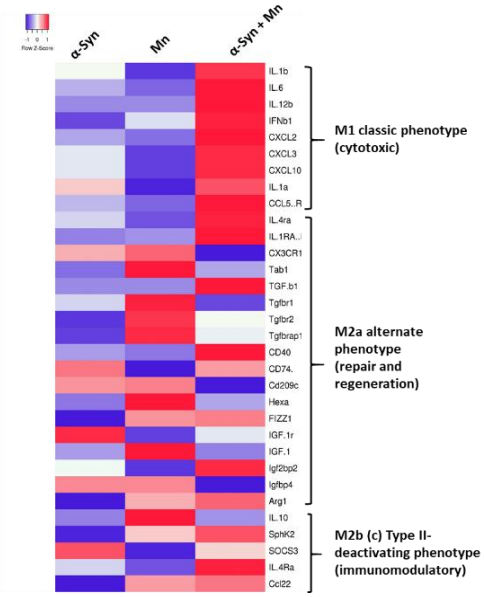

Figure 4: RNA-seq demonstrate distinct response in gene expression

(A) Schematic view of data from RNA-Seq using Venn diagram showing the overlaps between the differentially expressed genes (DEGs) in microglial responses to α-Syn, Mn, and their co-treatments. The overlap between the two circles indicates the number of genes differentially expressed by both treatments. (B) Heatmap representation of RNA-seq data showing inflammasome regulated gene transcripts in response to α-Syn, Mn and their co-treatments.

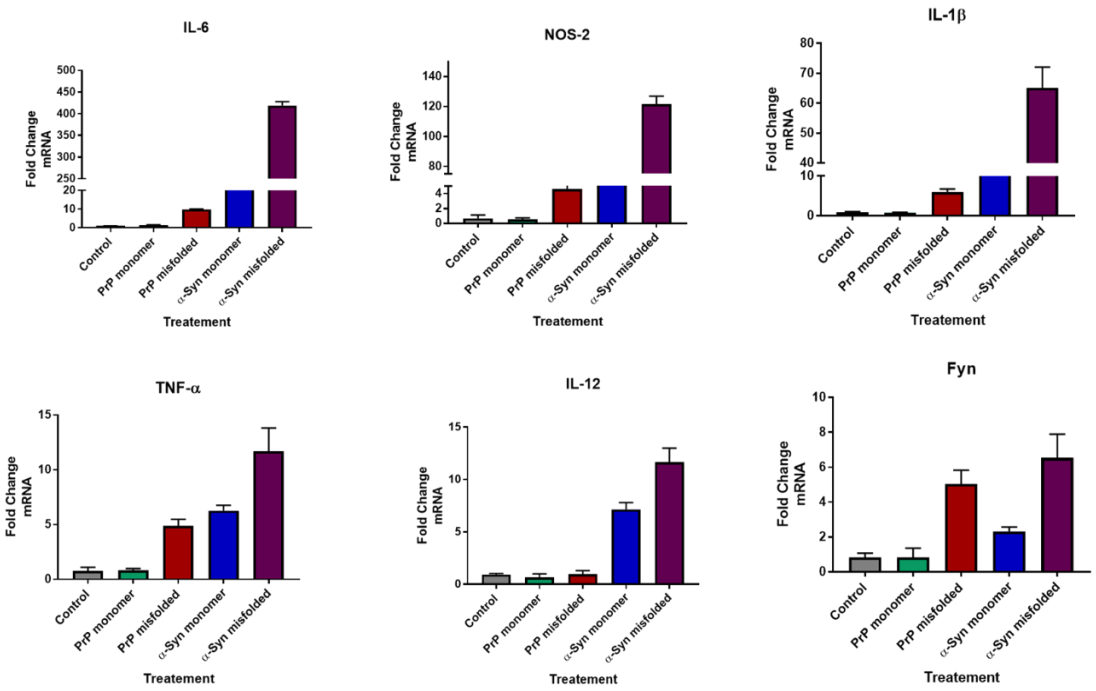

Figure 5: RNA-seq demonstrate distinct response in gene expression

RT-qPCR quantification of the genes expression levels in microglia in response to α-Synuclein and prion proteins. Increase in pro-inflammatory genes IL-6, NOS-2, IL-1β, TNF-α, IL-12 and non-receptor tyrosine kinase, Fyn, presented.

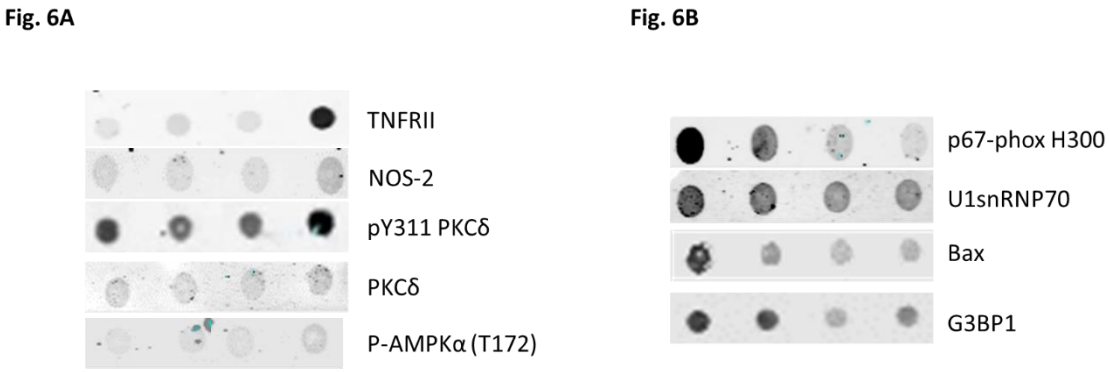

Figure 6: Verification of protein expression using dot blots increased or decreased genes

Dot blots to verify the protein expression changes as quantification of the genes expression levels in microglia in response to α-Syn, Mn and their co-treatments. Increase in pro-inflammatory genes (A) Proteins with increased response to treatments are shown on left, TNFRII, NOS-2, pY311 PKCδ, PKCδ and P-AMPKα (T172) were increased. (B) Proteins with the decreased trend to treatments are shown on right, p67-phox H300, U1snRNP7, Bax, G3BP1 were decreased.

CHAPTER VI: GENERAL CONCLUSION AND FUTURE DIRECTIONS

In this section, I present a general overview of the results from each chapter and how this fits in a global picture of each chapter in relation to their importance. We developed an organotypic brain slice culture model to understand the mechanism of misfolded protein pathology in the pathogenesis of protein misfolding disorders and overall implications of these findings in developing therapeutics (See Fig.1 below for other applications). We also used these models to understand mechanisms of neurotoxicity and characterized specific responses of Microglia in response to Manganese and α synuclein prions. The specific findings are covered under 'results' section and their implications can be found in 'discussion' section of the pertaining chapter.

In Chapter 1, we introduce an organotypic brain slice cultures as an *ex-vivo m*odel to study environmentally linked neurodegenerative diseases with a protein misfolding component as an etiological factor. We also reviewed, current knowledge on the applications of organotypic brain slices in diseases such as Alzheimer's, Parkinson's, Prion, Huntington's, ALS, and TBI. The brain slices recapitulate key features of several disease phenotype and neurotoxicity as compared to the cell cultures. Some of the key advantages of using the slice cultures are that they are feasible to study protein aggregation as they allow chronic/long-term studies involving several weeks in a controlled environment. Although there are several advantages of using the slice culture model for neurotoxicity studies, the notable caveat of this model includes the time-intensive protocol to generate slices and particularly labor-intensive nature of the long-term maintenance of the cultures. To overcome these challenges, new tools that allow slice preparation in a more time efficient manner are needed. Further technological

advancements in the slice preparation and maintenance may help to address some of these concerns.

In chapter II we provide a sensitive detection platform from prion-infected organotypic slice cultures termed as OSCAR assay (organotypic slice cultures coupled to RT-QuIC assay). Using this assay, lead compounds can be rapidly screened with very low protein requirement. This allows us to develop high-throughput models that are scalable. Further studies are underway to identify compounds that may uncouple seeding activity and or neurotoxicity in the slices. Neurodegenerative disorders such as Alzheimer's and Parkinson's have unique proteins that can be misfolded. Based on the existing evidence, we predict the OSCAR model can be translated to other protein misfolding disorders that obey protein-based aggregation phenomena. Another advantage of this model is that it requires less number of animals and is cost-effective. Further, we are using this model to understand mechanisms of protein aggregation.

The findings reported in Chapter III demonstrate that organotypic slice cultures can be effectively used to model chronic wasting disease (CWD). CWD prions are difficult to replicate in the mouse as the prion protein gene sequence doesn't effectively allow to cross seed the elk or deer prions. Therefore, we used a transgenic mouse that expresses elk prion protein sequence. Using Tg12 slice cultures we were able to develop a brain slice culture for CWD prions and thus reducing the time to study this chronic progressive disease that may take up to 3-5 years to study in cervids.

In Chapter IV, we investigated the role of microglia in Manganese and α-Syn induced inflammation at transcriptomic level. Mn is richly distributed in welding fumes and is also known to cross the blood-brain barrier as well as it could pass through the intranasal route to

lungs. Thus, Mn can enter the brain directly in high-risk groups such as welders and miners and cause a Parkinsonian syndrome. The interaction of Mn with α-Syn is investigated as it could trigger a deteriorating inflammation and thus may lead to neurological disease. Furthermore, we identified key genes and pathways related to microglial dysfunction caused by Mn, α-Syn and their interaction. Further biochemical and molecular studies would allow us to identify specific targets that are druggable. This not only enhances our understanding of the fundamental mechanisms of drug targets but also an optimization of rational drug targets. Previous studies suggested Fyn and PKCδ play a central role in the Parkinson's disease models. Misfolded aggregated α-synuclein can rapidly activate microglia and the effect of Mn on altering the phenotype is unknown. Using the transgenic knockout models of Fyn and PKCδ, we hope to understand the ability the key mechanisms involved in the microglia-mediated pathology. Further studies are being performed to validate promising targets *in-vitro* and *in-vivo* disease models.

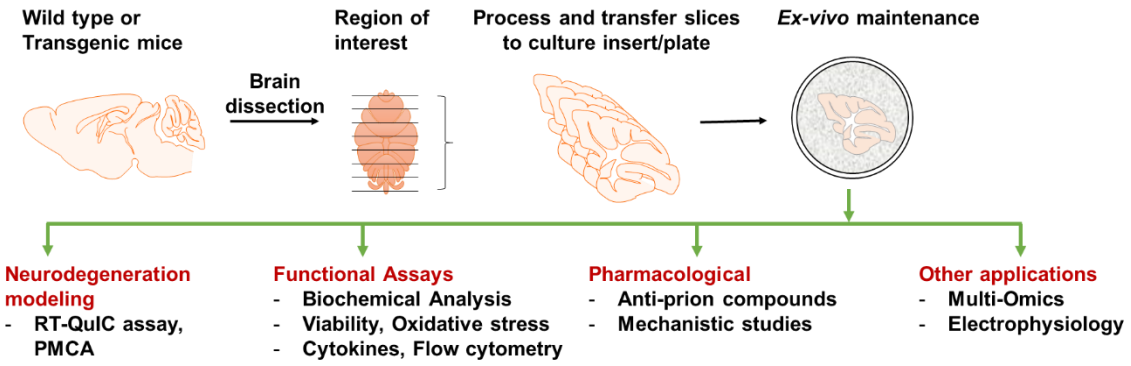

Figure 1: Schematic depiction of brain slice culture preparation and their applications

Brains were dissected out from neonatal mice and region of interest (for example, cerebellum) will be oriented to the cutting plane (sections derived from sagittal plane is

shown). Slices will be processed as desired such as treatments with materials such as homogenates and washed. The slices will be transferred to a culture insert with nutrient media supplied at the basal chamber to permit an air-media interface for the slice cultures. These slices are accessible for a variety of applications such as protein misfolding modeling, functional and biochemical assays, and other translational approaches.